Quantitative Analysis of the Shrinkage and Warpage Behavior of Injection Molded Parts Using Conventional and Microcellular Injection Molding and Microcellular Co-Injection Molding

By

Adam Jon Kramschuster

A thesis submitted in partial fulfillment of the requirement for the degree of

Master of Science

(Mechanical Engineering)

at the

UNIVERSITY OF WISCONSIN-MADISON

2005

Acknowledgements

First, I would like to thank Professor Lih-Sheng (Tom) Turng for his guidance and support throughout this research, and for giving me the opportunity to work with the Polymer Engineering Center at the University of Wisconsin-Madison. Without him, this work would not have been possible, and I only hope that I can be as good of a mentor to others as he has been to me.

I would like to thank Professor Don Ermer, whose patience with me when trying to fully understand design of experiments was extraordinary. Many hours were spent in his office reviewing data to ensure the validity of this research.

Ryan Cavitt, Dr. ZB Chen, and Chris Shen all deserve a special thank you for their large contributions to this research. Ryan and Chris helped extensively with running dozens of hours of preliminary experiments, and ZB provided me excellent advice many times during late nights in the office.

Professor Tim A. Osswald and Professor A. Jeffrey Giacomin also contributed greatly with their knowledge concerning polymers, and their class notes and books were consulted extensively during this research.

This research was partially supported by the National Science Foundation (DMI 0140396 and DMI 0323509), the UW–Madison Graduate School Industrial and Economic

Development Research (I&EDR) Award, and the industrial consortium of the Polymer Engineering Center at the University of Wisconsin-Madison. I would also like to thank EVCO Plastics, and especially Bob Pryzbilski, for use of their optical coordinate measurement machine (OCMM) for the S&W measurements, as well as ExxonMobil, Badger Color, and Moog Japan and Cornell Injection Molding Program (CIMP) for donating the polypropylene, color concentrate, and the box mold, respectively, used for the experiments.

Lastly, I would like to thank the student members of the Polymer Engineering Center for always asking tough questions during group meeting presentations, and for always being enjoyable to be around. My girlfriend Kate also spent many hours proofreading my thesis, and she deserves a special thank you for her hard work as well.

Dedication

To my parents, who always believed in me.

Table of Contents

Nomenclature

Acronym	Description
DOE	Design of Experiments
GCP	Gas counterpressure
MCP	Microcellular plastics
MFE	Mass flow element
MPP	MuCell® Process Pressure
OCMM	Optical coordinate measurement machine
PA	Polyamide
PC	Polycarbonate
PE	Polyethylene
PMMA	Polymethylmethacrylate
PP	Polypropylene
PS	Polystyrene
PTFE	Polytetrafluoroethylene
SCF	Supercritical fluid
SEM	Scanning electron microscope
T_g	Glass transition temperature

Description of Figures

List of Tables

Abstract

This research investigated the effects of processing conditions on the shrinkage and warpage (S&W) behavior of a box-shaped, polypropylene part using conventional and microcellular injection molding and microcellular co-injection molding. Three sets of 2^{6-1} fractional factorial design of experiments (DOE) were employed to perform the experiments and proper statistical theory was used to analyze the data. After the injection molding process reached steady state, molded samples were collected and measured using an optical coordinate measurement machine (OCMM), which had been evaluated using a proper repeatability and reproducibility (R&R) measurement study. By analyzing the statistically significant main and two-factor interaction effects, the results show that the supercritical fluid (SCF) content (nitrogen in this case, in terms of SCF dosage time) and the injection speed affect the S&W of microcellular injection and microcellular co-injection molded parts the most, whereas pack/hold pressure and pack/hold time have the most significant effect on the S&W of conventional injection molded parts. A reduction in cell size and increase in cell density is also noted when using high wt% SCF contents. Also, this study quantitatively showed that, within the processing range studied, a reduction in the S&W could be achieved with the microcellular injection molding and microcellular co-injection molding processes.

Chapter 1

Introduction

The plastics industry is one of the largest manufacturing industries in the United States, accounting for more than $409 billion in annual shipments and 2.4 million jobs [1]. Plastics play an indispensable role in a wide variety of markets, including packaging and building/construction; transportation; consumer and institutional products; furniture and furnishings; electronics and more. Plastics are one of the most utilized materials on a volume basis in the United States. Today, plastics are broadly integrated into people's lifestyles and make a major, irreplaceable contribution to virtually all product areas. The total thermoplastic consumption in the year 2000 was 26.8 million tons in United States, which accounted for 23% of the total plastic consumption in the world [2]. The total plastics usage in the United States is growing rapidly, much faster than the general

economy, as plastic is replacing conventional materials in old applications and finding newer applications because of its cost and processing benefits. As the need for thermoplastic resins for domestic consumption increases, there is a great demand for plastic processing technologies that can help provide environmentally friendly solutions to reduce plastics consumption per product, while maintaining the product quality and properties.

Microcellular injection molding is a major innovation in plastics technology that has the potential to significantly affect the plastics industry. The processing attributes of this novel technology opens up the avenue for newer applications with plastics and widens the processing window for manufacturing with polymers. This breakthrough foam process enhances product design, improves processing efficiency and reduces product cost. Microcellular injection molding enables molders to reduce material consumption while producing strong, lightweight products, and due to recent advancements, high quality surface finishes.

1.1 History

Professor Nam P. Suh and his graduate student, Jane Martini, in response to a problem posed by Mr. Gordon Brown of the Eastman Kodak Company, developed microcellular technology at the Massachusetts Institute of Technology (MIT). Eastman Kodak Co. aimed to reduce the plastic consumption in their products without compromising their toughness [3]. The idea was to replace the volume occupied by plastic material with tiny

bubbles smaller than the size of naturally occurring flaws in the polymer. This was accomplished by saturating the polymer with supercritical fluid (SCF) (e.g., nitrogen or carbon dioxide) and later inducing a thermodynamic instability to reduce the dissolubility of the gas in the polymer. The reduced solubility resulted in nucleation of the gas at numerous sites in the polymer, forming microcellular structures. Since its inception, much work has been done with microcellular plastics (MCP's) to advance them from a laboratory concept to a technology worthy of worldwide commercialization. Figure 1.1 shows an early design of equipment that was used to produce microcellular plastics. The equipment consisted of a pressure vessel, capable of holding highly pressurized atmospheric gases such as nitrogen or carbon dioxide in a supercritical state. Inside the

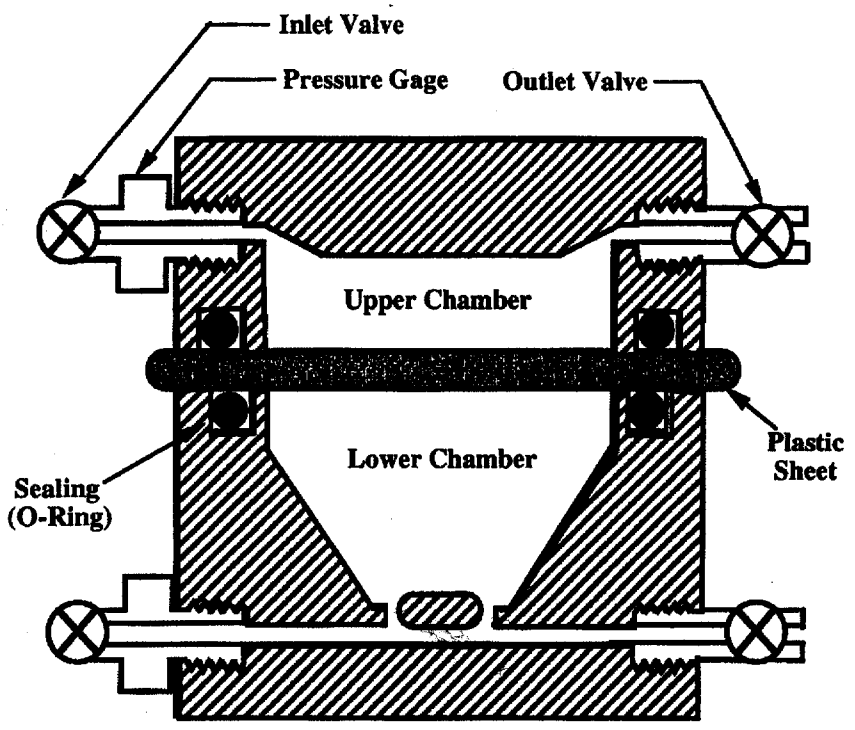

Figure 1.1 Batch processing equipment for manufacturing microcellular plastics [4].

pressure vessel, a plastic sheet or a batch of plastic sheets would be mounted. The polymer sheets could be heated and melted by electric heaters. Since only a batch of plastics could be foamed at a time, this process was known as the batch process of manufacturing microcellular plastics. The batch process consisted of supersaturating the heated polymer in a pressure chamber filled with gas, and later inducing a pressure drop in the chamber. The process of supersaturation was entirely diffusion driven and would take several hours, if not days, to complete. When a homogenous polymer-gas phase mixture was formed, nucleation was induced by a sudden thermodynamic instability (a significant pressure drop or rapid increase in temperature). This process was successful in producing lightweight parts with various thermoplastics such as polystyrene (PS), polypropylene (PP), polycarbonate (PC), polymethylmethacrylate (PMMA), polyethylene (PE) and some thermosets. Figure 1.2 shows micrographs of microcellular plastics foamed by the batch process [3].

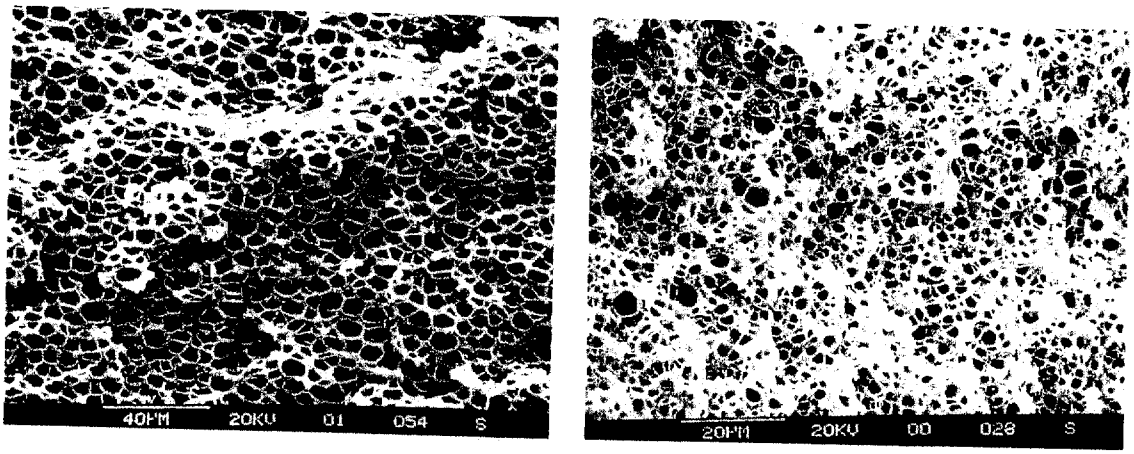

(a) (b)

pressure vessel, a plastic sheet or a batch of plastic sheets would be mounted. The polymer sheets could be heated and melted by electric heaters. Since only a batch of plastics could be foamed at a time, this process was known as the batch process of manufacturing microcellular plastics. The batch process consisted of supersaturating the heated polymer in a pressure chamber filled with gas, and later inducing a pressure drop in the chamber. The process of supersaturation was entirely diffusion driven and would take several hours, if not days, to complete. When a homogenous polymer-gas phase mixture was formed, nucleation was induced by a sudden thermodynamic instability (a significant pressure drop or rapid increase in temperature). This process was successful in producing lightweight parts with various thermoplastics such as polystyrene (PS), polypropylene (PP), polycarbonate (PC), polymethylmethacrylate (PMMA), polyethylene (PE) and some thermosets. Figure 1.2 shows micrographs of microcellular plastics foamed by the batch process [3].

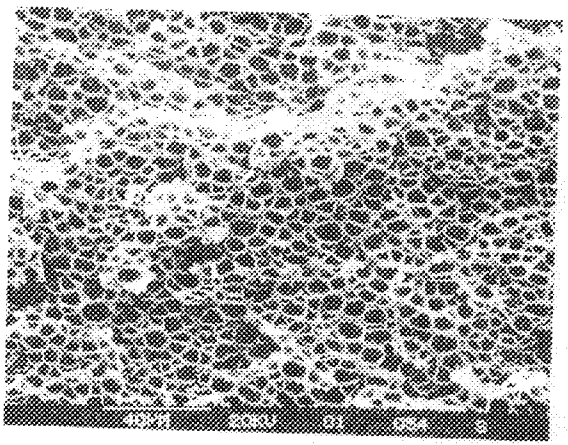

(a)

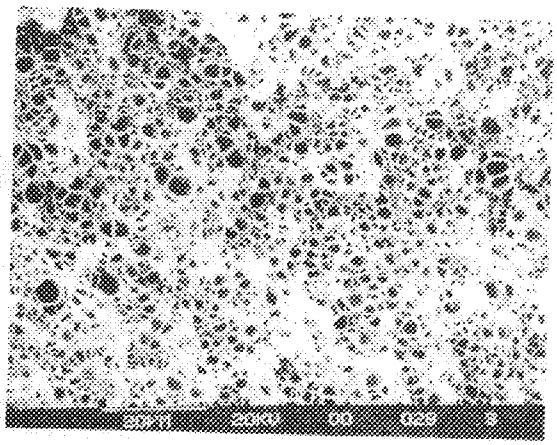

(b)

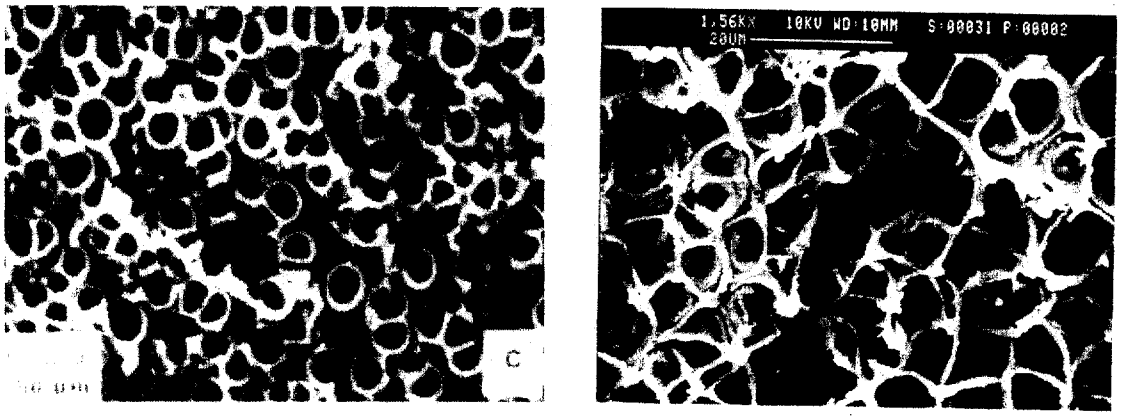

(c) (d)

Figure 1.2 (a) Microcellular PETG foamed at ambient temperature [4], (b) microcellular HDPE foamed at ambient temperature [4], (c) microcellular polystyrene nucleated at 10.3 MPa [5], and (d) microcellular perfluoroalkoxy produced at 228 °C [6].

While realizing part weight reduction by replacing plastics with gas, the microcells also serve as crack arrestors by blunting crack tips, thereby greatly enhancing part toughness [3]. For example, when properly prepared, microcellular PS has five times the impact strength of its unfoamed counterpart [7, 8]. The fatigue life of microcellular PC with relative foam density of 0.97 is four times that of its solid counterpart [9]. Furthermore, since the gas fills the interstitial sites between polymer molecules, it effectively reduces the viscosity [10 to 12] and the glass transition temperature of the polymer melt [3, 12 to 14]. This allows injection of such a material at a temperature below the normal processing temperature and at a lower and more uniform pressure [15]. Once the gas diffuses out of the MCP, the material recovers its glass transition temperature and vitrifies quickly (cf. Fig. 1.3).

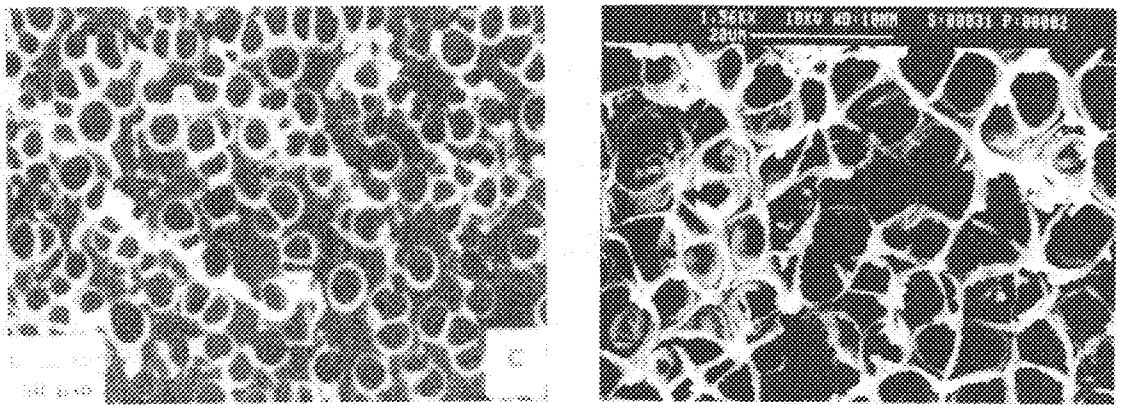

(c) (d)

Figure 1.2 (a) Microcellular PETG foamed at ambient temperature [4], (b) microcellular HDPE foamed at ambient temperature [4], (c) microcellular polystyrene nucleated at 10.3 MPa [5], and (d) microcellular perfluoroalkoxy produced at 228 °C [6].

While realizing part weight reduction by replacing plastics with gas, the microcells also serve as crack arrestors by blunting crack tips, thereby greatly enhancing part toughness [3]. For example, when properly prepared, microcellular PS has five times the impact strength of its unfoamed counterpart [7, 8]. The fatigue life of microcellular PC with relative foam density of 0.97 is four times that of its solid counterpart [9]. Furthermore, since the gas fills the interstitial sites between polymer molecules, it effectively reduces the viscosity [10 to 12] and the glass transition temperature of the polymer melt [3, 12 to 14]. This allows injection of such a material at a temperature below the normal processing temperature and at a lower and more uniform pressure [15]. Once the gas diffuses out of the MCP, the material recovers its glass transition temperature and vitrifies quickly (cf. Fig. 1.3).

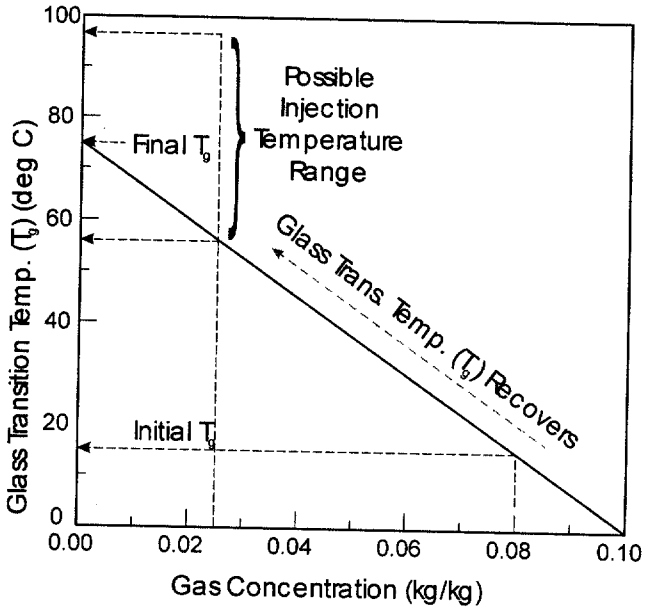

Figure 1.3 Glass transition temperature decreases with increasing gas content in the MCP for an amorphous PET. The solid curve is based on data reported in [3, 16].

Furthermore, since significantly less mass needs to be cooled and the endothermic reaction of cell nucleation and growth accelerates cooling, cooling time requirements are reduced. The significant benefits obtained with this process have made microcellular plastics a topic of significant research interest. From 1984 to 2005, much research has been conducted in this field with an aim to expand the knowledge base about microcellular plastics, process and applications. Substantial efforts have been made in the field of controlling cell nucleation and, thereby, the microstructure and mechanical properties of microcellular plastics through use of gases, materials, additives and by controlling process parameters during the manufacturing of MCP's.

1.2 Continuous Processing of Microcellular Plastics

1.2.1 MuCell® Process Overview

Although MCP's offered several advantages, one of the major shortcomings of the batch process is the slow production rate. The creation of saturated polymer-gas mixture within short cycle times and inducing nucleation by creating a sudden pressure drop posed some problems to manufacture MCP's in a continuous fashion. The work done by S. W. Cha [4], Vipin Kumar [5], Dan Baldwin [16] and Chul Park [17] led to the graduation of the batch process into semi-continuous and continuous applications such as injection molding, thermoforming and extrusion. Recently, these semi-continuous and continuous processes have been commercialized. Among them, microcellular injection molding is the most widely practiced commercial MuCell® process around the world, despite the fact that extrusion processing had at least a five year head start in development [18].

Injection molding with MCP's blends atmospheric gas (usually nitrogen or carbon dioxide) at a high-pressure, and sometimes high-temperature supercritical state, with polymer melt in the screw barrel to create a single-phase polymer-gas solution. To facilitate fast and homogeneous mixing of gas and polymer and maintain a single-phase solution prior to injection, the MuCell® Process Pressure (MPP) inside the screw barrel is typically kept between 70 and 250 bar. Such a pressure level is approximately one order of magnitude higher than the typical back pressure (generally between 3 to 30 bar) employed with the conventional injection molding process. During microcellular injection molding, the sudden pressure drop in the material as it flows through the nozzle

triggers the thermodynamic instability of the polymer-gas solution. The pressure drop rate required for homogeneous nucleation has been calculated to be 10^9 Pa/s [19]. As a result, the gas starts emerging from the polymer-gas solution forming numerous micro-scale cells. Figure 1.4 shows the schematic of injection molding with MCP's as well as the characteristic microstructures at the center and edge of the part cross section. In general, the size of the cells is inversely proportional to the cell density, both of which are determined by cell nucleation and growth, the amount of gas dissolved in the polymer, and other process conditions that affect the state and strength of the melt. As shown in Fig. 1.4, the typical cell diameter in microcellular injection molded parts is in the order of 5 to 100 microns (as opposed to 250 microns or more with the conventional structural foam molding process).

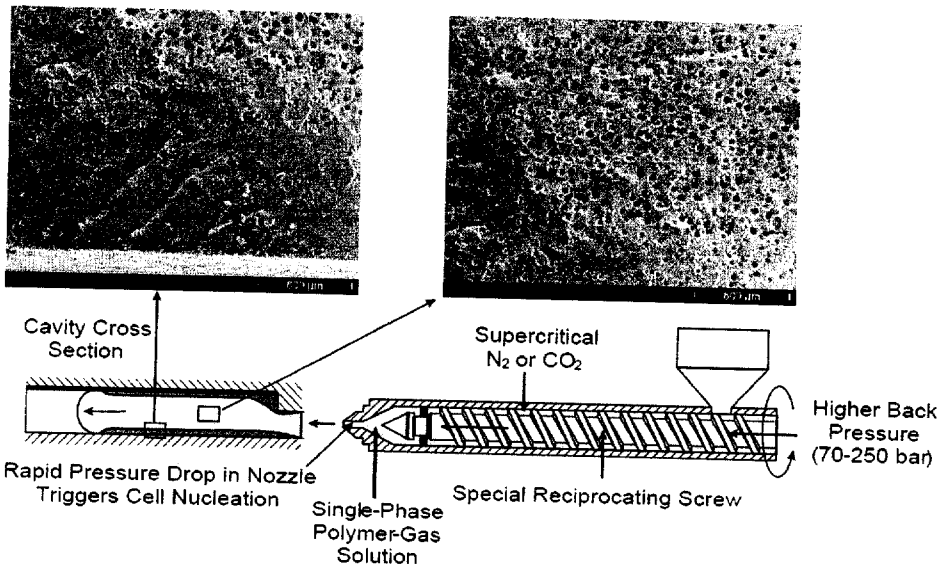

Figure 1.4 Schematic of injection molding of microcellular plastics with characteristic microstructures [20].

1.2.2 Optifoam Process

The advantages of the MuCell® process has motivated researchers to develop other methods of microcellular injection molding. Beginning with a new concept in 2000 at IKV in Aachen, Germany, the Optifoam system has been developed by Sulzer Chemtech in Switzerland [21]. The Optifoam system differs from Trexel's MuCell® system in that it injects the SCF at the nozzle during the injection phase of the injection molding cycle, while the MuCell® system injects the SCF into the barrel behind a special mixing section of the screw during the recovery phase. The Optifoam process uses a special nozzle, combined with a static mixer and porous sintered inserts (cf. Figure 1.5) to introduce gas into the polymer melt. By injecting the physical blowing agent into the melt through the inner and outer sintered inserts, the diffusion path is decreased, speeding up the

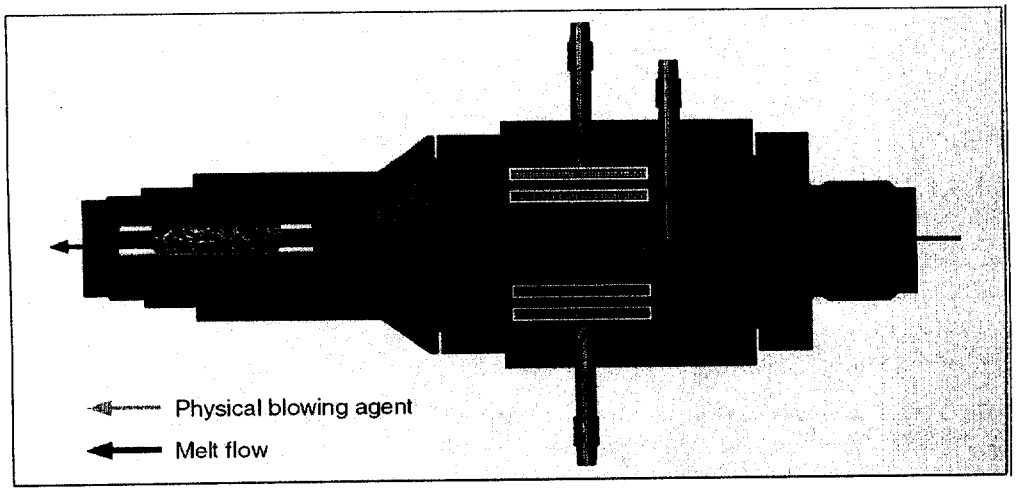

Figure 1.5 Schematic of an Optifoam nozzle showing the SCF entering the polymer melt and the static mixer in order to create a single-phase solution [21].

1.2.2 Optifoam Process

The advantages of the MuCell® process has motivated researchers to develop other methods of microcellular injection molding. Beginning with a new concept in 2000 at IKV in Aachen, Germany, the Optifoam system has been developed by Sulzer Chemtech in Switzerland [21]. The Optifoam system differs from Trexel's MuCell® system in that it injects the SCF at the nozzle during the injection phase of the injection molding cycle, while the MuCell® system injects the SCF into the barrel behind a special mixing section of the screw during the recovery phase. The Optifoam process uses a special nozzle, combined with a static mixer and porous sintered inserts (cf. Figure 1.5) to introduce gas into the polymer melt. By injecting the physical blowing agent into the melt through the inner and outer sintered inserts, the diffusion path is decreased, speeding up the

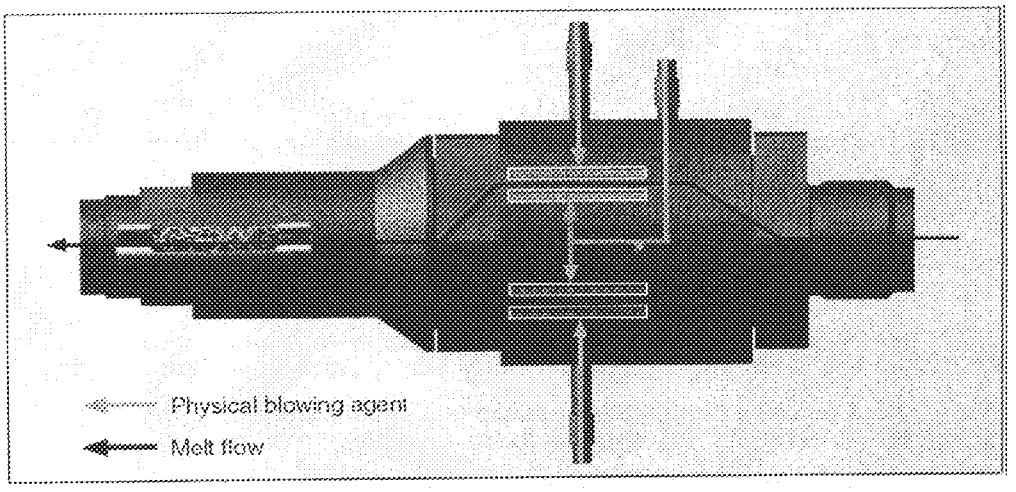

Figure 1.5 Schematic of an Optifoam nozzle showing the SCF entering the polymer melt and the static mixer in order to create a single-phase solution [21].

temperature and concentration distribution over the flow front's cross-section. According to Sulzer Chemtech, the melt flow changes directions frequently and undergoes efficient mixing as it flows past the obstacles, while the shear is considerably less than that encountered between the screw and the barrel. As with MuCell®, the Optifoam process is adaptable to any conventional injection molding machine through a commercial upgrade.

1.3 Process Description

Microcellular injection molding comprises of four steps, namely,

- Dissolution of gas in the polymer matrix.
- Nucleation of microcells.
- Growth and coalescence of microcells to form final foam structure.
- Shaping of the polymer into finished part.

These steps are described as follows.

1.3.1 Dissolution of gas in the polymer matrix

The dissolution of gas in the polymer matrix is achieved during the screw recovery phase of the injection molding cycle. Pure industrial grade nitrogen or carbon dioxide gas is pressurized with a positive displacement pump and is converted into a supercritical state. The temperature and pressure requirements of CO_2 and N_2 for becoming supercritical can be seen in Table 1.1. It is easier to measure the mass of the gas injected into the barrel when it is in a supercritical state compared to being in a gaseous state. A measured dose of supercritical fluid is then injected into the horizontal cylinder through an injector.

Table 1.1 Temperature and pressure requirements for supercritical state for carbon dioxide and nitrogen [18].

Property	Carbon Dioxide	Nitrogen
Critical Temperature (°C)	31	–147
Critical Pressure (bar)	73.7	34.0

As mentioned previously, the dosage of SCF into the barrel takes place during the screw recovery stage in the injection molding cycle. The melt is deliberately maintained at high pressure to ensure that the SCF remains in solution with the polymer. To verify that the gas injection is taking place, the gas delivery pressure is kept approximately 3 to 6 bar higher than the MPP. The amount of SCF being delivered into the barrel is thus controlled by the time the injector valve is open and the pressure difference between the gas inflow and the MPP. Vigorous mixing and diffusion accomplish the saturation of the polymer with the SCF. The diffusion coefficients in various polymers are in the order of 1×10^{-5} to 1×10^{-7} cm^2/sec for nitrogen and carbon dioxide respectively [3, 17]. As soon as the SCF is injected into the barrel, it is broken into several smaller pockets of bubbles by the swiping action of the screw during the recovery phase. This vigorous mixing in the barrel breaks the bubbles into smaller sizes by stretching them in the circumferential direction. Due to the slow diffusion rate of the SCF in the polymer, this vigorous mixing ensures that the size of the bubbles is small enough for the SCF to diffuse into the polymer in a small amount of time. Table 1.2 lists the estimated diffusion coefficients of nitrogen and carbon dioxide gas in commonly used polymers. Table 1.3 enumerates the estimated diffusion times determined by Park [17] at various striation thickness and diffusion coefficients.

Table 1.2 Estimated diffusion coefficients (D) of gases in common polymers at elevated temperatures [3].

Polymer	D of CO_2 (cm^2/s)		D of N_2 (cm^2/s)	
	at 188 °C	at 200 °C	at 188 °C	at 200 °C
PS	--	1.3×10^{-5}	--	1.5×10^{-5}
PP	4.2×10^{-5}	--	3.5×10^{-5}	--
PE	--	2.6×10^{-6}	--	8.8×10^{-7}
HDPE	5.7×10^{-5}	2.4×10^{-5}	6.0×10^{-5}	2.5×10^{-5}
LDPE	--	1.1×10^{-4}	--	1.5×10^{-4}
PTFE	--	7.0×10^{-6}	--	8.3×10^{-6}
PVC	--	3.8×10^{-5}	--	4.3×10^{-5}

Table 1.3 Estimated diffusion time by Park [17] at various striation thickness and diffusion coefficients.

Striation thickness (S)	Diffusion Coefficient (D)			
	10^{-5} cm^2/s	10^{-6} cm^2/s	10^{-7} cm^2/s	10^{-8} cm^2/s
1 μm	1×10^{-3} sec	0.01 sec	0.1 sec	1 sec
10 μm	0.1 sec	1 sec	10 sec	100 sec
50 μm	2.5 sec	25 sec	4 min	42 min
100 μm	10 sec	100 sec	17 min	3 hrs
250 μm	63 sec	10 min	2 hrs	17 hrs
500 μm	4 min	42 min	7 hrs	3 days
750 μm	9 min	94 min	16 hrs	7 days
1 mm	17 min	3 hrs	28 hrs	12 days

1.3.2 Nucleation of cells

During the injection phase, the shot is injected under pressure into the cavity. The suddenly induced thermodynamic instability (which can be obtained either by a rapid decrease in pressure or a rapid increase in temperature) decreases the gas solubility in the polymer so that the gas starts emerging from the solution via nucleation. Depending on the thermodynamic state, the gas nucleates at different points in the matrix. The number of sites at which the gas nucleates is governed by various factors [22, 23]:

- The amount of thermodynamic instability induced by the sudden pressure drop.
- The decrease in the interfacial tension between the polymer and the gas.
- Presence of high-energy sites like impurities, crystals, nucleating agents, etc. that facilitate the nucleation process. These opportunities will be further discussed later.

1.3.3 Growth and coalescence of microcells

The growth of the microcells and the final microstructure depend on [22, 23]:

- The number of nucleating sites and the time at which the microcells nucleate. The microcells that nucleate earlier have a tendency to grow larger. They have a lower energy level than the microcells nucleating at a later time. These smaller microcells coalesce into the larger cells to achieve a lower energy level, thus making the larger bubble grow even larger.

- The difference between the internal pressures of the gas and the surface tensions produced due to the interfacial forces produced between the polymer-gas interfaces and the strength of the solidifying polymer melt.

1.3.4 Shaping of the molded part, forming the final foam structure

Due to the absence of a high-pressure packing stage and the drastic reduction in viscosity due to the addition of the SCF, the parts produced are virtually stress and warpage free [18, 24]. The injection phase produces a short shot, and the growth of the cells fills the cavity and provides a homogeneous packing pressure throughout the part. Unlike conventional injection molding, where the packing pressure exists only until gate freeze-off, the packing pressure in microcellular injection molding is maintained until the polymer has solidified. A reduction in residual stress is realized due to the extended and homogeneous packing pressure and decreased viscosity. The result is parts with geometry that is near the actual mold design.

1.4 Process Advantages

Microcellular injection molding can reduce product costs significantly and impart better mechanical and physical qualities when compared to conventional injection molded parts.

1.4.1 Weight reduction

Recently, there has been an increasing need for lightweight, high performance parts in the industry. As compared to conventional injection molding, microcellular injection

molding can achieve weight reductions as high as 50%, though weight reductions of 5 to 10% are more typical [25]. Microcellular injection molding technology has been demonstrated to work with a myriad of commercial and engineering polymers [26]. On average, about 70% of the costs of plastic injection molded products are the raw material costs. Microcellular injection molding technology can bring about significant savings by producing lightweight parts with reduced material consumption.

1.4.2 Cycle time reductions

The savings due to reduction in total cycle time is realized by the reduction in cooling time and the elimination of the packing phase of the injection molding cycle. The endothermic process of cell nucleation and growth results in rapid cooling and solidification of polymer melt and thus reduces the total cooling time before the part is ejected from the mold [15]. Furthermore, because of the weight savings, there is a smaller mass of polymer to cool, which further reduces the cooling time. The foaming of the part provides the packing pressure to pack out the part during the cooling cycle, resulting in the reduction or elimination of the pack and hold stage. Cycle time savings as high as 50% have been reported for some applications [26].

1.4.3 Reduced energy requirements for injection and clamping

As the gas fills the interstitial sites between polymer molecules, it effectively reduces the viscosity of the polymer [10 to 12]. The reduced viscosity of the polymer melt allows the injection of the polymer inside the mold at significantly lower pressures. Because of the

lower injection pressures, the requirements on clamping are significantly reduced. Microcellular injection molding can lead to up to 48% reductions in injection pressures and 30% reduction in clamp pressures (and up to 80% in some situations) [25, 26].

1.4.4 Improvements in physical properties

As the gas forms a homogenous mixture with the polymer, it reduces the glass transition temperature of the polymer melt (3, 12 to 14). Therefore, processing temperatures of materials can be reduced significantly while maintaining viscosities typically seen in conventional injection molding. This opens a window to process temperature-sensitive additives in high-melting temperature, albeit high-performance engineering resins such as PC and polyamides (PA). Furthermore, the microcells also serve as crack arrestors by blunting crack tips, thereby greatly enhancing part toughness, fatigue life and impact strength (3).

1.4.5 Improvement in Dimensional Stability

Microcellular technology can be effectively used to increase the dimensional stability in injection molded components. Warpage, the bending or deformation of the part due to anisotropic shrinkage, presents a significant challenge in injection molding technology, wherein it impedes part assembly. The residual stresses formed as a result of the anisotropic shrinkage are caused by a myriad of factors such as unbalanced filling and cooling, poor part and mold designs, and anisotropy in molecular and fiber orientations. The residual stresses in microcellular injection molded parts are lower due to the use of lower injection pressures and the absence of a high-pressure packing stage. In addition,

sink marks are common surface defects formed on injection molded parts because of shrinkage of the plastic melt after cooling. Since the internal pressure arising from foaming eliminates the sink marks and improves the dimensional stability of the molded parts (cf. Fig. 1.6), little or no packing pressure is needed to pack out the mold [27]. This internal pressure of the nucleating gas provides a prolonged, low-pressure packing stage that is homogeneous throughout the part, making the shrinkage in the entire part more uniform and thus further reducing the warpage. Shrinkage and warpage (S&W) reductions using PP were reported to be around 90% when comparing microcellular injection molding and microcellular co-injection molding to conventional injection molding with a special box part molded with PP [24].

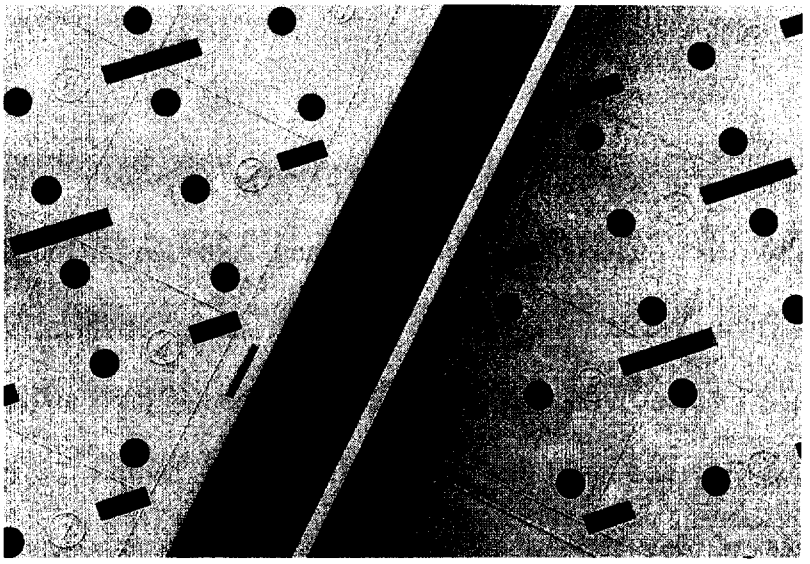

Figure 1.6 Elimination of sink marks with injection molding of microcellular plastics (left) in comparison to a solid plastic part (right). The microcellular part also exhibits greater dimensional stability. (Parts courtesy of Arburg, Inc.) [28].

sink marks are common surface defects formed on injection molded parts because of shrinkage of the plastic melt after cooling. Since the internal pressure arising from foaming eliminates the sink marks and improves the dimensional stability of the molded parts (cf. Fig. 1.6), little or no packing pressure is needed to pack out the mold [27]. This internal pressure of the nucleating gas provides a prolonged, low-pressure packing stage that is homogeneous throughout the part, making the shrinkage in the entire part more uniform and thus further reducing the warpage. Shrinkage and warpage (S&W) reductions using PP were reported to be around 90% when comparing microcellular injection molding and microcellular co-injection molding to conventional injection molding with a special box part molded with PP [24].

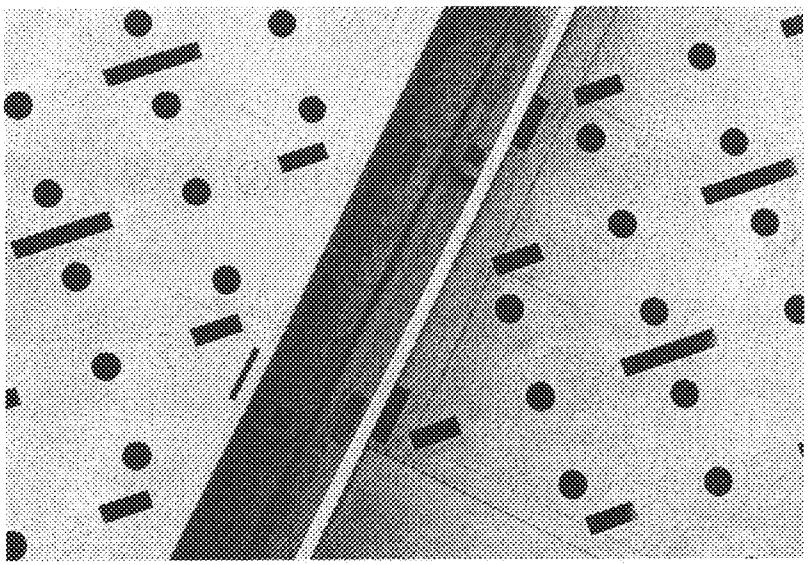

Figure 1.6 Elimination of sink marks with injection molding of microcellular plastics (left) in comparison to a solid plastic part (right). The microcellular part also exhibits greater dimensional stability. (Parts courtesy of Arburg, Inc.) [28].

1.5 Process Challenges

Despite the considerable advantages offered by this process, microcellular injection molding is by no means a panacea for all molding problems or superior to its conventional counterpart in all aspects. Unlike the simple batch process [3] or the continuous microcellular extrusion process [29], injection molding is inherently complex and dynamic. Two of the major problems with microcellular injection molding are (1) the control of the state of thermodynamic instability (via temperature and pressure variation) to create fine and uniform microcells throughout the part and (2) the maintenance of critical mechanical properties while realizing material savings. For example, experimental studies indicate that the microcellular injection molded parts tend to exhibit non-uniform distribution of cell size and cell density with certain materials, inadequate process setup, or high levels of SCF or weight reduction (see, e.g., Fig. 1.7).

Continuous and efficient generation of the single-phase polymer-gas solution with proper SCF content also poses a challenge during processing. Although microcellular injection molding offers a plausible means to improve the impact strength and bending stiffness-to-weight ratio, the inherent reduction in mechanical properties such as tensile strength, tensile modulus [30] and weld-line strength [20] could hamper broader industrial implementations of this process in areas of structural components and critical applications. At present, the process requires changes in the machinery components and licenses. The changes in machinery can be made with the MuCell® Modular Upgrade, or

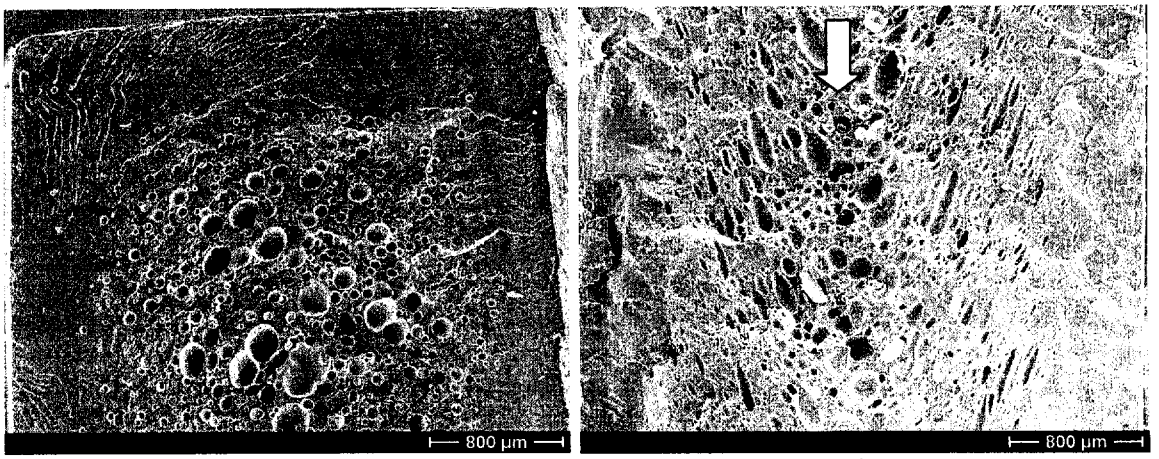

(a) (b)

Figure 1.7 SEM micrographs of a microcellular injection molded neat polyamide (PA)-6 part showing non-uniform cell sizes and cell densities. (a) Cross section normal to the melt flow direction near the edge of the part. Weight reduction 7.8%. (b) Cross section parallel to the melt flow direction showing deformation of microcells by shear. Weight reduction 20% [31].

ordered initially through most injection molding machine manufacturers. Due to the presence of microcells, it may have limited applications with parts that require clarity. Furthermore, as with other emerging processes, the processing know-how for microcellular injection molding has yet to be developed to enable the molding industry to fully materialize the process benefits.

Lastly, the frequently occurring swirling pattern on part surfaces could potentially affect the cosmetic appearance. Various post-molding operations such as spray painting or coating have been employed to improve the surface finish. A major drawback of these post-molding operations is that the gas diffuses out of the molded component even after it

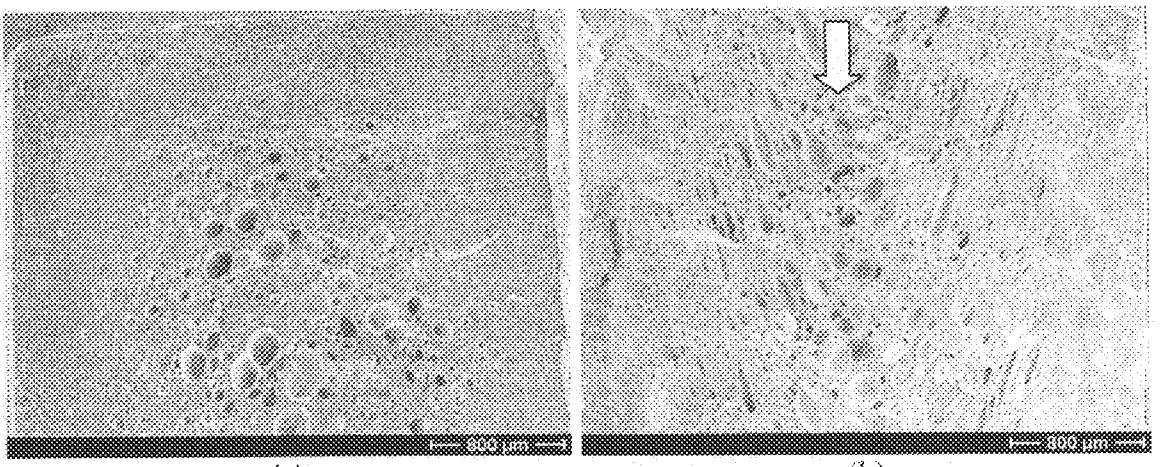

(a) (b)

Figure 1.7 SEM micrographs of a microcellular injection molded neat polyamide (PA)-6 part showing non-uniform cell sizes and cell densities. (a) Cross section normal to the melt flow direction near the edge of the part. Weight reduction 7.8%. (b) Cross section parallel to the melt flow direction showing deformation of microcells by shear. Weight reduction 20% [31].

ordered initially through most injection molding machine manufacturers. Due to the presence of microcells, it may have limited applications with parts that require clarity. Furthermore, as with other emerging processes, the processing know-how for microcellular injection molding has yet to be developed to enable the molding industry to fully materialize the process benefits.

Lastly, the frequently occurring swirling pattern on part surfaces could potentially affect the cosmetic appearance. Various post-molding operations such as spray painting or coating have been employed to improve the surface finish. A major drawback of these post-molding operations is that the gas diffuses out of the molded component even after it

is cooled and hence peels off the paint, further damaging the surface quality. Waiting for the gas to diffuse out before performing post-molding operations would adversely increase the flow-time of the components through the factory and the inventory in the production system. Recent innovations, however, have taken aim at producing high quality surface finishes while realizing the benefits of microcellular injection molding.

1.6 Overcoming Process Challenges

Three new technologies have been developed in an attempt to overcome the swirling pattern frequently observed with the microcellular injection molding process.

1.6.1 MuCell® Gloss®

Trexel, in a joint development with the Japanese molding company Ono Sangyo, has developed a process called MuCell® Gloss® for producing high quality surface finish parts with microcellular injection molding. This process combines Trexel's MuCell® technology with Ono Sangyo's rapid heat cycle molding (RHCM) process. This new technology heats the mold to near the melting temperature of the polymer prior to injection and then rapidly cools the polymer. This technology eliminates weld and knit lines while maintaining similar weight reductions and other advantages of the MuCell® process [32]. However, this technology results in a slight increase in cycle time (vs. microcellular injection molding without MuCell® Gloss®), and higher energy costs. An example of a part molded with MuCell® and MuCell® Gloss® can be seen in Figure 1.8.

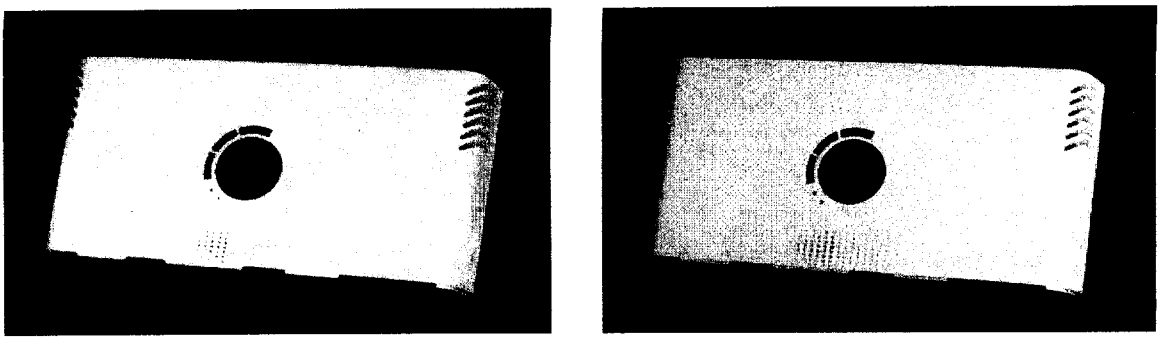

Figure 1.8 MuCell® on the left and MuCell® Gloss® on the right. The MuCell® Gloss® part has a uniform, high quality surface finish [26].

1.6.2 Gas Counterpressure (GCP)

Gas counterpressure (GCP) has been used to produce microcellular injection molded parts with a glossy finish and improved mechanical properties [33, 34]. Gas counterpressure is not a new process, but has just recently been employed in conjunction with microcellular injection molding to create high surface quality parts. The GCP process uses nitrogen gas to build up a pressure pad in the mold [cf. Figure 1.9].

The pressure pad is made possible by using an o-ring to seal the mold at the parting line. The pad maintains the single-phase solution during the injection phase and prevents the creation of the surface swirls caused by the dissolved SCF between the melt and the mold, which occurs when not using the GCP process. The pressure pad maintains control via pressure as it is pushed back by the melt. According to [33], PC test bars molded with the GCP process maintained almost 90% of the elongation at break when compared to solid polycarbonate test bars at a 5.5% weight reduction. At the same weight reduction,

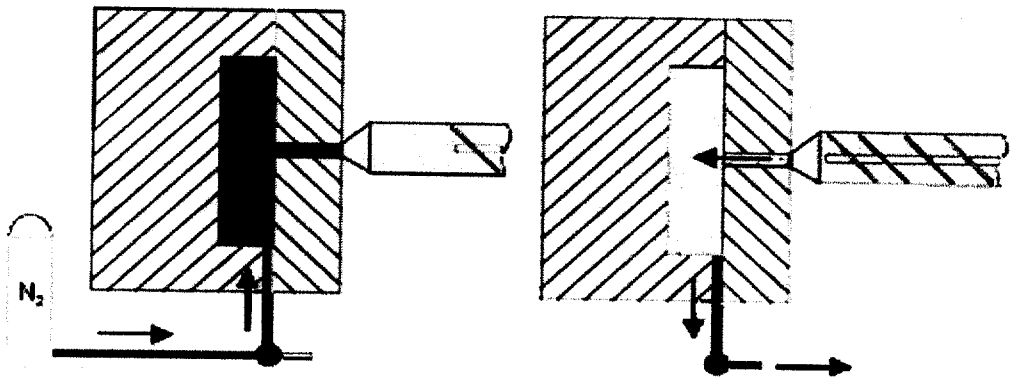

Figure 1.9 On the left, nitrogen gas is pumped into the cavity to create high pressure in the mold. The subsequent injection of polymer forces the nitrogen gas out through a valve while maintaining a single-phase solution [33].

foamed PC parts molded without the GCP process maintained less than 10% of the elongation at break. Different mechanical properties can be obtained by altering the thickness of the solid skin layer, which can be changed through control of the process conditions. Drawbacks of this technology include the added cost of a counterpressure system and the increased mold cost in order to create a sealed cavity. Additionally, current research gives no indication that high surface quality can be maintained at the gate area. An example of a PC tensile bar molded with the GCP process can be seen in Figure 1.10.

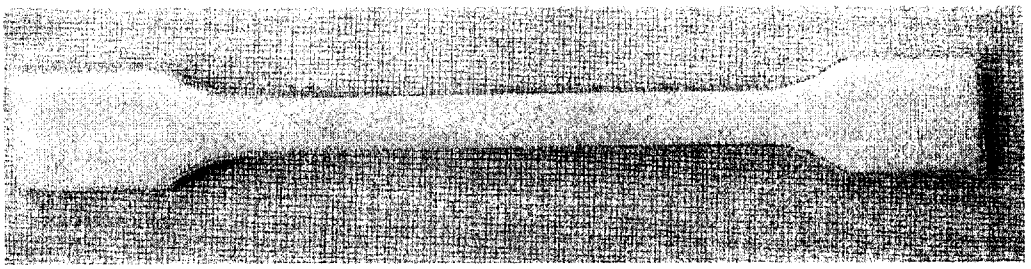

Figure 1.10 GCP molded part made of polycarbonate (PC). The part shows a clear, uniform skin layer everywhere except the gate location, which is located on the left end of the tensile bar.

1.6.3 Microcellular Co-Injection Molding

Microcellular co-injection molding, used for producing parts with a foamed structure and a high quality surface finish, has been developed at the University of Wisconsin - Madison by Turng et al [35]. Co-injection molding (also called sandwich molding) is a process where a laminated skin-core-skin structure, typically of two dissimilar albeit compatible materials, is produced within an injection molding cycle [cf. Figure 1.11]. The same material may be used for both the skin and the core, with the core ideally being recycled sprues, runners, and rejected parts. If dissimilar materials are used, the material with the higher shrinkage should be used as the skin material to avoid separation of the skin and the core during cooling. Generally, the co-injection process is used in industry to acquire unique mechanical or physical properties by employing different materials within a single molded component, or to save material costs by "hiding" inexpensive recycled or commodity materials in the core of the co-injection molded part. Co-injection was first reported in 1970 in an attempt to overcome the shortcomings of the structural foam

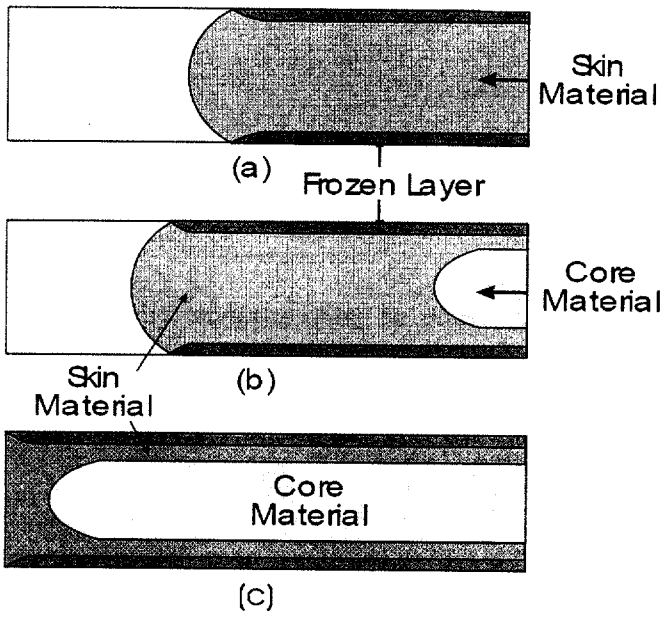

Figure 1.11 Drawing displaying a) the molten skin and the frozen layer during injection of the skin material, b) the injection of the core material, pushing the skin material towards the end of the cavity, and c) the end of injection, with the core material fully encapsulated by the skin.

molding process by combining the improved appearance with the benefits of structural foam molding [36]. In traditional co-injection molding, two sequential injections of skin and core material occur, respectively, from two different injection units into the same cavity through the sprue. This is accomplished with a manifold and switchover valve and is known as A-B co-injection molding. Co-injection molding may also consist of a third stage, in which a small amount of skin material is injected in order to purge the material in the hot manifold and seal the gate to encapsulate the core material for cosmetic and functional reasons. This sequence is known as A-B-A, and an A-AB-B-A co-injection

molding sequence can also used, where the skin and core are injected simultaneously. By injecting simultaneously, hesitation marks, caused by a halting of the melt front, are eliminated. The resulting co-injection molded parts have a core material embedded in a skin material. The thickness and uniformity of the skin layer are governed by the material combinations and processing parameters, such as viscosity and shot volume ratios of the materials, melt temperatures, mold wall temperature, and injection speeds [15, 37]. Figure 1.12 shows the stages for an A-B-A sequence using traditional co-injection molding. Despite these many benefits of co-injection molding, disadvantages do exist. The machine modifications usually increase the cost of a standard injection molding machine 50 to 100% [38].

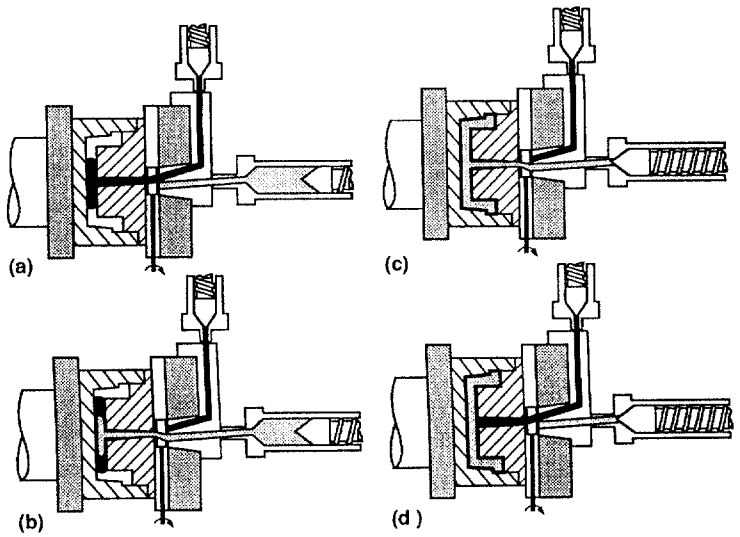

Figure 1.12 Stages of a sequential co-injection molding process. (a) Injection of skin material, (b) injection of core material, (c) near end of fill, and (d) final injection of skin material to purge the core material from the sprue [39].

Other methods exist for producing co-injection molded parts, such as Twinshot Co-Injection by Spirex [cf. Figure 1.13].

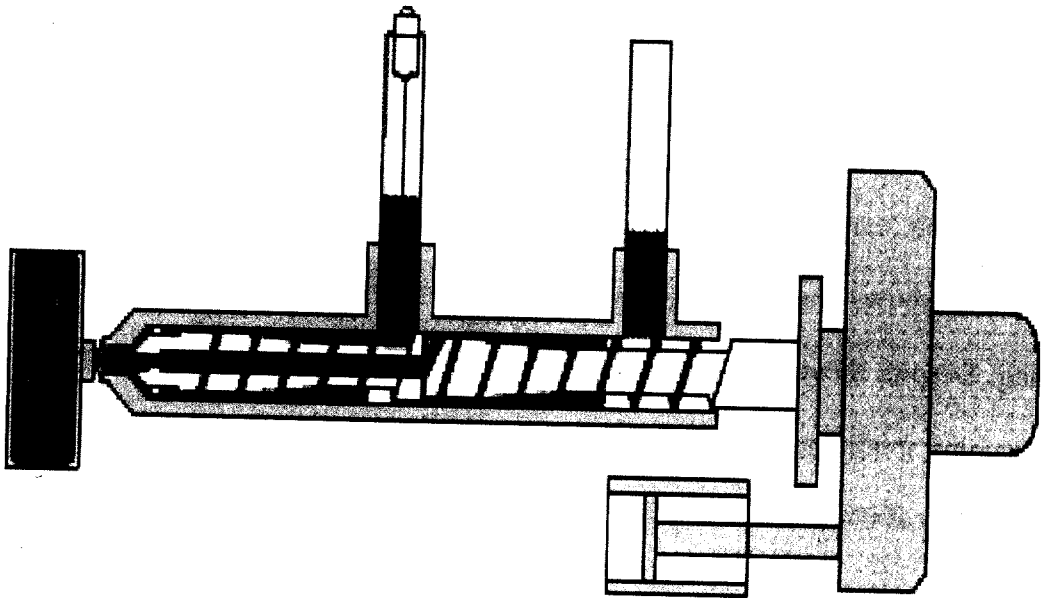

Figure 1.13 Schematic of Twinshot co-injection molding machine, showing the skin material in green in the back of the barrel and the core material in red in the front of the barrel [40].

This technology provides a lower cost option for co-injection molding, and can be adapted to existing injection molding machines. Twinshot utilizes a single screw and barrel arrangement that produces two independent melt streams within a single barrel. Metering of the two materials can occur simultaneously for using A-AB-B-A co-injection. Twinshot utilizes fewer machine components than traditional co-injection molding machines, and the lack of the need for a manifold eliminates the losses in melt pressure and velocity control associated with the compressible resin residing in a

manifold [40]. Other variations for co-injection molding exist, but will not be dwelled on here due to the traditional co-injection molding equipment used for this thesis. For more information regarding variations within the co-injection molding process, refer to [15, 37, 40, 41]. For this thesis, traditional co-injection molding was coupled with Trexel's MuCell® process to investigate processing parameters for reducing the S&W of a PP box part. This setup can be seen in Figure 1.14.

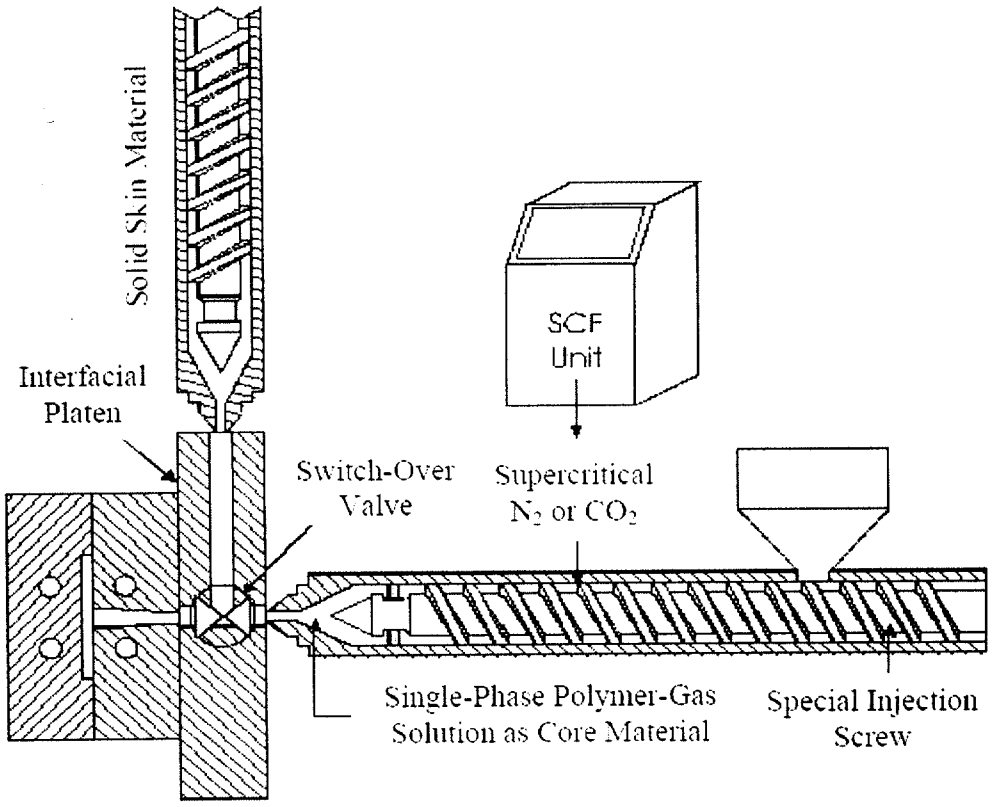

Figure 1.14 Schematic of a microcellular co-injection machine. The skin material is injected from the vertical barrel, and the microcellular core is injected from the horizontal barrel.

Due to the existing SCF unit on the horizontal barrel, the vertical unit was used for the solid skin layer and the horizontal injection unit was used for the foamed core. The microcellular core encapsulated by the solid skin layer provides many benefits of microcellular injection molding, such as reduced weight and an increase in dimensional stability, which will be highlighted in this thesis, while still maintaining a high surface quality.

In this research, we have focused on using design of experiments (DOE) to quantitatively compare the shrinkage and warpage (S&W) of a box-shaped part using conventional and microcellular injection molding and microcellular co-injection molding. These rigorous studies used polypropylene as the material for the three experiments due to its semi-crystalline structure and the difficulties previously experienced with foaming the material. The microstructure was also analyzed to observe the cell size and density, as these have been shown to be critical for maintaining the mechanical properties of microcellular injection molded parts.

Chapter 2

Motivation, Experimentation, and Analysis Methods

2.1 Motivation for Study

While it is widely agreed that microcellular injection molding and microcellular co-injection molding improve many aspects of part quality, no previous quantitative studies have reported on what process parameters affect the S&W and at what magnitude. The purpose of this study is to use design of experiments (DOE) to identify the significant

main and two-factor interaction effects for reducing the amount of S&W and quantitatively compare the S&W for three different processes:

1) Conventional Injection Molding
2) Microcellular Injection Molding
3) Microcellular Co-Injection Molding

Identification of these significant main and two-factor interaction effects will contribute to the process know-how for microcellular injection molding and microcellular co-injection molding. Furthermore, reduction of the S&W in a part that violates many conventional injection molding design rules may indicate the ability to overcome outside disturbances and the existing design rules.

2.1.1 Background of S&W

While the factors affecting dimensional stability in conventional injection molding have been widely studied and a wealth of information is available [42, 43], this study used DOE to verify these findings and to determine optimal process conditions for reducing the S&W of a special box part. The S&W at the optimal process conditions for conventional injection molding was then used as a baseline for comparing the S&W to microcellular injection molding and microcellular co-injection molding. In addition, the conventional injection molding experiment served as a testing ground for planning, executing, and analyzing a DOE. As expected for the conventional injection molding

process, the two most significant effects affecting the S&W were the pack/hold time and the pack/hold pressure, referenced throughout this thesis as simply the hold time and the hold pressure. These results agree with previous information in [44], validating the DOE procedure in place. In addition to quantitatively comparing the S&W, the information gathered from the microcellular injection molding and microcellular co-injection molding experiments was used to verify existing theory for reducing S&W, as well as provide further insight into the S&W behavior.

Several reasons exist as to why microcellular injection molding can be used to increase dimensional stability and reduce S&W. First, the introduction of the supercritical fluid (SCF) into the polymer reduces the viscosity of the material, therefore requiring less injection pressure. These lower pressures translate into a reduction in residual stresses in the part, reducing anisotropic shrinkage and increasing the dimensional stability. Along with this decrease in residual stresses, the homogeneous internal pressure arising from cell nucleation and growth continues to pack the part against the mold walls until the polymer has solidified. This differs from conventional injection molding, where the high-pressure packing stage creates a large pressure gradient from the gate to the end of fill, and does not allow the polymer to relax, resulting in residual stresses frozen in the part. In addition, the packing of the cavity only exists until the gate freezes off.

2.1.2 Material Selection

To study the worst-case scenario and to be fair to both processes, a PP resin, ExxonMobil PP7032E2, injection molding grade with a melt flow index of 3.6 g/10 min, was selected for this study. It was anticipated that the S&W of the semi-crystalline PP resin would be more significant than that of amorphous materials for conventional injection molded parts. On the other hand, due to its semi-crystalline structure and the fact that PP has a weak melt strength, it has been known to be difficult to foam when compared to other plastics [45, 46]. Studies have shown nucleating agents can result in an increase in cell density and decrease in cell size [28, 30, 47, 48]. The PP was hand-blended with talc to obtain a mixture of 1 wt% talc for the microcellular injection molding and microcellular co-injection molding experiments. The talc, with a nominal diameter of 5 microns and a density of 2.8 g/cm^3, acted as a nucleating agent [49] and resulted in a smaller cell size as well as a greater cell density [50, 51]. Lastly, 2 wt% blue colorant was added to the skin material for the microcellular co-injection molding experiments to help distinguish between the core and skin material.

2.1.3 Part Geometry Selection

A difficult-to-mold box part manufactured to produce high amounts of warpage was used for this study. The overall outside dimensions of the molded part were 7.4 x 9.8 x 4.5 cm. The walls perpendicular to the x-direction were 1.25 mm thick and the walls perpendicular to the y-direction had four stepwise changes in thickness of 3.5 mm, 3 mm, 2.5 mm, and 2 mm. As seen in Figures 2.1 and 2.2, the mold violates many of the known

design rules for injection molding, including sharp corners, a tendency for the material to race-track with the variable wall thickness, and abrupt changes in thickness. Choosing mold geometry such as this provided for a measurable difference in the shrinkage and warpage between injection molding processes.

Figure 2.1 Solid models showing the box part used for the experiments. The photos display the stepwise changes in thickness, the sprue gate, and the sharp corners of the part.

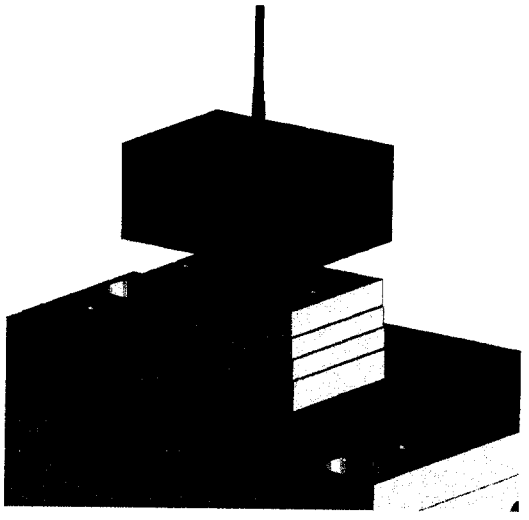

Figure 2.2 Solid model of the box part and the core side of the mold, clearly showing the step-wise changes molded into the part.

design rules for injection molding, including sharp corners, a tendency for the material to race-track with the variable wall thickness, and abrupt changes in thickness. Choosing mold geometry such as this provided for a measurable difference in the shrinkage and warpage between injection molding processes.

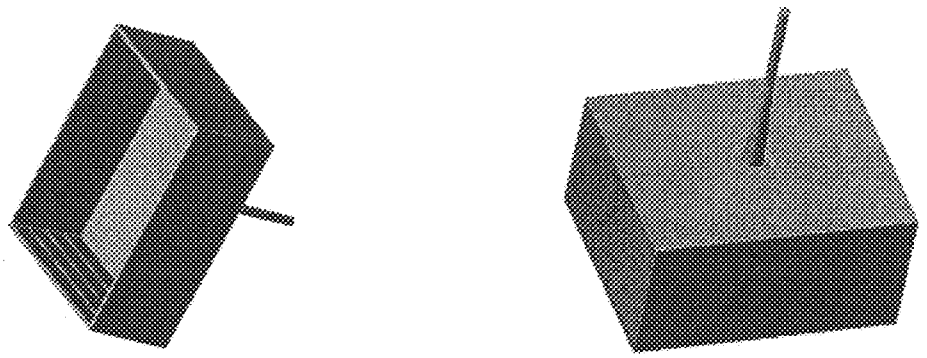

Figure 2.1 Solid models showing the box part used for the experiments. The photos display the stepwise changes in thickness, the sprue gate, and the sharp corners of the part.

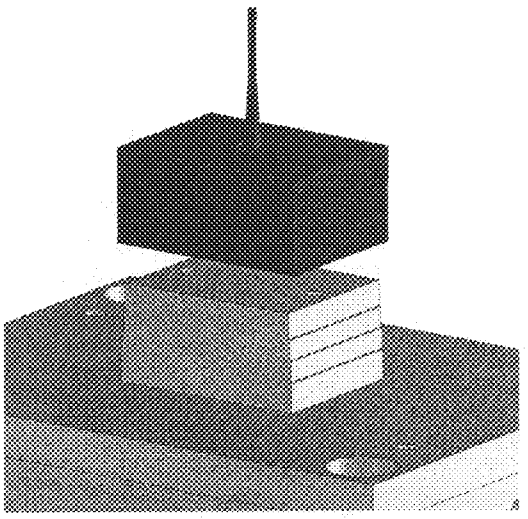

Figure 2.2 Solid model of the box part and the core side of the mold, clearly showing the step-wise changes molded into the part.

2.2 Factorial Design of Experiments (DOE)

2.2.1 DOE Background

Scientists and engineers around the world perform engineering experiments daily. One of the common approaches employed by scientists and engineers today is the One-Variable-At-a-Time (OVAT) method, where one variable is varied at a time, keeping all other variables in the experiment fixed. However, this type of experimentation requires large resources to obtain a limited amount of information about the process. It is often unreliable, inefficient, time consuming, and may yield false optimum conditions for the process [52]. Many experiments involve a study of the effects of two or more factors. It can be shown that, in general, factorial designs are most efficient for this type of experiment [53]. In a designed factorial experiment, an engineer makes deliberate changes in the input variables (referred to as factors or independent variables in this study) and then determines the change in the output (referred to as the response in this study). Not all factors will affect the response in the same manner. Some may have strong influences, some may have no influence at all, and interaction effects between two factors may also exist. Therefore, a factorial design, also known as a design of experiments (DOE), can be used to identify significant main and two-factor interaction effects, as well as the magnitude of these effects.

Most DOE are 2^k or 3^k factorial designs, where k represents the number of independent variables, and the base number (2 or 3) represents the number of levels of the independent variables. In this thesis, two levels were used for each factor, and therefore,

the three level DOE will not be discussed. If the effect of the independent variables is known to be nonlinear, then a 3^k factorial design should be used, while 2^k factorial designs are based on the principle of linearity. Information regarding 3^k factorial designs can be found in [53]. A simple DOE with four trials would be a 2^2 factorial design, and an example is shown in Table 2.1.

Table 2.1 This example of a 2^2 factorial DOE is shown in standard order, with the "–" and "+" signs indicating the low and high level of the factor, respectively. The AB interaction is simply the product of the levels of factors A and B.

Trial #	A	B	AB	Response
1	–	–	+	20
2	+	–	–	50
3	–	+	–	40
4	+	+	+	12

From this result, statistical methods can be used to determine the significant main and two-factor interaction effects, as well as their magnitudes. Determining how the factors affect the response with a 2^2 factorial DOE becomes increasingly complicated for experiments approaching five or six factors, such as 2^5 or 2^6 factorial designs. Additionally, regression models can be derived from the data in order to determine the optimal parameters for achieving a set response.

2.2.2 Fractional Factorial DOE

As the number of factors in a 2^k factorial design increases, the number of runs required for a complete DOE can become enormous. For example, a complete replicate of a 2^6

design requires 64 runs. In this design, only 6 of the 63 degrees of freedom correspond to main effects, and only 15 degrees of freedom correspond to two-factor interactions. The remaining 42 degrees of freedom are associated with three-factor and higher interactions, which can generally be assumed to be negligible [53]. Therefore, the information on the main effects and two-factor interactions may be obtained by running a fraction of the complete factorial experiment. For this thesis, six factors were used for each of the three injection molding experiments. However, due to the time required to achieve steady state between each run, in addition to the time required to perform each run of the experiment, 64 trials could not be completed in one day. Therefore, a resolution VI (six), 2^{6-1} fractional factorial DOE consisting of 32 trials was implemented for this study. Resolution VI means that all main effects and two-factor interactions are clear of each other, and are confounded only with four-order and higher interactions. All three-factor interactions are confounded with other three-factor interactions. Confounded means it is impossible to determine which factor or interaction is responsible for the effect. However, as noted earlier, three-order interactions and higher can generally be considered negligible. Therefore, confounding main effects and two-order interactions with higher-order interactions will still result in meaningful information. Further analysis performed in this study presents evidence that in each of the three experiments, the three-order interactions and higher were indeed negligible. The alias structure, which displays the way the effects are confounded, is shown in Table 2.2.

Table 2.2 Alias structure indicating how factors and interactions are confounded. Using the 2^{6-1} fractional factorial DOE, the experimenter can be certain that any significant main effects or two-factor interactions are not the result of the interaction they are confounded with.

Factor/Interaction	**Confounded with**
A	B*C*D*E*F
B	A*C*D*E*F
C	A*B*D*E*F
D	A*B*C*E*F
E	A*B*C*D*F
F	A*B*C*D*E
A*B	C*D*E*F
A*C	B*D*E*F
A*D	B*C*E*F
A*E	B*C*D*F
A*F	B*C*D*E
B*C	A*D*E*F
B*D	A*C*E*F
B*E	A*C*D*F
B*F	A*C*D*E
C*D	A*B*E*F
C*E	A*B*D*F
C*F	A*B*D*E
D*E	A*B*C*F
D*F	A*B*C*E
E*F	A*B*C*D
A*B*C	D*E*F
A*B*D	C*E*F
A*B*E	C*D*F
A*B*F	C*D*E
A*C*D	B*E*F
A*C*E	B*D*F
A*C*F	B*D*E
A*D*E	B*C*F
A*D*F	B*C*E
A*E*F	B*C*D

2.3 Basic Experimental Procedure

2.3.1 Determination of Process Parameters

Upper and lower settings of the six most influential process parameters were determined experimentally to create as large of a process window as possible without creating defective parts, such as a short-shot or post-blow (a surface blister defect in microcellular injection molding). The defects varied for each of the injection molding processes, as post-blow is not possible with conventional injection molding, and breakthrough (when core material breaks through the skin layer during co-injection molding) does not occur in conventional injection molding or microcellular injection molding. Further detail into the determination of the process parameters is given in Chapters 3 through 5.

2.3.2 Steady State Conditions

In addition to experimentally determining the proper process parameters, a steady state condition needed to be determined before collecting parts for each molding trial. This is critical to ensure the accuracy of the experiment. While it is obvious when the barrel temperature achieves a steady state condition, this does not mean the melt temperature of the polymer has achieved steady state. The melt temperature is a process parameter that is very important, but is difficult to measure. By monitoring the mold-wall temperature, one can determine when the melt temperature has achieved steady state. Additionally, while the cooling time and chiller temperature can be adjusted quickly, their effects on the mold temperature are not instantaneous. Therefore, the mold-wall temperature was monitored to determine when the process had achieved a steady state with respect to temperature.

Graphs indicating the steady state mold temperature were generated and used during the experiments to verify steady state conditions had been met. Figure 2.3 shows the cyclic change in temperature (due to the injection and subsequent cooling of the polymer), as well as the overall mold temperature decrease, when the chiller temperature setting is changed from 40°C to 20°C, with all other parameters remaining constant.

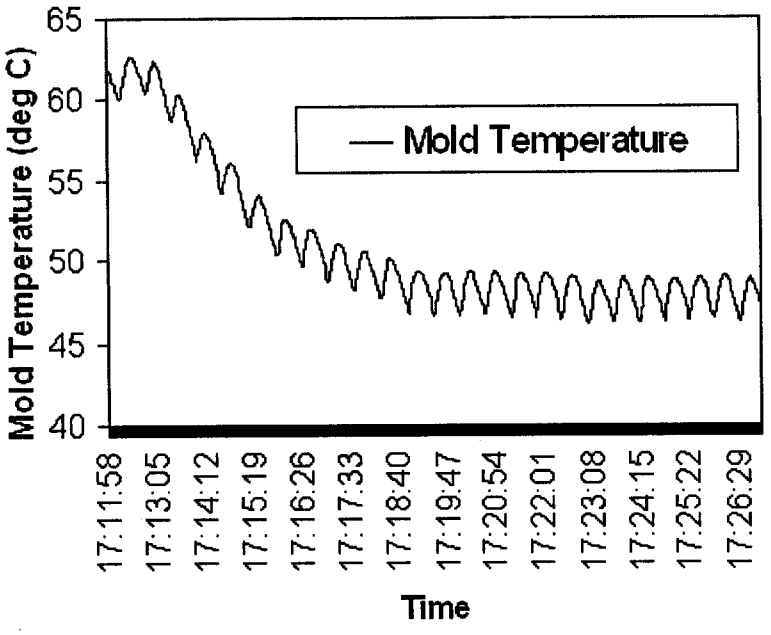

Figure 2.3 Graph of mold temperature as a function of time. The cyclic nature of the graph is due to the injection and ensuing cooling of the polymer. Note the mold temperature decreases from a steady state condition at the first set of parameters and then achieves steady state at the second set of parameters [24].

In addition to verifying that the process temperatures had achieved steady state, microcellular injection molding and microcellular co-injection molding represented new challenges for determining the steady state. As described earlier, the introduction of the SCF into the polymer reduces the viscosity of the melt. As the shot volume (core shot volume, in the case of microcellular co-injection molding) of the polymer and the amount of the SCF injected into the polymer are adjusted throughout the experiments, this viscosity changes. Therefore, the switchover pressure was monitored as an indication of the viscosity of the single-phase polymer-gas solution. The switchover pressure is the injection pressure when the injection phase switches from velocity control to pressure control, also known as the VPT (velocity to pressure transfer) point. For microcellular injection molding and microcellular co-injection molding, there is no pack/hold stage, so the VPT point is the pressure at the end of injection, just prior to screw recovery. Due to the introduction of the SCF, drastic reductions in the switchover pressure were observed due to process changes [cf. Figure 2.4].

Using the mold temperature and the switchover pressure, steady state conditions corresponding to all of the molding trials were determined during the preliminary experiments. During the running of the three DOE's, the process conditions observed between molding trials were checked against the predetermined steady state conditions. Once the current and predetermined steady state conditions matched, ten parts were collected for that molding trial. This method for determining the steady state between molding trials was used (in place of arbitrarily selecting a set number of parts to discard

between each mold trial) in order to improve the accuracy of the experiments. It was observed that the actual mold temperature obtained during the DOE's were within +/– 1°C of the steady state mold temperatures determined during the preliminary experiments.

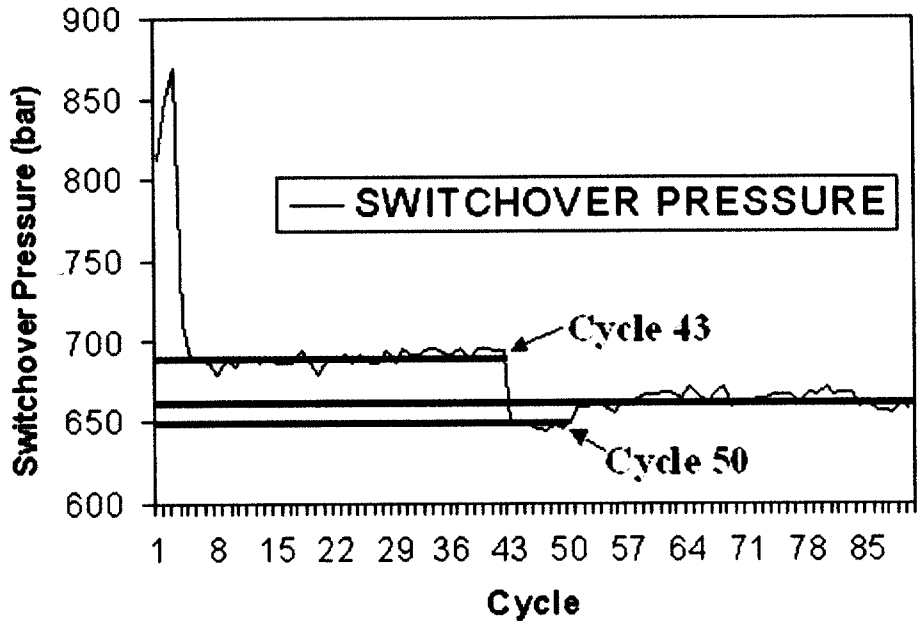

Figure 2.4 Graph of the switchover pressure, which can be used to indirectly measure the viscosity of the material. Process changes were made at cycles 43 and 50, resulting in switchover pressure changes of approximately 30 and 20 bar, respectively [24].

2.3.3 Additional Data

In addition to monitoring the mold temperature and the switchover pressure, other variables such as injection time, screw recovery time, and cycle time were collected.

During analysis of the data, any abnormalities could be investigated further to see if there was any correlation between the abnormality and the process conditions. An example of the data collected can be seen in Figure 2.5.

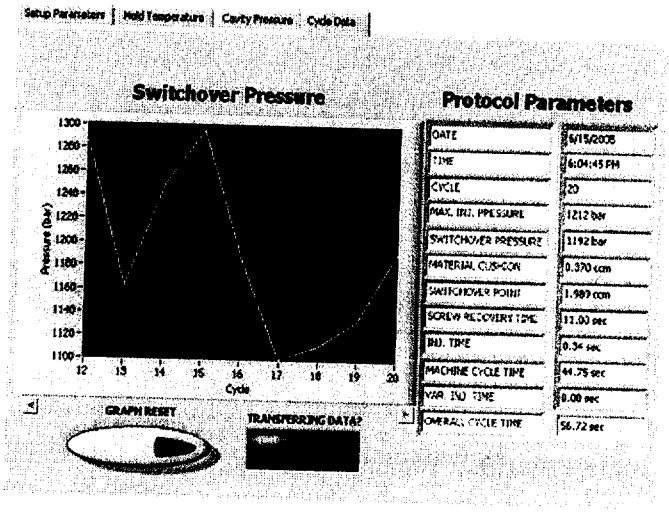

Figure 2.5 Screenshot displaying the switchover pressure, as well as the other variables collected during the experiments. This data could then be referenced to determine if correlations existed between responses and process conditions.

2.3.4 Part Collection

For each of the three experiments, a total of ten parts were collected for each of the 32 molding trials. These ten parts were collected when the steady state conditions (described in Section 2.3.2) were met. Each set of ten parts was individually labeled and stored separately for several weeks at room temperature. Because of the complexity of the measurement method (described in Section 2.4), coupled with fatigue, parts five through nine were measured for S&W and the average of these five values was used for each trial.

During analysis of the data, any abnormalities could be investigated further to see if there was any correlation between the abnormality and the process conditions. An example of the data collected can be seen in Figure 2.5.

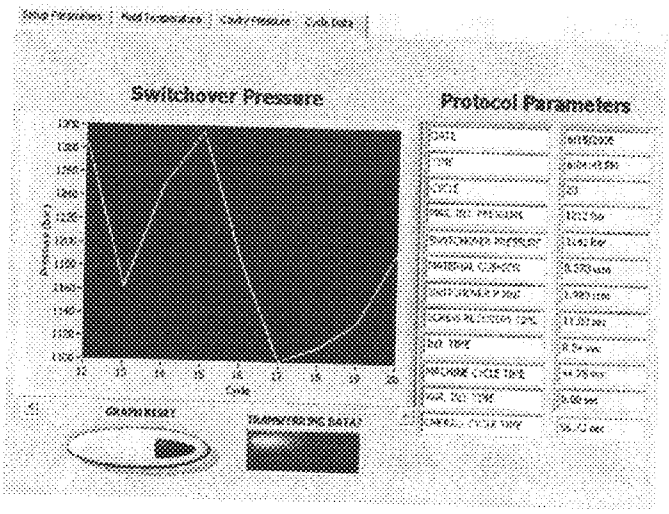

Figure 2.5 Screenshot displaying the switchover pressure, as well as the other variables collected during the experiments. This data could then be referenced to determine if correlations existed between responses and process conditions.

2.3.4 Part Collection

For each of the three experiments, a total of ten parts were collected for each of the 32 molding trials. These ten parts were collected when the steady state conditions (described in Section 2.3.2) were met. Each set of ten parts was individually labeled and stored separately for several weeks at room temperature. Because of the complexity of the measurement method (described in Section 2.4), coupled with fatigue, parts five through nine were measured for S&W and the average of these five values was used for each trial.

The exception to this is the conventional injection molding experiment, where only parts 5 through 7 were measured due to an error measuring parts 8 and 9 for several trials.

2.3.5 Trial Randomization

According to [53], randomization of the experimental trials is the cornerstone underlying the use of statistical methods in experimental design, and it assists in "averaging out" the effects of extraneous effects that may be present. Noting this, a random number generator was used to determine the order in which the trials were run. Separate sheets detailing each run of the experiments and containing the parameters held constant can be seen in Appendix 1 (A.1 through A.3). This was also used to record any abnormal phenomena that occurred throughout the experiments, which could then be interpreted and lead to further insight into the cause of any error.

2.4 Part Measurement

2.4.1 Coupling Shrinkage and Warpage

While the shrinkage and warpage were grouped into an S&W term in this research, the shrinkage was also investigated as its own entity. The shrinkage was measured using a digital caliper on the closed side of the box part, where there was no measurable deformation of the part. A comparison of the molded parts between processes did not show any difference in the shrinkage of the box part. Therefore, the more accurate measurement of the box part using an optical coordinate measurement machine (OCMM) was used to describe the S&W as one entity.

2.4.2 Measurement Method

The measurement procedure for acquiring the S&W on this part was extremely involved, mainly due to the fact that any physical means of measurement that involves contacting the part would have distorted the walls and adversely affected the accuracy of the S&W measurements. To overcome this challenge, a fixture was fabricated and mounted to the base of the OCMM that had a measurement accuracy of 2.5 microns. Each part was held securely, without distorting the walls, by placing a very small amount of force at the base of the part at the corners [cf. Figure 2.6].

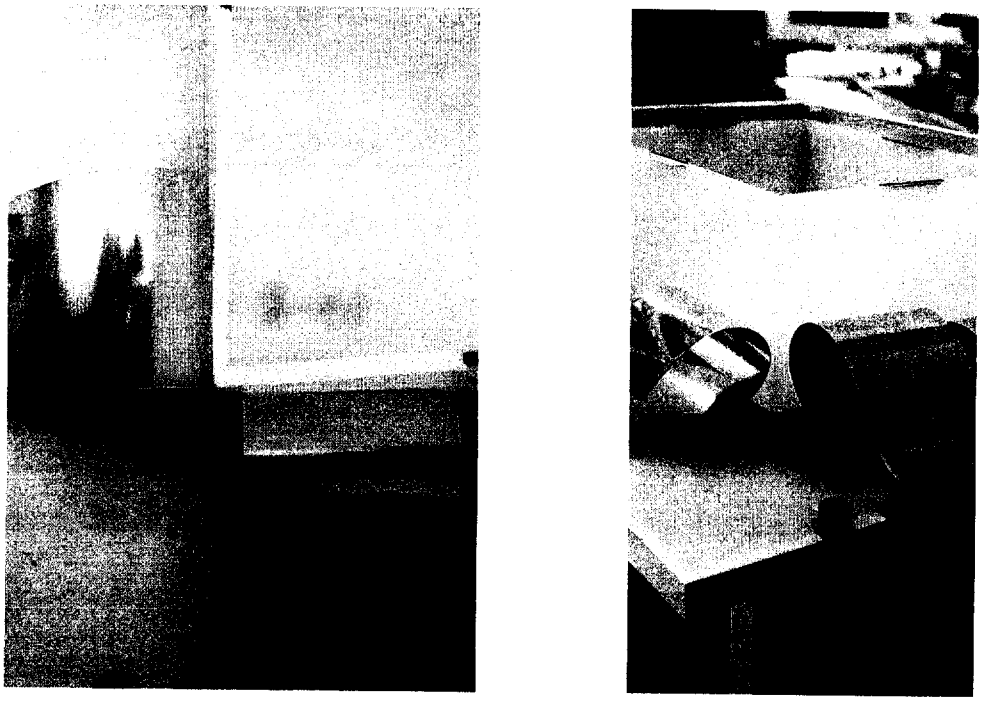

Figure 2.6 The photo on the left clearly shows the contact point is at or near the corner of the part, with a gap separating the clamp from the part as it moves towards the center. The photo on the right shows the small force is applied to the bottom of the part, causing no distortion of the wall.

2.4.2 Measurement Method

The measurement procedure for acquiring the S&W on this part was extremely involved, mainly due to the fact that any physical means of measurement that involves contacting the part would have distorted the walls and adversely affected the accuracy of the S&W measurements. To overcome this challenge, a fixture was fabricated and mounted to the base of the OCMM that had a measurement accuracy of 2.5 microns. Each part was held securely, without distorting the walls, by placing a very small amount of force at the base of the part at the corners [cf. Figure 2.6].

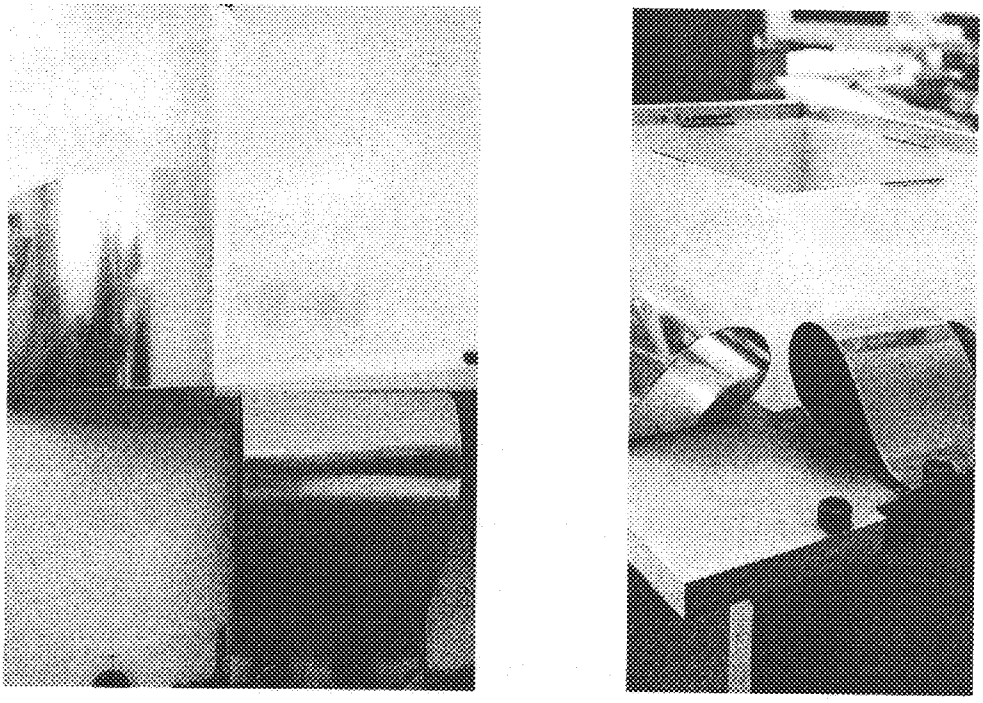

Figure 2.6 The photo on the left clearly shows the contact point is at or near the corner of the part, with a gap separating the clamp from the part as it moves towards the center. The photo on the right shows the small force is applied to the bottom of the part, causing no distortion of the wall.

The S&W measurement needed to be taken from a center position to the inside edge of each of the four walls. Through experimentation, it was determined that a witness line left by a pressure transducer hole was aligned with the center of the part vertically, and was offset 14 mm in the horizontal direction. Therefore, the center of the transducer witness line was found for each part, which could then be used to determine the center position of the part using the 14 mm offset. The number of data points needed to obtain the S&W data, and the order they were collected in, can be seen in Figure 2.7.

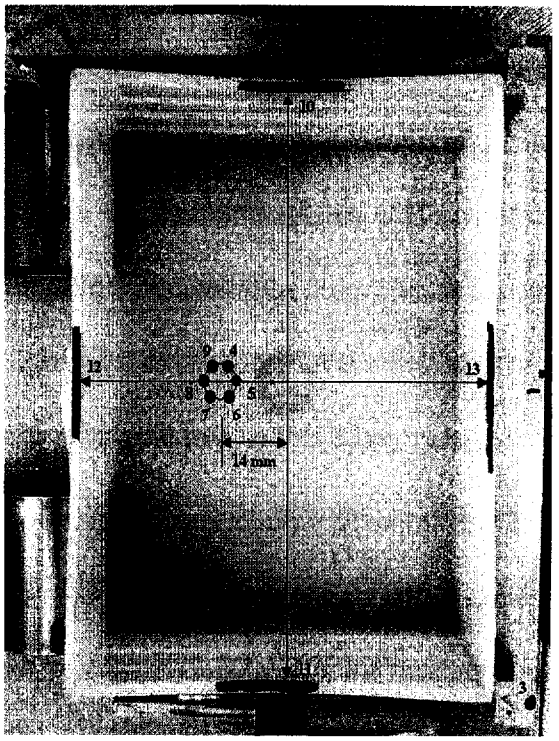

Figure 2.7 Photo of a typical box part molded with conventional injection molding. The edges were marked with black marker to help distinguish them from the rest of the part. After the center position was determined, the four S&W measurements were collected with data points 10 to 13.

The S&W measurement needed to be taken from a center position to the inside edge of each of the four walls. Through experimentation, it was determined that a witness line left by a pressure transducer hole was aligned with the center of the part vertically, and was offset 14 mm in the horizontal direction. Therefore, the center of the transducer witness line was found for each part, which could then be used to determine the center position of the part using the 14 mm offset. The number of data points needed to obtain the S&W data, and the order they were collected in, can be seen in Figure 2.7.

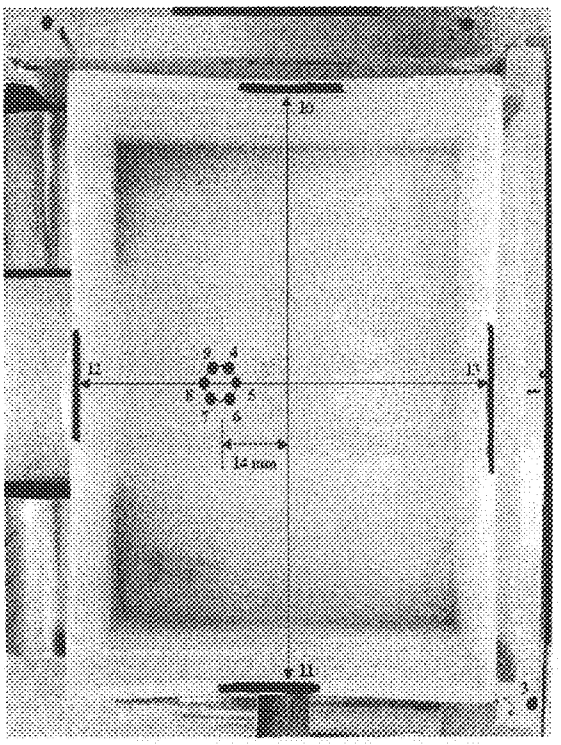

Figure 2.7 Photo of a typical box part molded with conventional injection molding. The edges were marked with black marker to help distinguish them from the rest of the part. After the center position was determined, the four S&W measurements were collected with data points 10 to 13.

2.4.3 Measurement Reporting

To report the vast amount of experimental data more concisely, the final S&W measurement for each part was presented as an average of the absolute values of all four S&W measurements. For example, each part has four S&W values; –X, +X, –Y, and +Y. The absolute value of each of the measurements (i.e., the deviation from the design geometry) was added and then averaged to determine the average S&W for that part. Therefore, the S&W of the box part is dependent on all four measurement directions. Note that a positive S&W value indicates the wall warps inwards, while a negative S&W value indicates the walls warps outward. Further on in this study, it will be shown that the optimal process parameters for the X directions can differ from the optimal process parameters in the Y directions. This can be attributed to differences in wall thickness, abrupt changes in thickness of the Y walls, and the degree of race-tracking.

2.5 Measurement Validation

The success of using DOE's to improve product quality and productivity depends highly on the accuracy and precision of the measurements. If the data collected are not accurate and precise, they will not represent the true characteristics of the parts being measured, even though manufacturers may be using the quality tools correctly [54]. Therefore, it is very important to have valid measurement studies to ensure that the data and measurements collected are accurate and precise, so that the effectiveness of the DOE is fully utilized. For this research, gage repeatability and reproducibility (GAGE R&R) studies were performed for each of the four measurement directions. Two ratios, called

the intraclass correlation coefficient (ICC) and the discrimination ratio (D_R), can be used to determine the capability of the measurement process [55]. A measurement process with a D_R greater than four denotes that the measurement process is capable of detecting significant product variation [54, 55]. While the ICC can also be used to determine a valid measurement process, it does not contain the appraiser variation (A.V.), known more simply as the operator error. Therefore, it is only valid when a single operator is performing all of the measurements. Using a system of two trials and two operators, the D_R was found to be well above four in each of the four directions. The actual D_R values for each of the four measurements can be found in Table 2.3, while the data collected and the GAGE R&R calculations can be seen in Tables 2.4 and 2.5, respectively. Note that the lower value of 5.68 in the –X direction can be attributed to the presence of flash on the inside edge of the part when compared to the other three directions, making determining the exact edge more challenging. Nevertheless, the measurement validation procedure ensured that the data gathered in this study were repeatable and reproducible. When not taking the part variation into account, it was determined that the actual measurement variation was approximately 70 microns in the X directions and 50 microns in the Y directions. For a more detailed description of how to accurately perform a GAGE R&R study, refer to [54, 55].

Table 2.3 Intraclass correlation coefficients (ICC) and discrimination ratios (D_R) for the four measurement directions.

GAGE Repeatability & Reproducibility (GAGE R&R)		
Measurement Direction	**ICC**	**D_R**
–X	0.940	5.68
+X	0.979	9.69
–Y	0.982	10.40
+Y	0.983	10.76

Table 2.4 Example of the data collected for the +Y direction.

+Y	Operator	A - Adam			B - Ryan			OVERALL
Part ID	Sample #	1st Trial	2nd Trial	Range	1st Trial	2nd Trial	Range	Part AVG
1	1	47.635	47.634	0.201	47.604	47.595	0.009	47.667
2	2	47.614	47.61	0.004	47.553	47.601	0.048	47.5945
3	3	47.599	47.617	0.018	47.595	47.573	0.022	47.596
4	4	47.638	47.607	0.031	47.54	47.604	0.064	47.59725
5	5	47.62	47.67	0.05	47.611	47.566	0.045	47.61675
6	6	46.48	46.538	0.058	46.598	46.52	0.078	46.534
7	7	46.498	46.525	0.027	46.399	46.419	0.02	46.46025
8	8	46.583	46.647	0.064	46.637	46.638	0.001	46.62625
9	9	46.39	46.516	0.126	46.42	46.455	0.035	46.44525
10	10	46.694	46.672	0.022	46.662	46.601	0.061	46.65725
	Totals	470.951	471.036	0.601	470.619	470.572	0.383	470.7945
		↓→	470.951	0.0601	↓→	470.619	0.0383	1.22175
			Sum 941.987	WR_A		Sum 941.191	WR_B	R_P
			AVG X_A 47.09935			AVG X_B 47.05955		

WR_A	0.0601
WR_B	0.0383
Sum	0.0984
WR_{AVG}	0.0492

	Max. X_{AVG}	47.09935
	Min. X_{AVG}	47.05955
R_O	X_{AVG} Diff.	0.0398
	X_{AVG}	47.07945

# Trials	D_4
2	3.27

WR_{AVG} x D_4 = UCL_R
UCL_R = 0.160884

Table 2.5 Calculations used for determining the ICC and D_R in the +Y direction.

Measurement Unit Analysis

# Trials (r)	# Appraisers (k)	# of Parts (n)	WR_{AVG}	R_O	R_P	X_{AVG}	E.V. d^*_2	A.V. d^*_2	P.V. d^*_2
2	2	10	0.0492	0.0398	1.22175	47.07945	1.14	1.41	3.18

Repeatability - Equipment Variation (E.V.)

$E.V. = WR_{AVG}/d^*_2$
E.V.= 0.043157895

Intraclass Correlation Coefficient (IC

$ICC = 1-(R\&R/T.V.)^2$
ICC = 0.962858

Reproducibility - Appraiser Variation (A.V.)

$A.V. = \sqrt{[(R_O/d^*_2)^2-(E.V.^2)/(nxr)]}$
A.V. = 0.026526035

Discrimination Ratio (D_R)

$D_R = \sqrt{[(1+ICC)/(1-ICC)]}$
D_R = 10.75527

Repeatability and Reproducibility (R&R)

$R\&R = \sqrt{[E.V.^2+A.V.^2]}$
R&R = 0.050658014

Appraiser Bias Effect

Operator Averages
AVG X_A AVG X_B
47.09935 47.05955

$\sigma_{e\ avg} = E.V./\sqrt{[nxr]}$
$\sigma_{e\ avg}$ = 0.00965

Control Limits
$X_{AVG} \pm 3\sigma_{e\ avg}$ =
+ = 47.108401
- = 47.050499

Check operator avg. outside the control limits

Product Variation

$P.V. = \sqrt{[(R_P/d^*_2)^2-(E.V.^2)/(kxr)]}$
P.V. = 0.383591631

Total Variation

$T.V. = \sqrt{[(R\&R)^2+(P.V.)^2]}$
T.V. = 0.38692218

2.6 Analysis

DOE analysis software (Minitab®) was used to analyze the data collected from the three experiments. The S&W value for each direction and process was input into Minitab® as shown in Figure 2.8.

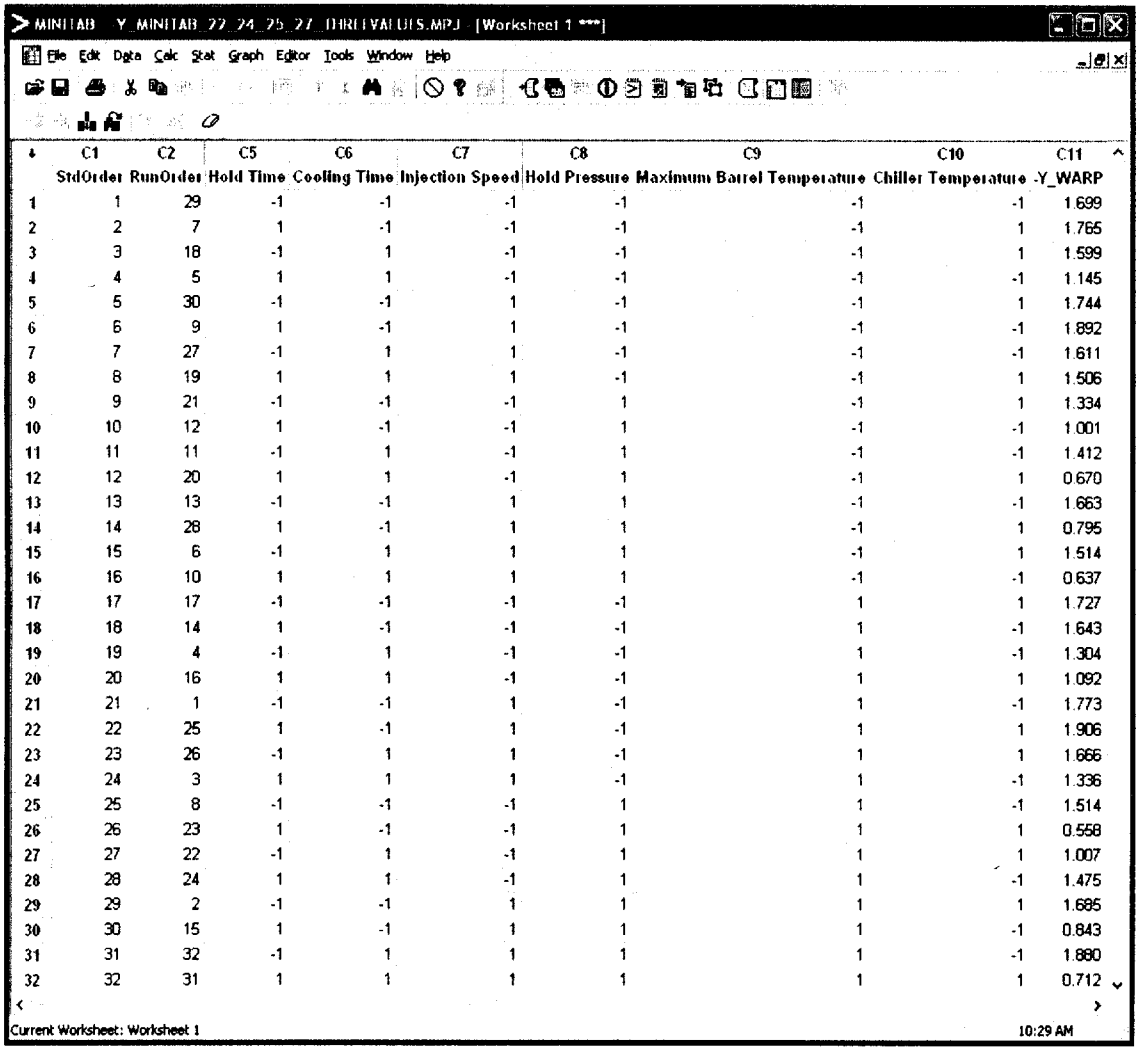

MINITAB - Y_MINITAB_22_24_25_27_THREEVALUES.MPJ - [Worksheet 1 ***]

File Edit Data Calc Stat Graph Editor Tools Window Help

	C1	C2	C5	C6	C7	C8	C9	C10	C11
	StdOrder	RunOrder	Hold Time	Cooling Time	Injection Speed	Hold Pressure	Maximum Barrel Temperature	Chiller Temperature	-Y_WARP
1	1	29	-1	-1	-1	-1	-1	-1	1.699
2	2	7	1	-1	-1	-1	-1	1	1.765
3	3	18	-1	1	-1	-1	-1	1	1.599
4	4	5	1	1	-1	-1	-1	-1	1.145
5	5	30	-1	-1	1	-1	-1	1	1.744
6	6	9	1	-1	1	-1	-1	-1	1.892
7	7	27	-1	1	1	-1	-1	-1	1.611
8	8	19	1	1	1	-1	-1	1	1.506
9	9	21	-1	-1	-1	1	-1	1	1.334
10	10	12	1	-1	-1	1	-1	-1	1.001
11	11	11	-1	1	-1	1	-1	-1	1.412
12	12	20	1	1	-1	1	-1	1	0.670
13	13	13	-1	-1	1	1	-1	-1	1.663
14	14	28	1	-1	1	1	-1	1	0.795
15	15	6	-1	1	1	1	-1	1	1.514
16	16	10	1	1	1	1	-1	-1	0.637
17	17	17	-1	-1	-1	-1	1	1	1.727
18	18	14	1	-1	-1	-1	1	-1	1.643
19	19	4	-1	1	-1	-1	1	-1	1.304
20	20	16	1	1	-1	-1	1	1	1.092
21	21	1	-1	-1	1	-1	1	-1	1.773
22	22	25	1	-1	1	-1	1	1	1.906
23	23	26	-1	1	1	-1	1	1	1.666
24	24	3	1	1	1	-1	1	-1	1.336
25	25	8	-1	-1	-1	1	1	-1	1.514
26	26	23	1	-1	-1	1	1	1	0.558
27	27	22	-1	1	-1	1	1	1	1.007
28	28	24	1	1	-1	1	1	-1	1.475
29	29	2	-1	-1	1	1	1	1	1.685
30	30	15	1	-1	1	1	1	-1	0.843
31	31	32	-1	1	1	1	1	-1	1.880
32	32	31	1	1	1	1	1	1	0.712

Current Worksheet: Worksheet 1 10:29 AM

Figure 2.8 Screen dump of Minitab®, showing the –Y warp in the far right column corresponding to its respective trial for conventional injection molding.

2.6.1 Normal Probability Plots

Because unreplicated experiments were employed, a graphical method called a normal probability plot (cf. Figure 2.9) was used to estimate significant main and two-factor interaction effects. The effects that are negligible are normally distributed, with mean zero and variance σ^2, and will tend to fall along a straight line on this plot, whereas significant effects will have nonzero means and will not lie along the straight line [53]. If a significant main or two-factor interaction effect lies on the left side of the straight line, increasing the level of the effect will decrease the response (the S&W of the molded part in this case). Conversely, if a significant main or two-factor interaction effect lies on the right side of the straight line, increasing the level of the effect will increase the response.

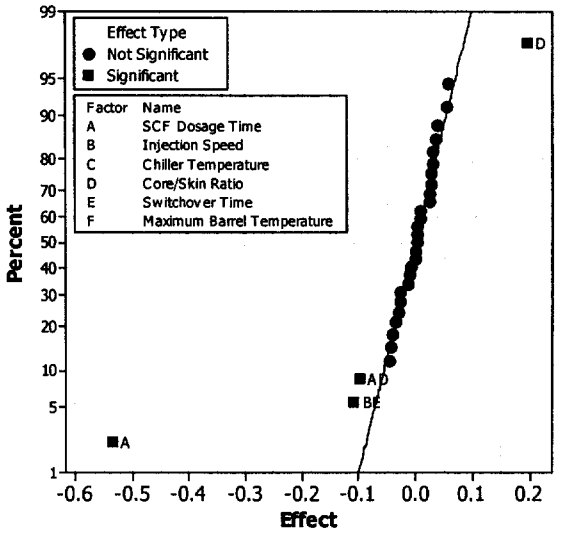

Figure 2.9 Example of a normal probability plot for the microcellular co-injection molding experiment. This plot indicates the SCF dosage time and core/skin ratio are significant main effects, while two interaction effects also exist.

2.6.2 Interaction Diagrams

When two-factor interactions exist, one must examine the interaction diagrams to determine the optimal process conditions. Even if the two factors in a significant two-factor interaction are deemed to be significant main effects, the results of the main effects must be neglected due to the interaction effect. The interaction diagrams will lend insight into determining the optimal parameters for achieving the ideal response. Two-factor interaction diagrams will be examined in detail in Chapters 3 through 5.

2.6.3 Regression Models

Using the significant main and two-factor interaction effects, multiple linear regression models were derived for each of the four directions for each process. A regression model is a mathematical model used to predict the response. For example, if main effect A, main effect B, and interaction effect AB are all deemed significant, the regression model would look like:

$$\hat{y} = b_0 + b_A X_A + b_B X_B + b_{AB} X_A X_B \qquad (2.1)$$

where:

$\hat{y}$ is the predicted response,

b_0 is the average response for all trials,

$b_i = \frac{E_i}{2}$ = effect of independent variable i (i = A or B) divided by 2,

$b_{AB} = \frac{E_{AB}}{2}$ = effect resulting from interaction between variables A and B divided by 2, and

X_i is the level of independent variable i, (i = A or B) either –1 (low setting) or +1 (high setting).

Regression models serve to validate the actual measurements taken after the experiments. The difference between the model and the actual data is known as the residual (see equation 2.2), and experimental runs with high residuals indicate that the actual data may not be accurate.

$$\varepsilon = y - \hat{y} \tag{2.2}$$

where:

ε is the residual error and

y is the observed response.

Therefore, the regression model can be used to verify the actual data obtained for each experiment. The residuals can be standardized using the following equation from [53].

$$d_{ij} = \frac{\varepsilon_{ij}}{\sqrt{MS_E}} \tag{2.3}$$

where:

d_{ij} is the standardized residual,

ε_{ij} is the residual (model data subtracted from actual data), and

$MS_E = \sigma^2$ (expected mean square).

These standardized residuals should be approximately normally distributed with mean zero and unit variance. Thus, about 68 percent of the standardized residuals should fall within the limits +/– 1, about 95 percent of them should fall within +/– 2, and virtually all of them should fall within +/– 3 [53]. A residual bigger than 3 or 4 standard deviations from zero is a potential outlier. Noting this, a series of tests/checks were performed on the residuals to ensure they behaved as they should in order to prove the regression models were adequate. Additionally, regression models are especially useful for fractional factorial DOE, as it allows us to estimate the other 32 combinations of factors that are not performed in a 2^{6-1} fractional factorial DOE's.

2.6.4 Manual Checking

While all analysis was performed automatically using Minitab®, the results were verified by performing the calculations manually. By checking results manually, the experimenter gains a better understanding of the calculations the software performs when asked to analyze the data. Additionally, the manual checking will identify if any mistakes were made when using Minitab®, which is common when using new software.

Chapter 3

Examining Shrinkage and Warpage with Conventional Injection Molding

3.1 Experiments

As discussed previously, the factors affecting dimensional stability in conventional injection molding have been widely studied, and a wealth of information is available [42, 43]. Therefore, a DOE was used for conventional injection molding in order to validate the procedures developed for data collection and analysis, as well as to determine the

optimal parameters for achieving the minimum S&W so that it could be used as a baseline. This minimum S&W baseline could be used to compare to the minimum S&W obtained with microcellular injection and microcellular co-injection molding to determine the percent change in S&W between these three injection molding processes.

3.1.1 Preliminary Experiments

Before performing a DOE, it is very important to properly identify the most influential factors to be used in the experiment, as well as the high and low levels of these factors. Because of the in-house experience, coupled with the abundance of information available, the options for independent variables were narrowed to six for this DOE. The factors and levels of the settings can be seen in Table 3.1.

Table 3.1 Independent variables and their high and low settings used for the conventional injection molding experiment.

Parameter Settings for Conventional Injection Molding Experiment		
Parameter	**Low (–1)**	**High (+1)**
A – HOLD TIME (sec)	3	6
B – COOLING TIME (sec)	20	35
C – INJECTION SPEED (mm/sec)	40	100
D – HOLD PRESSURE (bar)	400	600
E – MAX BARREL TEMP (°C)	205	230
F – CHILLER TEMP (°C)	20	40

As described earlier, these settings represent the largest processing window for producing the box part without creating a defective part. For instance, if one were to increase the maximum cooling time from 35 to 40 seconds, the actual mold-wall temperature would

decrease, due to the less frequent injection of molten polymer. As this mold surface cooled, it would result in a short shot, and the entire experiment would be sacrificed due to defective parts for that trial. On the other hand, if one were to reduce the cooling time from 20 seconds to 15 seconds, the part would not be fully solidified upon part ejection, again sacrificing the validity of the experiment.

Machine limitations also played a role in determining the independent variable settings. The maximum shot size of the barrel was 54 cm^3, which was nearly the volume of the part. Therefore, if the hold time or hold pressure was increased above the levels in Table 3.1, there would be no material cushion, and packing would no longer be taking place (the screw bottomed out in the nozzle). While this was initially cause for concern, as too small of a process window may not accurately depict the impact of either of these variables, the hold time and hold pressure turned out to have the most significant effect on the S&W. This proved that the processing window was large enough to produce a significant difference in the S&W.

3.1.2 DOE

The 2^{6-1} fractional factorial DOE used for this study consisted of 32 trials run in random order. The random order was determined using a random number generator, and the predetermined steady state conditions were met before switching from one trial to the next. Ten parts were collected for each trial, and parts five through seven were then

measured to determine the S&W as described in Section 2.4. The DOE matrix used for this experiment can be seen in Table 3.2.

Table 3.2 2^{6-1} DOE matrix used for conventional injection molding experiment, shown in standard order.

Standard Order	Hold Time (sec)	Cooling Time (sec)	Injection Speed (mm/sec)	Hold Pressure (bar)	Max Barrel Temp (°C)	Chiller Temp (°C)	Trial Number
1	3	20	40	400	205	20	29
2	6	20	40	400	205	40	7
3	3	35	40	400	205	40	18
4	6	35	40	400	205	20	5
5	3	20	100	400	205	40	30
6	6	20	100	400	205	20	9
7	3	35	100	400	205	20	27
8	6	35	100	400	205	40	19
9	3	20	40	600	205	40	21
10	6	20	40	600	205	20	12
11	3	35	40	600	205	20	11
12	6	35	40	600	205	40	20
13	3	20	100	600	205	20	13
14	6	20	100	600	205	40	28
15	3	35	100	600	205	40	6
16	6	35	100	600	205	20	10
17	3	20	40	400	230	40	17
18	6	20	40	400	230	20	14
19	3	35	40	400	230	20	4
20	6	35	40	400	230	40	16
21	3	20	100	400	230	20	1
22	6	20	100	400	230	40	25
23	3	35	100	400	230	40	26
24	6	35	100	400	230	20	3
25	3	20	40	600	230	20	8
26	6	20	40	600	230	40	23
27	3	35	40	600	230	40	22
28	6	35	40	600	230	20	24
29	3	20	100	600	230	40	2
30	6	20	100	600	230	20	15
31	3	35	100	600	230	20	32
32	6	35	100	600	230	40	31

3.2 Analysis

With proper planning and execution, the analysis portion of a DOE can be relatively straightforward. The analysis involves examination of the normal probability plots, two-factor interaction diagrams, and a series of tests/checks on the residuals. This analysis is detailed in the following sections for conventional injection molding.

3.2.1 Normal Probability Plots

Normal probability plots for the –X, +X, –Y, and +Y directions are shown in Figure 3.1. These were used to determine significant main and interaction effects. From these four normal probability plots, it can be seen that the hold time and the hold pressure are the two most significant effects for all four directions. For the two X directions, the cooling time and a two-factor interaction, cooling time and chiller temperature, also affect the S&W. In the two Y directions, there is an interaction effect between hold pressure and hold time.

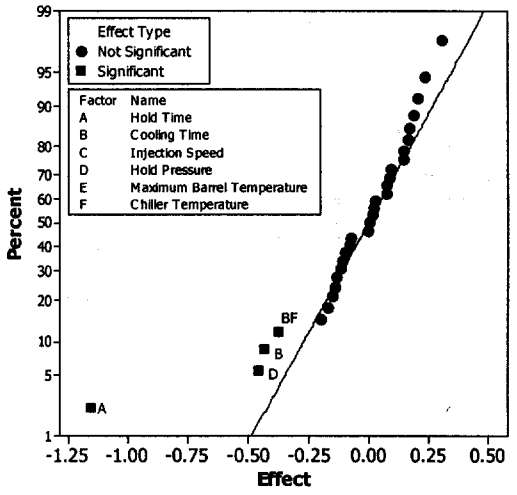

(a)

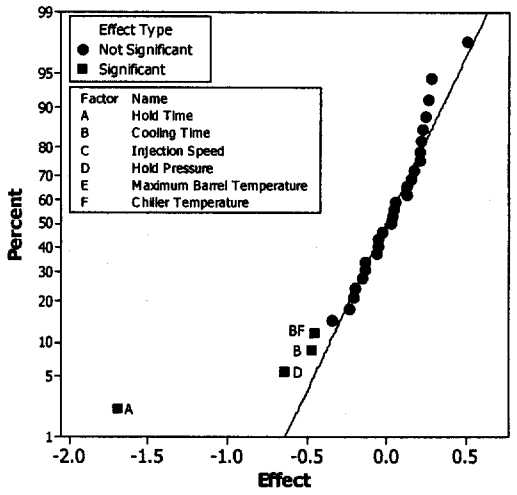

(b)

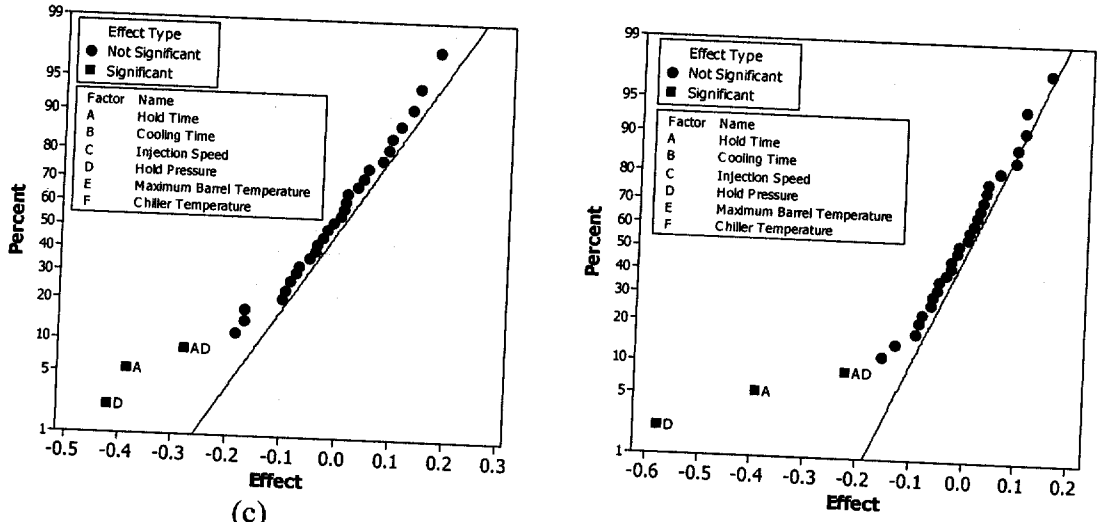

Figure 3.1 Normal probability plots for conventional injection molding in the (a) –X direction, (b) +X direction, (c) –Y direction, and (d) +Y direction.

3.2.2 Interaction Diagrams

Using two-factor interaction diagrams, the interaction effect between cooling time and chiller temperature, and between hold pressure and hold time will be explored. The interaction diagrams provide insight into how the interactions affect the S&W, as well as aid in determining the cause for the interaction.

3.2.2.1 Cooling Time and Chiller Temperature Interaction

The interaction between cooling time and chiller temperature in conventional injection molding has a large effect on the cooling rate. At the high chiller temperature and low cooling time, the lowest cooling rate exists, due to the high mold temperature. At the low chiller temperature and high cooling time, the highest cooling rate exists. The cooling time has an influence due to the less frequent injection of molten polymer, resulting in a

cooler mold-wall temperature. The cyclic change in mold temperature due to the injection of molten polymer was discussed previously in Section 2.3.2.

The cooling time and chiller temperature interaction for the –X and +X directions can be seen in Figure 3.2. Initially looking at them, the figures appear to be identical. However, while the shape of them is the same, where they lie on the y-scale is different. The sprue is centrally located on the part, and the part is symmetrical in the X directions and the Y directions. However, the +X wall exhibits a tendency to warp outward, rather than inward. It can be seen in Figure 3.2 that as one adjusts the parameters, the walls respond in the same fashion. The explanation for the peculiar behavior of the X walls may be attributed to the cooling line location in the box mold. Due to the location of the cooling lines, it is presumed that a warm spot lies on the outside edge of the +X wall, attributing

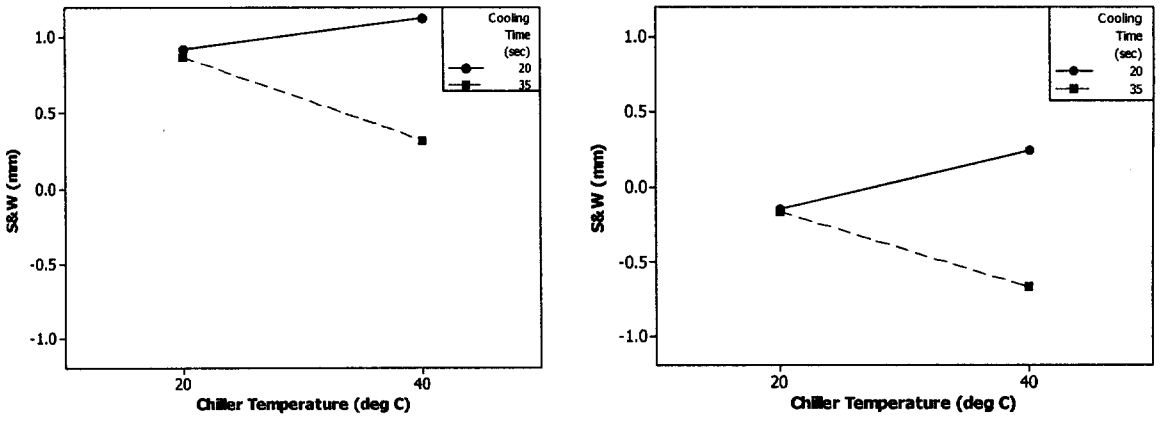

Figure 3.2 Interaction between the cooling time and the chiller temperature for conventional injection molding in the (a) –X direction, and (b) +X direction.

to its tendency to warp in that direction. Due to the complex geometry of the box part and the cooling line location, no obvious solution exists for optimal process parameters to use for obtaining the minimum S&W. A method for determining the optimal process parameters will be discussed in the following sections.

3.2.2.2 Hold Time and Hold Pressure Interaction

As expected, the hold time and hold pressure had the most significant effect on the S&W for the Y directions. However, an interaction effect existed, which can easily be seen in Figure 3.3. If no interaction effect existed, the two lines would be parallel to each other. It can be seen in Figure 3.3 that with the low hold time and the high hold pressure, the S&W reduction in not as great as when the high hold pressure is coupled with the high hold time. It is possible this is due to the freezing of the sprue gate with this particular

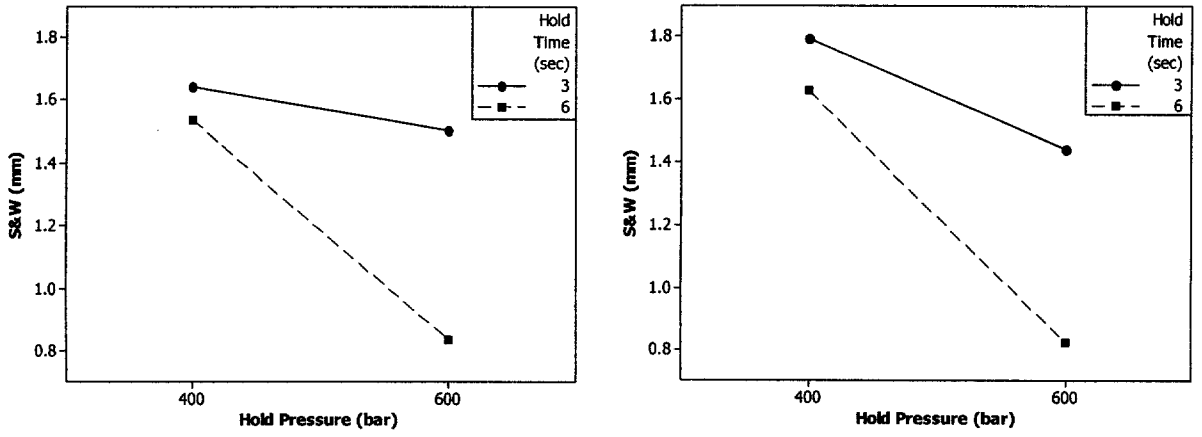

Figure 3.3 Interaction between the hold time and the hold pressure for conventional injection molding in the (a) –Y direction, and (b) +Y direction.

part geometry. If the sprue gate did not freeze off during the hold time, the high hold pressure, which is known to reduce warpage, would be released. Therefore, the pressure in the cavity would rapidly decay as material oozed out of the gate, whereas with a high hold time and subsequent gate freezing, the cavity pressure would decay due only to the shrinkage of the material. At the high hold pressure, the amount of material oozing out of the cavity would be larger than at the low hold pressure. The different amounts of material oozing out of the gate at the different hold pressures is potentially the cause for the lines to not be parallel.

3.3 Results and Discussion

Complying with previous studies, increasing the hold time and hold pressure reduced the S&W most significantly in all four of the measurement directions. Additionally, the cooling time and chiller temperature affected the S&W of the X walls.

3.3.1 The Hold Time and Hold Pressure Interaction

Examination of the sprue on the box part (cf. Figure 2.1) shows the thickness of the sprue at the gate location, which is approximately 8 mm in diameter. Moving up the sprue, it tapers down to three millimeters, where it is possible it would freeze during the holding stage of the injection molding cycle. However, this section is very close to a hot manifold (cf. Figure 1.14), which may hinder the freezing of the sprue. Due to the thickness of the sprue gate and the presence of the hot manifold, it is possible that the sprue gate did not freeze during the holding stage. Therefore, the aforementioned gate freeze is actually a

sprue freeze, probably at the point where it tapers, which has the minimum cross-sectional area and is also furthest away from the hot manifold. Regardless of the cause for the interaction, it can easily be seen that in order to reduce the S&W as much as possible, increasing both the hold time and hold pressure at the same time yields the best results.

3.3.2 Optimal Parameters

3.3.2.1 S&W in X directions

The optimal parameters for reducing the S&W in the X directions are very complicated due to the interaction effect between the cooling time and chiller temperature. As seen in Figure 3.1, increasing the hold time and hold temperature will have the most significant effect on reducing the S&W in these directions. Using the regression models in Appendix 2, one can estimate the S&W for each of the X directions.

3.3.2.2 S&W in Y directions

The optimal parameters for reducing the S&W in the Y directions is much more simple and direct than in the X directions. Understanding this is significant, because the end user of the plastic component may only care about one or two critical dimensions, potentially the S&W of the Y walls. If this were the case, one could use the regression models to determine the optimal parameters for the Y directions, neglecting the X directions. The magnitude of the effects are different, but the direction of the effects is the same, and using the maximum hold time and the maximum hold pressure will result in the S&W closest to zero for each of the Y directions.

3.3.2.3 Average S&W

In order to determine optimal process parameters for reducing the average S&W, the method detailed in Section 2.4.3 was used, and then compared to the actual values. The estimated average S&W for each trial, as well as the actual average S&W, can be seen in Table 3.3.

Table 3.3 Predicted and actual S&W for each trial of the experiment.

Standard Order	Regression Model (mm)	Actual (mm)
1	1.547	1.328
2	1.058	1.207
3	1.261	1.123
4	1.091	1.017
5	1.691	1.489
6	1.100	1.203
7	1.528	1.386
8	1.099	1.030
9	1.295	1.136
10	0.768	1.083
11	1.132	0.975
12	0.996	0.918
13	1.151	1.351
14	0.727	0.560
15	0.940	1.160
16	0.760	0.687
17	1.691	1.704
18	1.100	1.144
19	1.528	1.492
20	1.099	1.068
21	1.547	1.955
22	1.058	1.694
23	1.261	1.310
24	1.091	1.112
25	1.151	1.441
26	0.727	0.760
27	0.940	0.796
28	0.760	1.222
29	1.295	1.567
30	0.768	0.753
31	1.132	1.235
32	0.996	0.670

This data, along with the estimated S&W for the other 32 trials, can be seen in Figure 3.4. The method used for determining the estimated average S&W for the other 32 trials is described in the following section. While the results from Table 3.3 do not agree exactly, one must take into account the measurement variability, as well as machine and material fluctuations, even at constant parameter settings. These variations in part quality at constant parameter settings, due to machine and material fluctuations, have been documented at the Polymer Engineering Center at the University of Wisconsin-Madison. Furthermore, the residual analysis passed the tests/checks needed to validate the regression models.

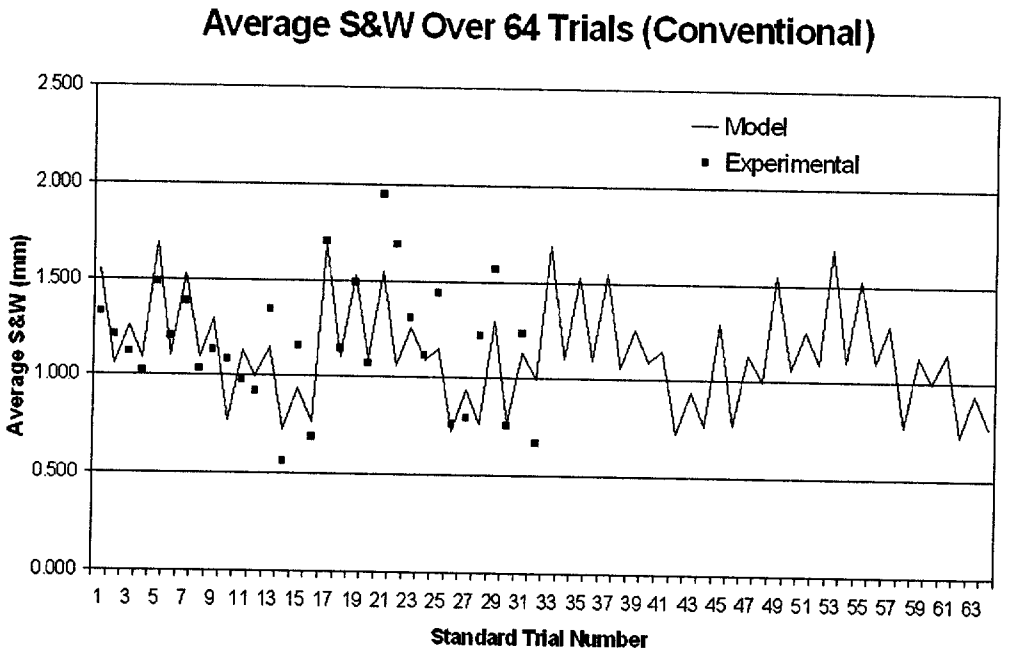

Figure 3.4 The average S&W determined from the regression models for all 64 trials. The lowest S&W values correlate to the high hold time and high hold pressure.

Examination of the data reveals that standard order 14 has the lowest predicted S&W and the lowest actual S&W. The predicted and actual values of 0.727 mm and 0.560 mm are not identical, but considering error is compounded for all four measurement directions, it is within the measurement variation of 0.070 mm in both X directions and 0.050 mm in both Y directions, excluding any variation due to uncontrollable variables. Compounding the measurement error results in a total allowable error of 0.240 mm. Referring to Table 3.2, one can find the processing parameters corresponding to the minimal S&W. These optimal processing conditions can be seen again in Table 3.4.

Table 3.4 Optimal parameters for achieving the minimum average S&W.

Standard Order	Hold Time (sec)	Cooling Time (sec)	Injection Speed (mm/sec)	Hold Pressure (bar)	Maximum Barrel Temperature (°C)	Chiller Temp. (°C)
14	6	20	100	600	205	40

Further examination of the data shows that several other combinations of parameter settings result in S&W values near the lowest predicted and actual values. All of the trials have a six second hold time and 600 bar hold pressure, with the exception of trials 15 and 27. While these trials sacrifice S&W results in the Y directions by having a three second hold time, the X direction S&W is improved, resulting in an overall S&W of less than 1 mm on average in all directions.

Standard order 32 has an actual S&W value of 0.670 mm, while the regression model estimates the S&W to be 0.996 mm. While the residual analysis indicates no glaring error was made, the data was examined further. The only variation between standard order 14

and 32 is the cooling time and chiller temperature. The steady state mold temperature for standard order 14 is approximately 4°C above the steady state mold temperature for standard order 32. However, looking back at the data, the mold temperature difference was only 2 to 3°C. This indicates that the cooling rate for standard order was not as high as it should have been, and potentially allowed more residual stresses to relax than normally would have, hence the reason for the actual data being lower than the estimated S&W derived from the regression equations.

3.3.3 Estimating the other 32 trials

Using the regression models, the other 32 possible combinations of parameters can be evaluated. While there is no actual data for these parameter combinations, residual analysis provided the means by which to accept the estimated results as accurate. Table 3.5 displays the estimated S&W value for the four best parameter combinations, along with the actual values for the first two, which were run in the DOE. All of these combinations have a high hold time and high hold pressure and share a low cooling time and high chiller temperature. The result of this is a higher mold wall temperature, which in turn, results in a slower cooling rate compared to a colder mold wall temperature. This slower cooling rate allows residual stresses due to the injection of the molten polymer to relax, therefore leaving less frozen-in residual stresses in the part.

Table 3.5 Estimated and actual S&W for optimal parameter combinations.

St. Order	Hold Time (sec)	Cooling Time (sec)	Injection Speed (mm/sec)	Hold Pressure (bar)	Max. Barrel Temperature (°C)	Chiller Temp. (°C)	Regression Model (mm)	Actual Data (mm)
14	6	20	100	600	205	40	0.727	0.560
26	6	20	20	600	230	40	0.727	0.760
n/a	6	20	20	600	205	40	0.727	n/a
n/a	6	20	100	600	230	40	0.727	n/a

3.3.4 Dimensional Stability

The standard deviation of the parts for each trial was evaluated to determine the part-to-part variation. This indicates the ability of the process to resist outside disturbances. The standard deviation for each of the four measurement directions was then averaged to determine the average standard deviation for each direction. These dimensional stability results will be compared to results from the other two experiments and discussed in the conclusions chapter of this thesis.

3.4 Chapter Summary

The S&W is most highly affected by the hold pressure and hold time. Due to the cooling channel location in the mold, the effect of these parameters tends to be opposite for the X directions, while increasing the hold time and hold pressure will always result in S&W closest to zero for both Y directions. The cooling rate, which is mainly a function of the cooling time and chiller temperature, also has a large impact on the thinner X directions. The thicker Y walls are not as sensitive to the change in these parameters due to the thickness of these walls.

Chapter 4

Examining Shrinkage and Warpage with Microcellular Injection Molding

4.1 Experiments

Microcellular injection molding is similar to conventional injection molding in the fact that the process is complex and dynamic. When compared to conventional injection molding, however, little information is available for understanding and harnessing the process dynamics. Understanding this process becomes more complex due to additional

process variables used with microcellular injection molding, as well as the importance of maintaining a single-phase polymer-gas solution for achieving consistent cell structure and part quality. The use of DOE in microcellular injection molding allows us to observe how parameters affect the response of the molded part, whether the response is weight, tensile or impact strength, S&W, or a myriad of other options for part quality. In this study, the box part was evaluated in order to determine the significant main and two-factor interaction effects affecting the S&W, and quantitatively compare the results to conventional injection molding and microcellular co-injection molding.

4.1.1 Preliminary Experiments

When determining factors for the microcellular injection molding experiment, the amount of time available to run the entire experiment was taken into account. It was estimated that any more than 32 trials could not be performed in one day, based on prior experience obtained performing the conventional injection molding experiment. In order to obtain optimal results, preliminary experiments were performed prior to running the 2^{6-1} fractional factorial DOE. Before these preliminary experiments were started, two independent variables used with conventional injection molding, hold time and hold pressure, were eliminated. These were eliminated due to the absence of the packing stage in microcellular injection molding. Literature reviews and experience indicated that the wt% supercritical fluid (SCF) content would play a significant role in the reduction of the S&W of the PP box part. The SCF content is dependent on three variables; SCF dosage time, SCF mass flow rate, and shot weight. The SCF dosage time is the time that the SCF

is allowed to flow into the barrel during screw recovery. The SCF mass flow rate is controlled using a mass flow element (MFE). The flow rate range on the equipment used for this experiment was 0.05 to 0.16 kg/hr, and was set at a constant 0.11 kg/hr. The calculation for obtaining the wt% SCF is shown in equation 4.1.

$$wt\%SCF = \frac{(\dot{m}_{SCF})(t) * 27.8}{m_{part}} \tag{4.1}$$

where,

$\dot{m}_{SCF}$ = SCF mass flow rate (kg/hr),

t = SCF dosage time (sec),

27.8 = conversion factor, and

m_{part} = shot weight (g).

Because of the dependence on shot weight and SCF dosage time, predicting the wt% SCF content for each of the 32 trials could prove to be difficult, especially if one decides to vary both the SCF dosage time and the shot volume. In this study, the SCF dosage time and the shot volume were both used as independent variables in place of the hold time and the hold pressure used previously in conventional injection molding. The wt% SCF content was calculated after the experiment was done, and in this study, the shot volume was found to have virtually no effect on this. This is mainly due to the fact that the process window for shot volume was very small due to the production of defective parts,

mainly short shot for low shot volumes. The factors and level of the settings can be seen in Table 4.1.

Table 4.1 Independent variables and their high and low settings used for the microcellular injection molding experiment.

Parameter Settings for Microcellular Injection Molding Experiment		
Parameter	**Low (–1)**	**High (+1)**
A – SCF DOSAGE TIME (sec)	4	7
B – SHOT VOLUME (cm^3)	51	53
C – MAX BARREL TEMP (°C)	205	230
D – INJECTION SPEED (mm/sec)	40	120
E – CHILLER TEMP (°C)	20	40
F – COOLING TIME (sec)	32	44

The preliminary experiments run for the microcellular injection molding study were used to determine the levels of the independent variables. Two defects are prevalent when using microcellular injection molding; short shot and post blow. Short shot occurs in microcellular injection molding when the polymer solidifies before the foaming action of the polymer-gas solution completely fills the cavity. This can be attributed to:

- Low SCF levels
- Low shot volume
- Low melt temperature
- Low injection speed
- Low chiller temp and a long cooling time, resulting in a colder mold wall.

Post blow occurs in microcellular injection molding when the polymer has not completely solidified and the mold is opened. Post blow can be attributed to:

- High SCF levels
- High shot volume
- High melt temperature
- High injection speed
- High chiller temp and a short cooling time, resulting in a hotter mold wall

Free from the constraints of the mold upon mold opening, the internal pressure in microcellular injection molding causes the part to swell until the internal pressure and atmospheric pressure achieve equilibrium, or the polymer solidifies sufficiently to resist the internal pressure. The "in microcellular injection molding" is emphasized because in conventional injection molding, post blow does not occur, and short shot occurs under different circumstances in conventional injection molding. Using preliminary experiments, the largest processing window without producing a defective part was determined. Because of this, even a small deviation from the independent variable settings found in Table 4.1 would result in a defective part.

4.1.2 DOE

The 2^{6-1} fractional factorial DOE used for this study consisted of 32 trials run in random order. The random order was determined using a random number generator, and the predetermined steady state conditions were met before switching from one trial to the next. Ten parts were collected for each trial, and parts five through nine were then measured to determine the S&W as described in Section 2.4. The DOE matrix used for this experiment can be seen in Table 4.2.

Table 4.2 2^{6-1} DOE matrix used for microcellular injection molding experiment, shown in standard order.

Standard Order	SCF Dosage Time (sec)	Shot Volume (cm^3)	Max Barrel Temp (°C)	Injection Speed (mm/sec)	Chiller Temp (°C)	Cooling Time (sec)	Trial Number
1	4	51	205	40	20	32	13
2	7	51	205	40	20	44	14
3	4	53	205	40	20	44	6
4	7	53	205	40	20	32	7
5	4	51	230	40	20	44	21
6	7	51	230	40	20	32	16
7	4	53	230	40	20	32	5
8	7	53	230	40	20	44	18
9	4	51	205	120	20	44	28
10	7	51	205	120	20	32	20
11	4	53	205	120	20	32	11
12	7	53	205	120	20	44	1
13	4	51	230	120	20	32	26
14	7	51	230	120	20	44	17
15	4	53	230	120	20	44	2
16	7	53	230	120	20	32	27
17	4	51	205	40	40	44	29
18	7	51	205	40	40	32	31
19	4	53	205	40	40	32	9
20	7	53	205	40	40	44	15
21	4	51	230	40	40	32	19
22	7	51	230	40	40	44	32
23	4	53	230	40	40	44	3
24	7	53	230	40	40	32	25
25	4	51	205	120	40	32	30
26	7	51	205	120	40	44	10
27	4	53	205	120	40	44	22
28	7	53	205	120	40	32	8
29	4	51	230	120	40	44	4
30	7	51	230	120	40	32	24
31	4	53	230	120	40	32	12
32	7	53	230	120	40	44	23

4.2 Analysis

With proper planning and execution, the analysis portion of a DOE can be relatively straightforward. The analysis involves examination of the normal probability plots, interaction diagrams, and a series of tests/checks on the residuals. This analysis is detailed in the following sections for microcellular injection molding.

4.2.1 Normal Probability Plots

Normal probability plots for the –X, +X, –Y, and +Y directions are shown in Figure 4.1. These were used to determine significant main and two-factor interaction effects. From these four normal probability plots, it can be seen that the SCF dosage time has the most significant effect on the S&W in all four directions. Because it falls on the left side of the normal probability plot, increasing the SCF dosage time will decrease the S&W. This

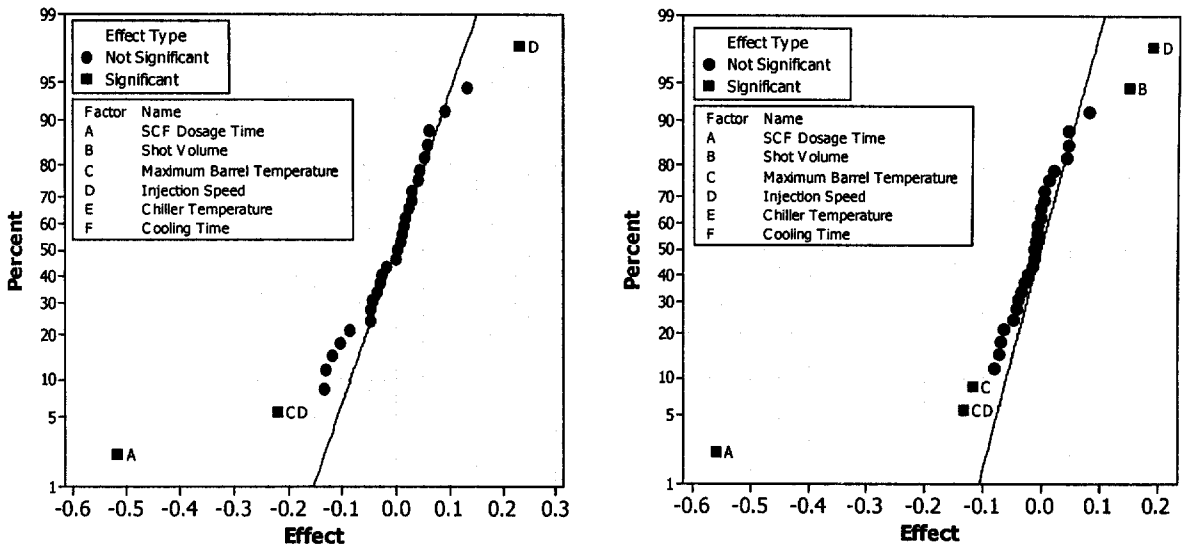

(a) (b)

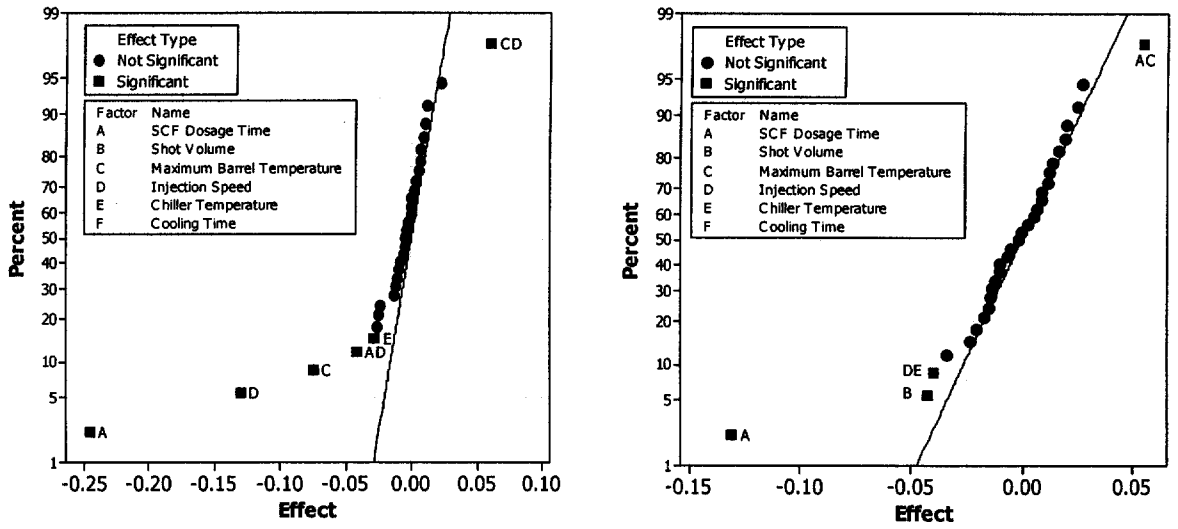

Figure 4.1 Normal probability plots for microcellular injection molding in the (a) –X direction, (b) +X direction, (c) –Y direction, and (d) +Y direction.

effect is in the same direction for all four directions. It can also be seen that the injection speed has an effect on the S&W, albeit an opposite effect when observing the X directions and the Y directions.

4.2.2 Interaction Diagrams

Using two-factor interaction diagrams, the interaction effects between maximum barrel temperature and injection speed will be examined. Other interaction effects exist, such as SCF dosage time and injection speed, SCF dosage time and maximum barrel temperature, and injection speed and chiller temperature. However, each of these interaction effects exist for only one of the four directions, and their magnitude is less than the maximum barrel temperature and injection speed interaction. Therefore, these will only be shown in Appendix 3 (A.16 through A.18). The interaction diagrams between maximum barrel

temperature and injection speed will be examined further, as they provide insight into how the process parameters affect the S&W.

4.2.2.1 Maximum Barrel Temperature and Injection Speed Interaction

The maximum barrel temperature, commonly referred to as the melt temperature, and the injection speed interact in the X directions and the –Y direction. However, the response of S&W is different when comparing the X walls to the Y walls. It has been shown in [15, 25] that decreasing the melt temperature and increasing the injection speed generally results in greater cell density and a smaller cell size. The cell density and cell size have been shown to be extremely important in determining the mechanical properties of microcellular injection molded parts [56].

The maximum barrel temperature and injection speed interaction for the –X, +X and –Y directions can be seen in Figure 4.2. Figures 4.2(a) and 4.2(b), while not identical, both represent similar results. Reducing the maximum barrel temperature and injection speed results in the S&W closest to zero. However, in the –Y direction, it appears that increasing the injection speed and either barrel temperature (at the high injection speed) will result in the S&W closest to zero. Close examination of the part geometry and the flow of the polymer in the mold cavity lends insight into the results and will be discussed later on.

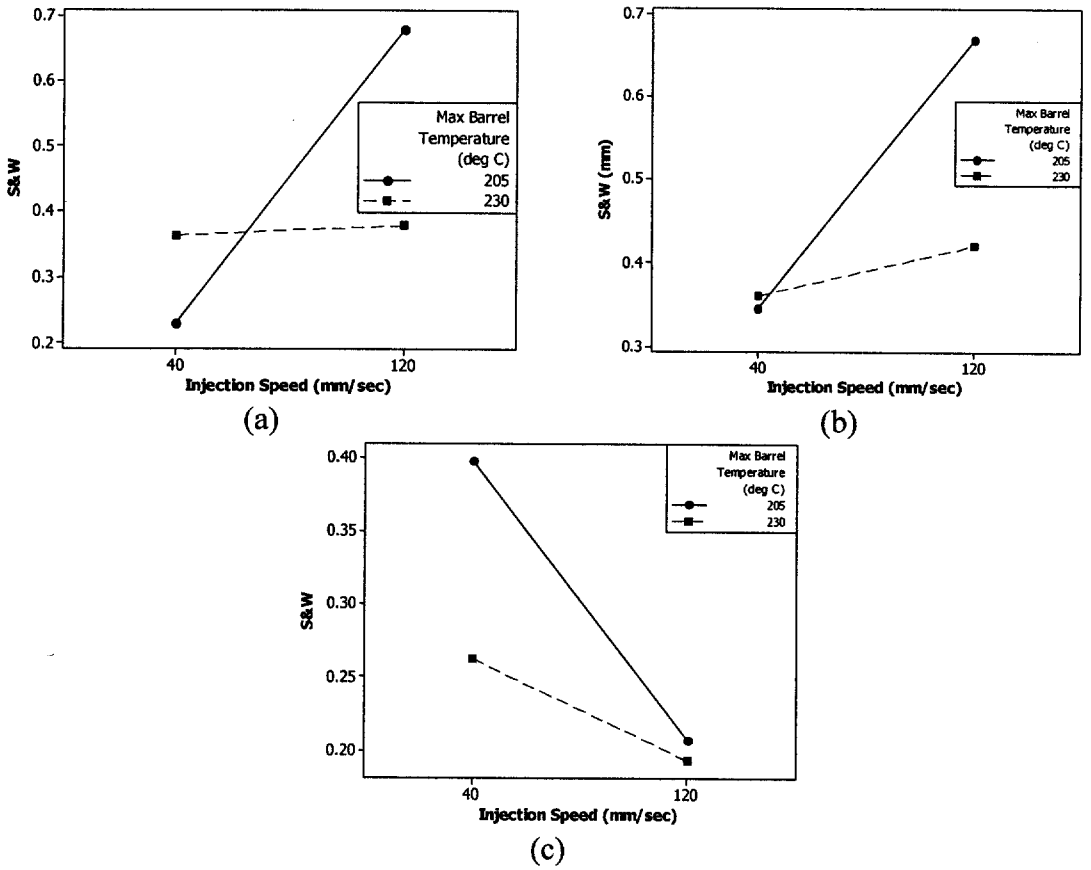

Figure 4.2 Interaction between the maximum barrel temperature and the injection speed for microcellular injection molding in the (a) –X direction, (b) +X direction, and (c) –Y direction.

4.2.2.2 Other Interactions

Three other interaction effects existed in the microcellular injection molding experiments. The results of these interactions may be viewed in Appendix 3 (A.16 through A.18). These three interactions were much less significant than the maximum barrel temperature and injection speed interaction, as well as only being significant for one direction. These interaction effects were included in the regression models for predicting the S&W, but

are not detailed due to their relative insignificance and lack of consistency throughout the four measurement directions.

4.3 SEM Analysis

The cell structure of the microcellular injection molded parts was examined using a JEOL JSM-6100 scanning electron microscope (SEM). Images of the microstructure were taken along the flow length of the box part, as well as each side of the part corresponding to the four walls measured for S&W. The locations at which the images were taken can be seen in Figure 4.3. Standard order 14 showed excellent S&W results and thus was chosen to analyze along the length of fill. These images can be seen in Figure 4.4.

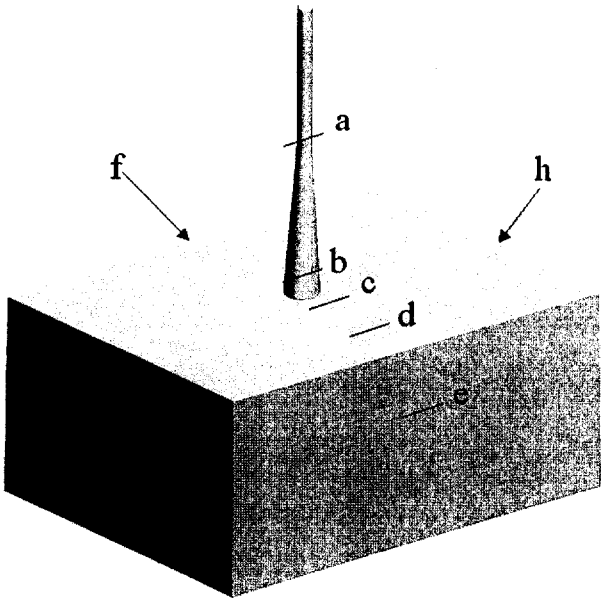

Figure 4.3 Solid model of the box part; letters indicate where the SEM images were taken.

are not detailed due to their relative insignificance and lack of consistency throughout the four measurement directions.

4.3 SEM Analysis

The cell structure of the microcellular injection molded parts was examined using a JEOL JSM-6100 scanning electron microscope (SEM). Images of the microstructure were taken along the flow length of the box part, as well as each side of the part corresponding to the four walls measured for S&W. The locations at which the images were taken can be seen in Figure 4.3. Standard order 14 showed excellent S&W results and thus was chosen to analyze along the length of fill. These images can be seen in Figure 4.4.

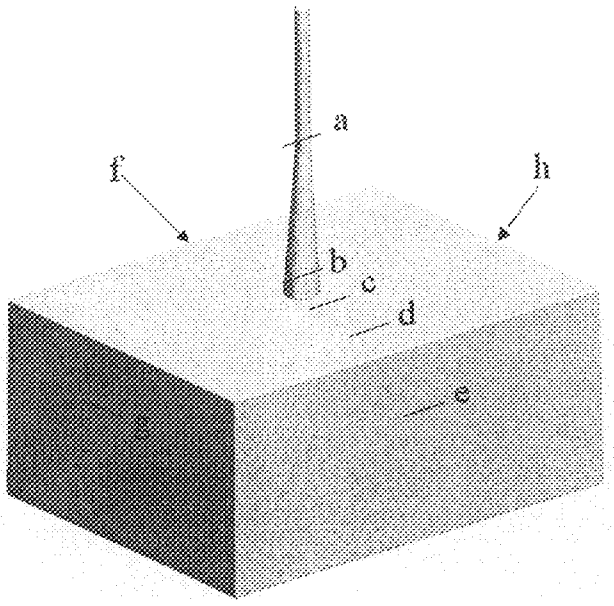

Figure 4.3 Solid model of the box part; letters indicate where the SEM images were taken.

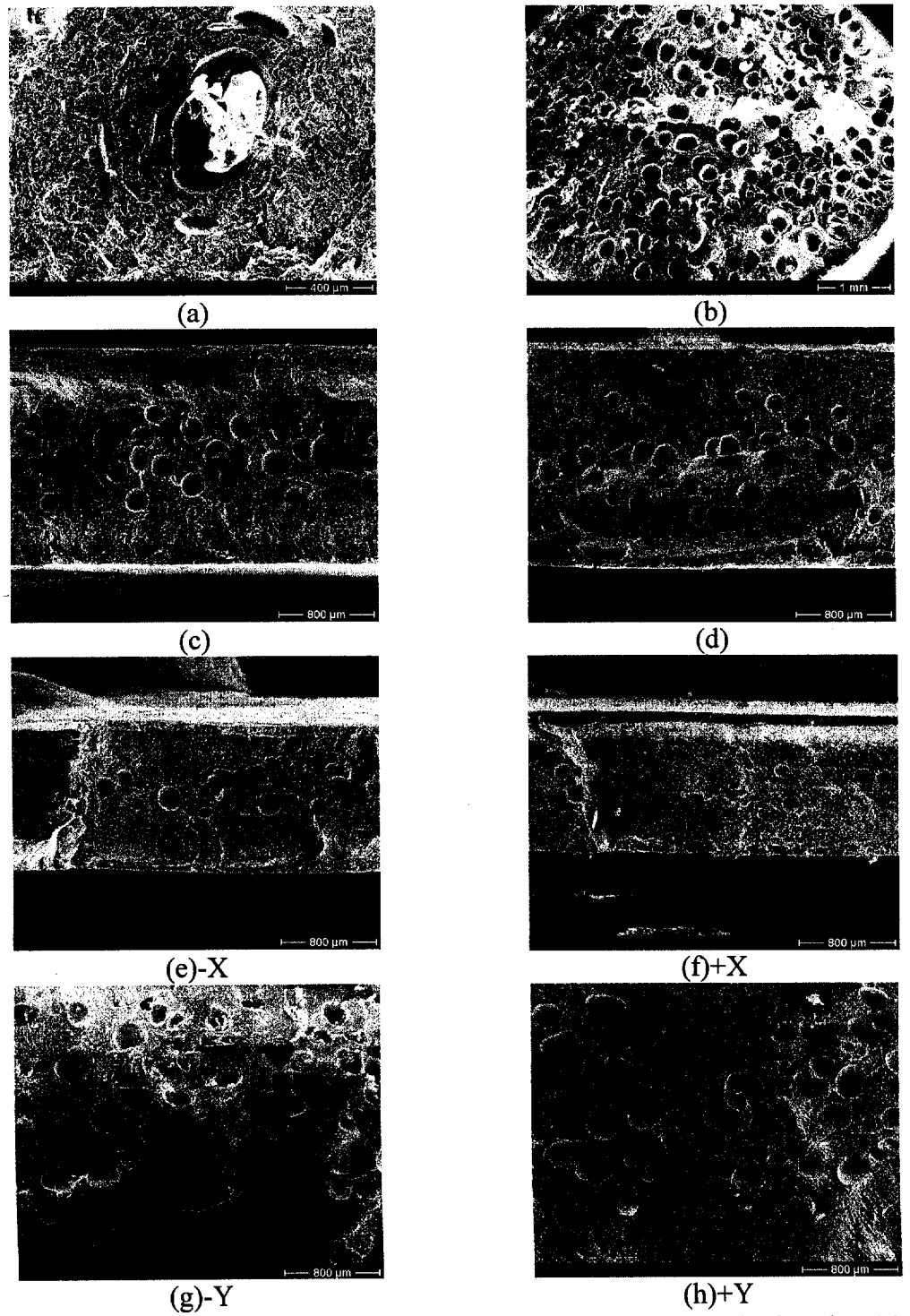

Figure 4.4 SEM images along the length of the fill for standard order 14. The locations of the images can be seen in Figure 4.3.

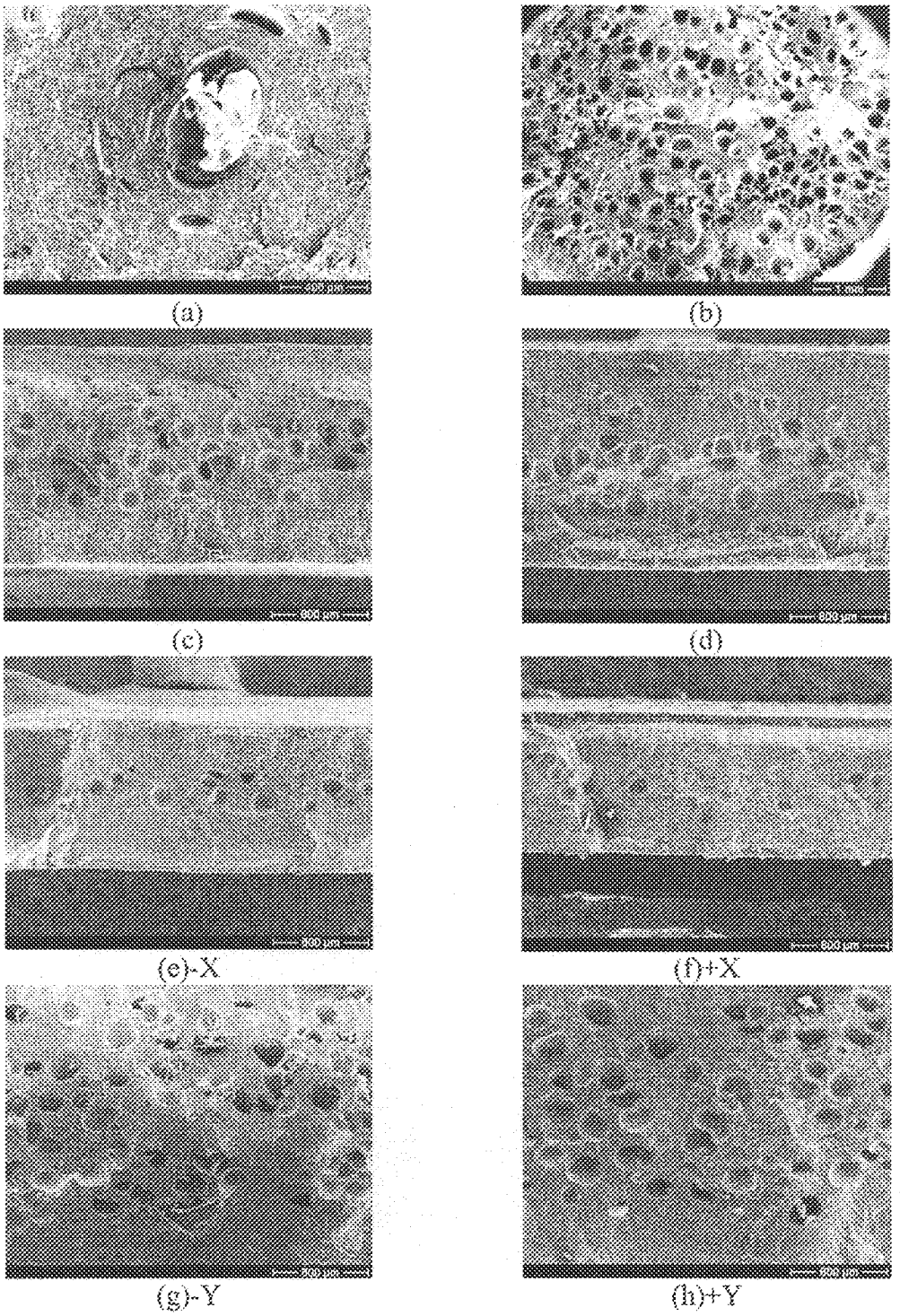

Figure 4.4 SEM images along the length of the fill for standard order 14. The locations of the images can be seen in Figure 4.3.

The density of the cells is much greater in the thicker sections of the part, most notably in the thick portion of the sprue and the two Y walls. The relatively few cells in the X walls may be attributed to three factors: 1) rapid cooling on the surface hampers cell nucleation and growth, 2) nitrogen gas diffuses out of the polymer-gas solution and escapes through the mold vents, and 3) cell embryos dissolve back into the polymer melt due to increased solubility at lower temperatures [57]. This is not to say that microcellular injection molding cannot be used for thin-wall injection molding, as it has been shown that this process is ideal for thin-wall molding due to its low viscosity [26]. The microstructure was not unexpected, however, due to the low melt strength of the PP and previous studies noting the poor cell structure when using PP. In order to achieve a higher cell density and smaller cell size, PP may be compounded with talc concentrations of 30 to 40%, which has been shown to result in a better cell structure. In this experiment, small pockets of cells with a diameter of 1 to 10 microns were discovered (cf. Figure 4.5). Such localized

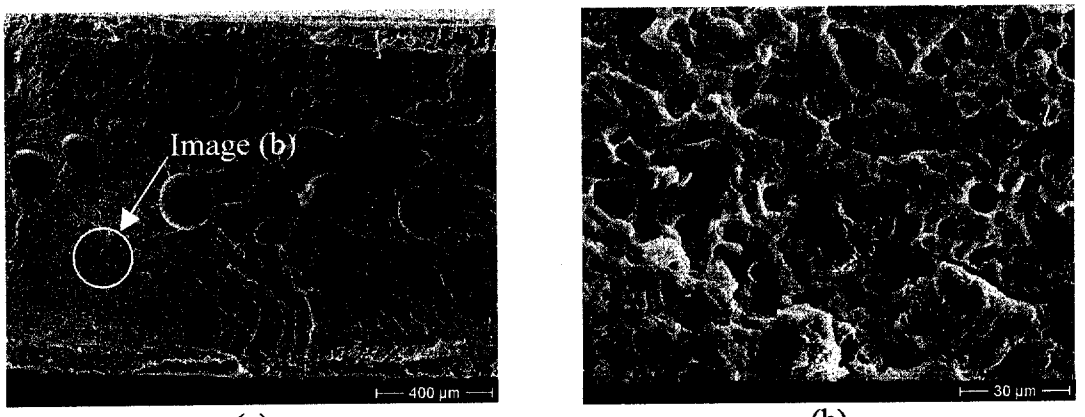

(a) (b)

Figure 4.5 (a) SEM image of the –X wall at position e for standard order 14, and (b) zoomed in view of the cell structure highlighted in image (a).

The density of the cells is much greater in the thicker sections of the part, most notably in the thick portion of the sprue and the two Y walls. The relatively few cells in the X walls may be attributed to three factors: 1) rapid cooling on the surface hampers cell nucleation and growth, 2) nitrogen gas diffuses out of the polymer-gas solution and escapes through the mold vents, and 3) cell embryos dissolve back into the polymer melt due to increased solubility at lower temperatures [57]. This is not to say that microcellular injection molding cannot be used for thin-wall injection molding, as it has been shown that this process is ideal for thin-wall molding due to its low viscosity [26]. The microstructure was not unexpected, however, due to the low melt strength of the PP and previous studies noting the poor cell structure when using PP. In order to achieve a higher cell density and smaller cell size, PP may be compounded with talc concentrations of 30 to 40%, which has been shown to result in a better cell structure. In this experiment, small pockets of cells with a diameter of 1 to 10 microns were discovered (cf. Figure 4.5). Such localized

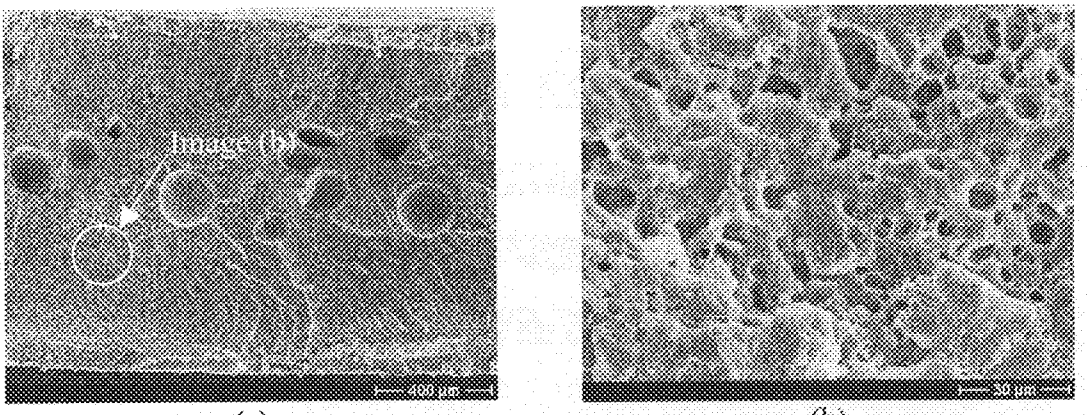

(a) (b)

Figure 4.5 (a) SEM image of the –X wall at position e for standard order 14, and (b) zoomed in view of the cell structure highlighted in image (a).

regions of small and dense cells are believed to be due to talc's effect as a nucleating agent and local talc concentrations resulting from hand mixing the talc with the polymer pellets prior to injection molding. Even with such a non-uniform cell size distribution, the result of this study suggests that the cell size and density are not as critical for achieving S&W reduction. However, a dense and uniform cell size and structure is crucial concerning the mechanical properties of microcellular injection molding parts [56].

4.4 Results and Discussion

For all four measurement directions, the wt% SCF content was the most significant factor for reducing the S&W of the microcellular injection molded box part. In all cases, increasing the wt% SCF content led to a decrease in the amount of S&W. Additionally, the maximum barrel temperature and the injection speed played a role in the S&W in the X directions, as well as the –Y direction. Using this information, optimal parameters for obtaining the part with the minimal S&W were determined and presented on the following pages.

4.4.1 The Interaction between Barrel Temperature and Injection Speed

In the –Y direction, traditional microcellular injection molding theory holds true with respect to the high injection speed. Due to the increase in injection speed, more cells are nucleated, resulting in a higher cell density and smaller cell size. The result is a wall with minimal S&W. Due to the part geometry, a large amount of race-tracking was observed in the X walls. This amount of race-tracking increased with a higher injection speed.

Therefore, while the X walls follow traditional microcellular injection molding theory with respect to lower melt temperatures leading to finer and more dense cells, it contradicts the theory by indicating that a slower injection speed minimizes the S&W. Observation of the race-tracking phenomena, pictured in Figure 4.6, gives a more graphic description of the scenario.

The race-tracking effect is amplified when using high injection speeds (cf. Figure 4.6). This phenomenon occurs due to the relatively thin X walls. The polymer easily flows along the Y walls and then wraps around to fill the X walls. This results in molecular

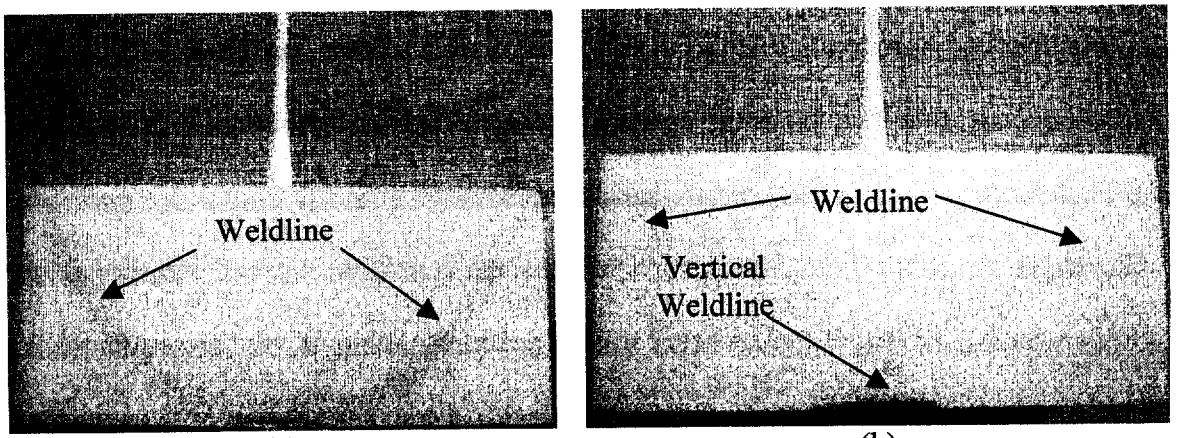

Figure 4.6 (a) Box part on the left indicates the race-tracking effect at low injection speeds. No vertical weldline is generated at these processing conditions. (b) The box part on the right incurs more race-tracking and results in a vertical weld-line in the middle of the X walls. This part is typical of high injection speeds.

Therefore, while the X walls follow traditional microcellular injection molding theory with respect to lower melt temperatures leading to finer and more dense cells, it contradicts the theory by indicating that a slower injection speed minimizes the S&W. Observation of the race-tracking phenomena, pictured in Figure 4.6, gives a more graphic description of the scenario.

The race-tracking effect is amplified when using high injection speeds (cf. Figure 4.6). This phenomenon occurs due to the relatively thin X walls. The polymer easily flows along the Y walls and then wraps around to fill the X walls. This results in molecular

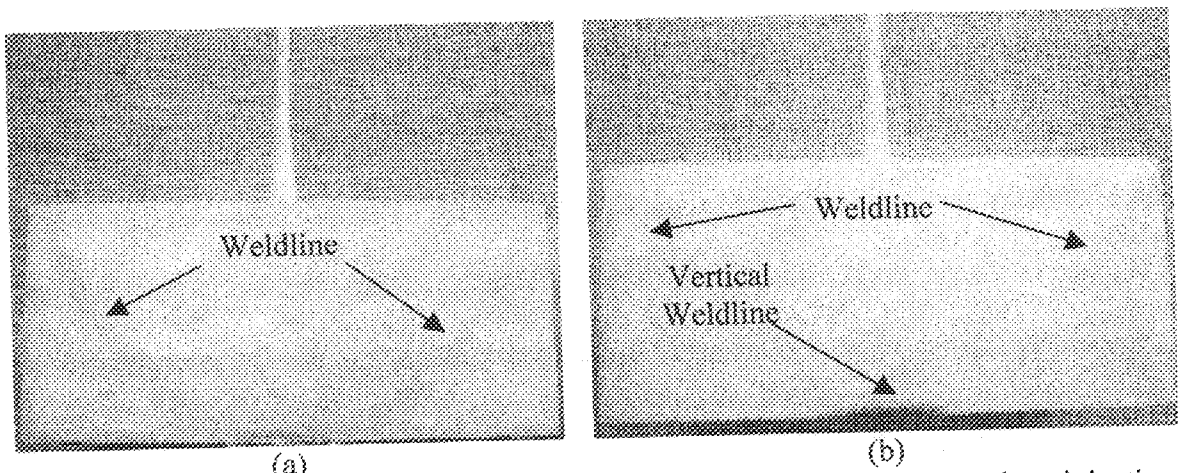

Figure 4.6 (a) Box part on the left indicates the race-tracking effect at low injection speeds. No vertical weldline is generated at these processing conditions. (b) The box part on the right incurs more race-tracking and results in a vertical weld-line in the middle of the X walls. This part is typical of high injection speeds.

orientation along the length of the wall. As the part cools, these molecules may tend to distort the X walls molded at high injection speeds more than the X walls molded at low injection speeds, due to the increased portion of the wall with molecules aligned perpendicular to the weld line on the X walls.

4.4.2 Optimal Parameters

4.4.2.1 S&W in the X directions

The optimal parameters for reducing the S&W in the X directions are fairly straightforward. Examination of the normal probability plots indicate that increasing the SCF dosage time and decreasing the maximum barrel temperature (the melt temperature) and the injection speed would result in the S&W closest to zero for the X directions. It may seem confusing then to see the optimal parameters for the best overall S&W include the high maximum barrel temperature and, in some cases, the high injection speed. This is due to the fact that the effect of these interactions is greater in the Y directions, and accommodating the Y walls gives better overall results for achieving the minimum S&W. If one were able to neglect the Y walls and their S&W response, the optimal parameters would include the lower barrel temperature and the slow injection speed. Using the regression models in Appendix 2, one can calculate the predicted S&W for each of the X directions.

4.4.2.2 S&W in the Y directions

The optimal parameters for reducing the S&W in the Y directions are more complicated than the X directions. However, the basic principle is still the same. The majority of the S&W reduction that can be realized for the Y walls in microcellular injection molding can be achieved simply by increasing the wt% SCF content (in terms of SCF dosage time in this experiment). If required, and if the S&W in the X directions is not as important as it is for the Y directions, increasing the melt temperature (the maximum barrel temperature, in this experiment) and the injection speed will further reduce the S&W. This can be attributed to the potential increase in cell density due to better cell nucleation and growth due to high injection speeds and shear nucleation [58].

4.4.2.3 Average S&W

In order to determine optimal process parameters for reducing the average S&W, the method detailed in Section 2.4.3 was used, and then compared to the actual values. The estimated average S&W for each trial, as well as the actual average S&W, can be seen in Table 4.3. This data, along with the estimated S&W for the other 32 trials, can be seen in Figure 4.7. While the results in Table 4.3 do not agree exactly, one must take into account the measurement variability, as well as machine and material fluctuations, even at constant parameter settings. These variations part quality at constant parameter settings, due to machine and material fluctuations, was discussed in Section 3.3.2.3. Furthermore, the residual analysis passed the tests/checks needed to validate the regression models.

Table 4.3 Predicted and actual S&W for each trial of the experiment.

Standard Order	Regression Model (mm)	Actual (mm)
1	0.443	0.396
2	0.096	0.101
3	0.470	0.404
4	0.121	0.118
5	0.428	0.348
6	0.090	0.073
7	0.455	0.416
8	0.116	0.228
9	0.611	0.639
10	0.224	0.199
11	0.638	0.722
12	0.251	0.186
13	0.451	0.555
14	0.092	0.051
15	0.478	0.422
16	0.119	0.152
17	0.448	0.425
18	0.101	0.126
19	0.475	0.606
20	0.123	0.134
21	0.433	0.476
22	0.095	0.100
23	0.460	0.335
24	0.122	0.207
25	0.596	0.628
26	0.210	0.148
27	0.623	0.605
28	0.237	0.241
29	0.436	0.363
30	0.077	0.107
31	0.463	0.569
32	0.104	0.047

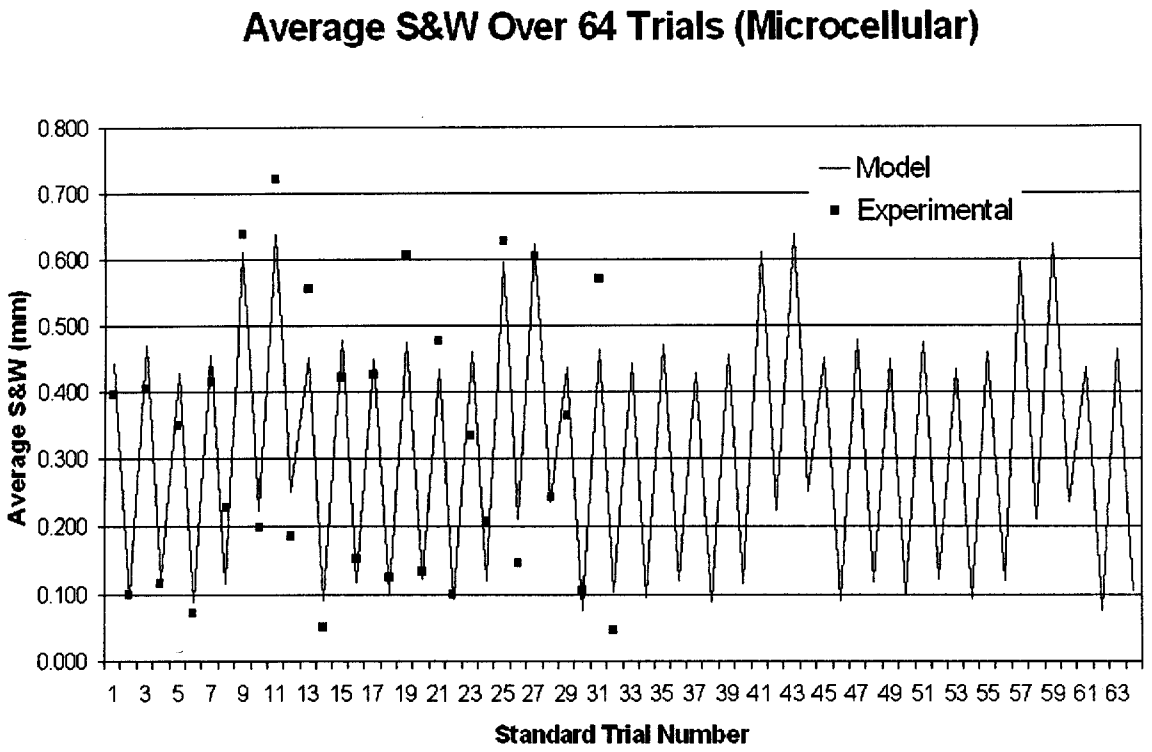

Figure 4.7 The average S&W determined from the regression models for all 64 trials. The peaks and valleys correlate to the high and low values of the SCF dosage time, which determines the wt% SCF content (cf. Figure 4.8).

Examination of the data reveals that standard order 30 has the lowest predicted S&W, while standard order 14 had the lowest actual S&W. The predicted and actual values are in the range of 0.050 mm to 0.100 mm at the best combinations of parameters. This discrepancy is exceptionally small when one examines the measurement error discussed in Section 3.3.1.1. Referring to Table 4.2, one can find the processing parameters corresponding to three trials ideal for obtaining the minimal S&W. These optimal processing conditions can be seen in Table 4.4.

Table 4.4 Optimal parameters for achieving the minimum average S&W.

Standard Order	SCF Dosage Time (sec)	Shot Volume (cm^3)	Maximum Barrel Temperature (°C)	Injection Speed (mm/sec)	Chiller Temp. (°C)	Cooling Time (sec)	Regression Model (mm)	Actual Data (mm)
30	7	51	230	120	40	32	0.077	0.107
6	7	51	230	40	20	32	0.090	0.073
14	7	51	230	120	20	44	0.092	0.051

Examination of the data indicates that increasing the SCF dosage time, or more accurately, the wt% SCF content can eliminate the majority of the S&W. From the regression models seen in Appendix 2 or the normal probability plots in Figure 4.1, the cooling time was not a significant factor for any of the four directions. Therefore, one could choose to use a 32 second cooling time and the other parameters in standard order 14 and expect similar results as those obtained in the experiment.

4.4.2.3 Wt% SCF Content

The wt% SCF content has been shown to reduce the S&W of the microcellular injection molded parts, and increasing it can potentially result in achieving near optimal results regardless of the other parameters. The average S&W at the two different wt% SCF contents can be seen in Figure 4.8. Regardless of the level of the independent variables used in the experiment, Figure 4.8 indicates that an S&W reduction of approximately 0.350 mm can be achieved just by using a higher wt% SCF content. This is important due to the fact that levels of independent variables that may result in undesirable responses (i.e., material degradation due to high barrel temperatures) can be set to minimize the undesirable response.

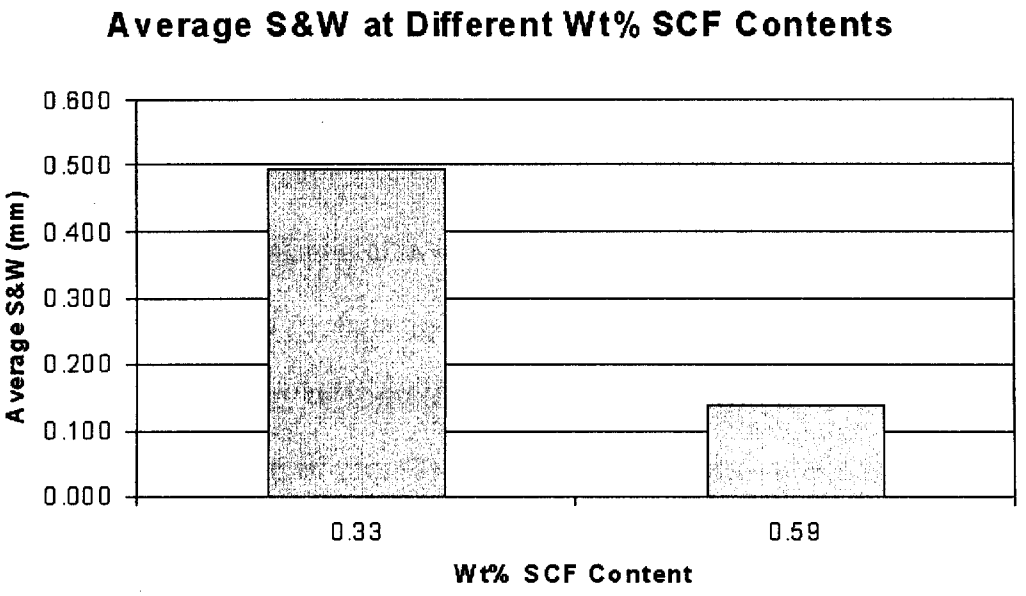

Figure 4.8 - The average S&W at the two different wt% SCF contents for microcellular injection molding.

4.4.3 Estimating the other 32 trials

Because the cooling time was not deemed significant for any of the four measurement directions, the estimation of the other 32 trials will yield the same results as those shown in Table 4.3. This is ideal, as all predicted S&W values, determined by the regression models, could be compared to the actual data.

4.4.4 Dimensional Stability

As discussed in Section 3.3.4, the standard deviation of the parts for each trial was evaluated to determine the part-to-part variation. These dimensional stability results will be compared to results from the other two experiments and discussed in the conclusions chapter of this thesis.

4.5 Chapter Summary

In order to decrease the S&W of difficult-to-mold parts, increasing the wt% SCF content will have the largest effect. Care must be used to maintain the single-phase polymer-gas solution as the polymer becomes saturated, as well as to prevent post blow upon ejection when using a high wt% SCF content. The microstructure of the PP box part has been shown to exhibit cell structure that could be classified as not ideal when discussing microcellular injection molding. This size of the cells may be improved by compounding a higher wt% of nucleating with the PP prior to injection molding. With respect to S&W, however, the cell size has shown to have little effect, as long as a wt% SCF content of around 0.59% or higher is used.

Chapter 5

Examining Shrinkage and Warpage with Microcellular Co-Injection Molding

5.1 Experiments

Microcellular co-injection molding allows a molder to capture the benefits of microcellular injection molding while maintaining several benefits of conventional injection molding. The aforementioned challenge of creating a smooth, glossy surface can be overcome using microcellular co-injection molding [35]. Experiments utilizing

DOE to determine optimal parameters for reducing the S&W of a PP box part have already been discussed for conventional and microcellular injection molding, and the results of this experiment will be compared to the previous results. The microcellular co-injection molding process is the least understood process of the three processes, and a considerable amount of preliminary experiments were run in order to determine the most influential independent variables, as well as their high and low levels. For details regarding the microcellular co-injection process used for this experiment, please refer to Section 1.6.3.

5.1.1 Preliminary Experiments

Due to the addition of the vertical injection unit, narrowing the list of independent variables was more difficult than in the previous two experiments. Independent variables that proved to have little or no significance with respect to reducing S&W in the previous experiments (i.e., cooling time) were set to constant values for this experiment. Instead of using the horizontal barrel temperature and horizontal injection speeds as independent variables, they were set to 230°C and 120 mm/sec for the duration of the experiment, based on optimal processing conditions observed for microcellular injection molding. In the place of these independent variables, the maximum vertical barrel temperature and the vertical injection speed were used. The shot volume was held constant, but the core/skin ratio was varied to produce parts with varying skin thickness and core penetration. Appendix 1 contains more information regarding variables held constant throughout the experiment. A new independent variable, the switchover time, is

introduced in this study. The switchover time is the time from the end of the skin injection to the beginning of the core injection. During simultaneous co-injection, the switchover time is not a variable. Ideally, the switchover time would be zero, because hesitation lines develop when the skin material momentarily stops flowing. The hesitation mark is further amplified because of an increase in the viscosity of the skin layer due to a reduction of the shear rate. The factors and level of the settings for the microcellular co-injection molding experiment can be seen in Table 5.1.

Table 5.1 Independent variables and their high and low settings used for the microcellular co-injection molding experiment.

Parameter Settings for Conventional Injection Molding Experiment		
Parameter	**Low (–1)**	**High (+1)**
A – SCF DOSAGE TIME (sec)	1.5	4
B – VERT. INJ. SPEED (mm/sec)	40	120
C – CHILLER TEMP (°C)	20	40
D – CORE/SKIN RATIO (cm^3/cm^3)	22/33	29/26
E – SWITCHOVER TIME (sec)	0.0	0.5
F – VERT. BARREL TEMP (°C)	205	230

These settings represent the largest processing window for producing the box part without creating a defective part. Defective parts were characterized as short shot or post blow, described in Section 4.1.1. Also described in Section 4.1.1 is the equation for calculating the wt% SCF content. In microcellular co-injection molding, it is nearly impossible to separate the core from the skin to accurately record the core shot weight. Therefore, while the wt% SCF content discussed in this chapter with respect to

microcellular co-injection molding is still calculated with equation 4.1, the shot weight is calculated with the following equation.

$$m_{part} = (V_{core} - S_{core}) * \rho_{PP} \tag{5.1}$$

where,

V_{core} is the shot volume of the core material,

S_{core} is the switchover position of the core material, and

ρ_{PP} is the density of the polypropylene (0.9 g/cm^3).

Another phenomenon prevalent in co-injection molding is breakthrough, which occurs when the core material breaks through the skin material. This defect has been studied, and has been shown to depend mainly on the core/skin ratio [59-62]. Due to the weak melt strength of the PP and the low viscosity of the core material (which enhances the core penetration), breakthrough did occur for selected trials. While attempts were made to eliminate this defect, the process window needed to be large enough to produce significant variations in the S&W of the part. Therefore, while breakthrough was not eliminated, efforts were made to minimize the number of occurrences and their magnitude. Throughout the experiment, all breakthroughs occurred at the high core/skin ratio, and were also influenced by a cool mold temperature and melt temperature of the skin (cf. Figure 5.1).

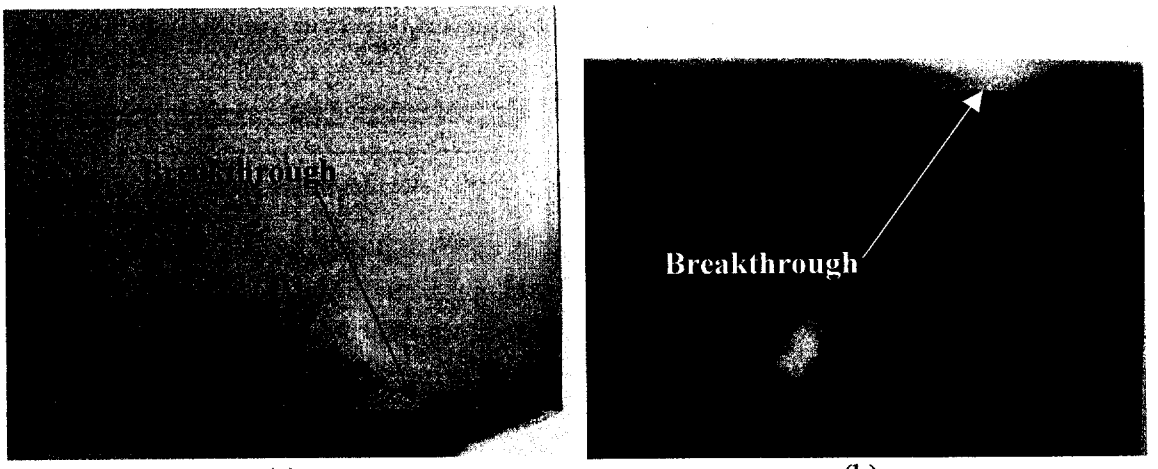

(a) (b)

Figure 5.1 (a) Side view of breakthrough on a microcellular co-injection molded part, (b) bottom view of the same part, showing a small white spot where the foamed core has broken through the solid skin layer.

5.1.2 DOE

The 2^{6-1} fractional factorial DOE used for this study consisted of 32 trials run in random order. The random order was determined using a random number generator, and the predetermined steady state conditions were met before switching from one trial to the next. Ten parts were collected for each trial, and parts five through nine were then measured to determine the S&W as described in Section 2.4. The DOE matrix used for this experiment can be seen in Table 5.2.

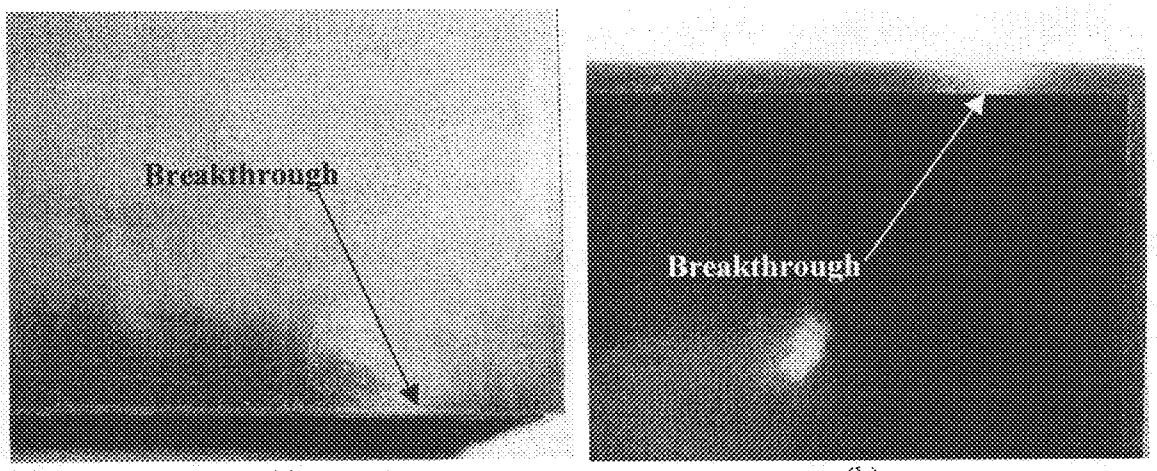

(a) (b)

Figure 5.1 (a) Side view of breakthrough on a microcellular co-injection molded part, (b) bottom view of the same part, showing a small white spot where the foamed core has broken through the solid skin layer.

5.1.2 DOE

The 2^{6-1} fractional factorial DOE used for this study consisted of 32 trials run in random order. The random order was determined using a random number generator, and the predetermined steady state conditions were met before switching from one trial to the next. Ten parts were collected for each trial, and parts five through nine were then measured to determine the S&W as described in Section 2.4. The DOE matrix used for this experiment can be seen in Table 5.2.

Table 5.2 2^{6-1} DOE matrix used for microcellular co-injection molding experiment, shown in standard order.

Standard Order	SCF Dosage Time (sec)	Vertical Injection Speed (mm/sec)	Chiller Temp (°C)	Core/ Skin Ratio	Switchover Time (sec)	Max Vertical Barrel Temp (°C)	Trial Number
1	1.5	40	20	40	0.0	205	23
2	4	40	20	40	0.0	230	17
3	1.5	120	20	40	0.0	230	9
4	4	120	20	40	0.0	205	32
5	1.5	40	40	40	0.0	230	18
6	4	40	40	40	0.0	205	12
7	1.5	120	40	40	0.0	205	1
8	4	120	40	40	0.0	230	6
9	1.5	40	20	53	0.0	230	7
10	4	40	20	53	0.0	205	14
11	1.5	120	20	53	0.0	205	25
12	4	120	20	53	0.0	230	19
13	1.5	40	40	53	0.0	205	15
14	4	40	40	53	0.0	230	11
15	1.5	120	40	53	0.0	230	28
16	4	120	40	53	0.0	205	22
17	1.5	40	20	40	0.5	230	2
18	4	40	20	40	0.5	205	31
19	1.5	120	20	40	0.5	205	3
20	4	120	20	40	0.5	230	27
21	1.5	40	40	40	0.5	205	4
22	4	40	40	40	0.5	230	29
23	1.5	120	40	40	0.5	230	30
24	4	120	40	40	0.5	205	21
25	1.5	40	20	53	0.5	205	24
26	4	40	20	53	0.5	230	8
27	1.5	120	20	53	0.5	230	16
28	4	120	20	53	0.5	205	20
29	1.5	40	40	53	0.5	230	26
30	4	40	40	53	0.5	205	10
31	1.5	120	40	53	0.5	205	13
32	4	120	40	53	0.5	230	5

5.2 Analysis

With proper planning and execution, the analysis portion of a DOE can be relatively straightforward. The analysis involves examination of the normal probability plots, interaction diagrams, and a series of tests/checks on the residuals. This analysis is detailed in the following sections for microcellular co-injection molding.

5.2.1 Normal Probability Plots

Normal probability plots for the –X, +X, –Y, and +Y directions are shown in Figure 5.2. These were used to determine significant main and interaction effects. From these four normal probability plots, it can be seen that increasing the SCF dosage time has the most significant effect on reducing the S&W for all four directions. This is in direct agreement with the results from the microcellular injection molding experiment. The core/skin ratio is highly correlated to the SCF dosage time through the wt% SCF content. The wt% SCF content is calculated using equations 4.1 and 5.1, and the amount of core material has a large effect on the wt% SCF content. This will be discussed in the results and discussion section.

The injection speed and chiller temperature effects fall on the right side of the normal probability plot. This means that decreasing these independent variables will decrease the S&W for both X directions. These injection speed results also agree directly with the previous study involving microcellular injection molding. When discussing the chiller

temperature, the cooling rate of the skin, the skin thickness, and the core penetration will all vary, and will be discussed further.

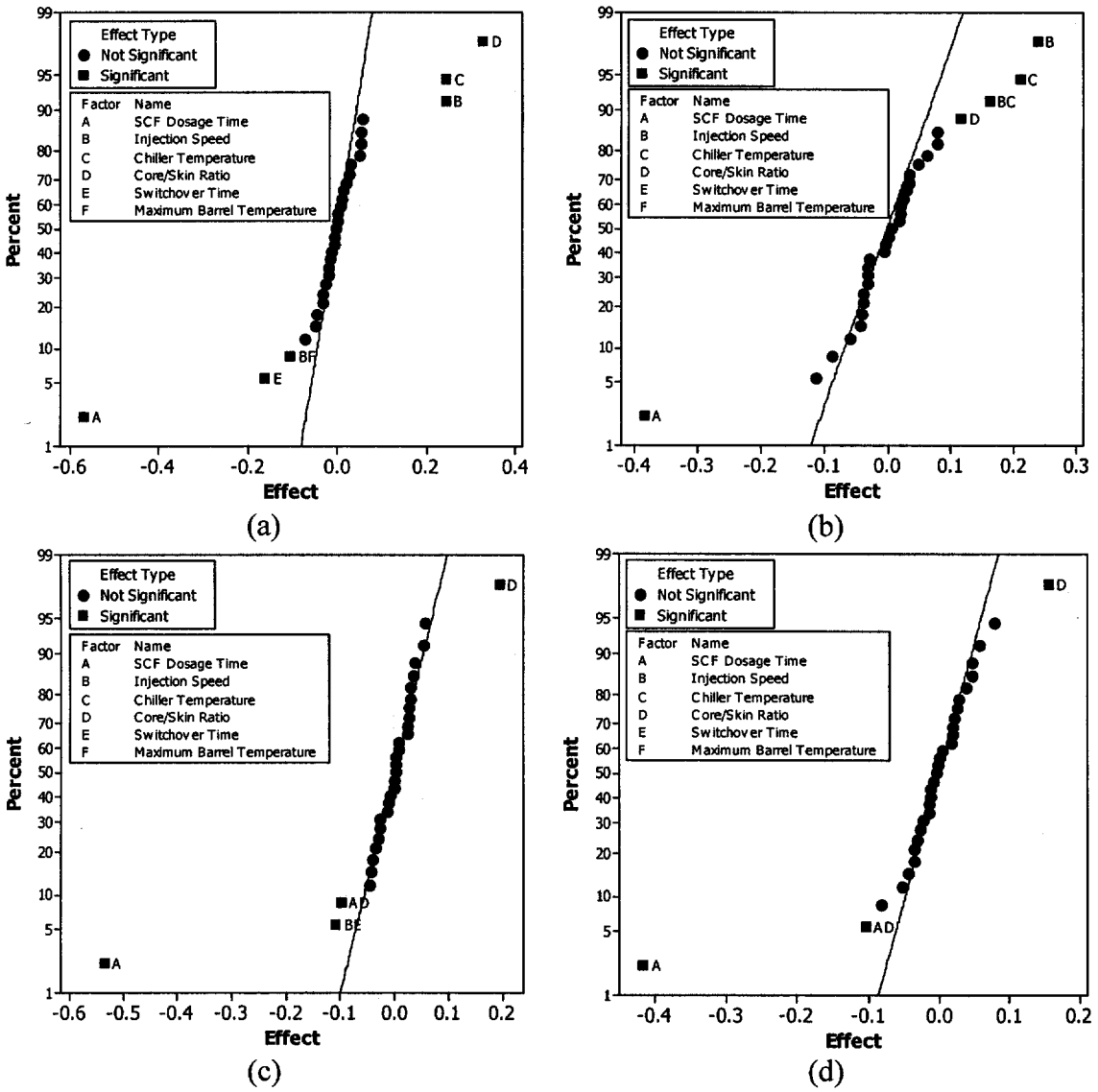

Figure 5.2 Normal probability plots for microcellular co-injection molding in the (a) –X direction, (b) +X direction, (c) –Y direction, and (d) +Y direction.

5.2.2 Interaction Diagrams

Using two-factor interaction diagrams, the interaction effects between SCF dosage time and core/skin ratio will be explored. Three other interaction effects exist, but each of the three exists for only one of the four directions. Therefore, these will be discussed briefly and the diagrams are shown in Appendix 3 (A.19 through A.21).

5.2.2.1 SCF Dosage Time and the Core/Skin Ratio

The interaction between the SCF dosage time and the core/skin ratio for the –Y and +Y directions can be seen in Figure 5.3. One can see at the low SCF dosage time, the core/skin ratio has a much larger effect than at the high SCF dosage time. This occurs because of the correlation between the SCF dosage time and the core/skin ratio. One needs to examine the effect of the wt% SCF content at each of the four processing conditions. It can be hypothesized that the two wt% SCF contents at the high SCF dosage times are high enough so that the difference between them has little effect on the S&W (they are different due to the different core/skin ratio). At the low SCF dosage time, the wt% SCF content is highly influenced by the core/skin ratio, resulting in drastic differences in the S&W reduction. A more in-depth analysis including the estimated wt% SCF contents will be shown in the results and discussion section.

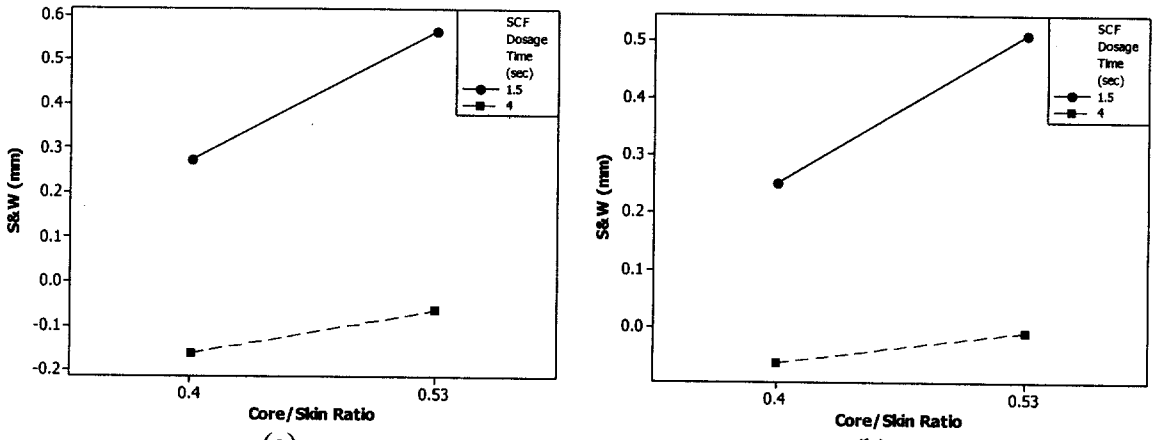

Figure 5.3 Interaction between the SCF dosage time and the core/skin ratio for microcellular co-injection molding in the (a) –Y direction, and (b) +Y direction.

5.2.2.2 Other Interactions

Three other interaction effects existed in the microcellular co-injection molding experiments. The results of these interactions may be viewed in Appendix 3 (A.19 through A.21). These three interactions were only significant for one direction, and analyzing them in detail would not lend any insight into determining the optimal parameters for minimizing the S&W in all four directions. These interaction effects were included in the regression models for predicting the S&W, but are not detailed due to their relative insignificance and lack of consistency throughout the four measurement directions.

5.3 SEM Analysis

As in Section 4.3, SEM images were used to examine the microstructure of microcellular co-injection molded parts using a JEOL JSM-6100 scanning electron microscope (SEM). Images of the microstructure were taken along the flow length of the box part as shown in Figure 4.3. Figure 5.4 displays the microstructure along the length of fill for standard trial 4. This trial exhibited excellent S&W results, and this microstructure was compared to the microstructure of standard trial 15 (cf. Figure 5.5), which exhibited very poor S&W results. These results will be discussed in detail in Section 5.4. The purpose of analyzing the microstructure is to determine if cell size or cell density plays a major role in determining the S&W of the PP box part.

Comparison of these SEM images shows differences in cell size and cell density at every position along the length of fill and at all four walls. Review of Table 5.2 indicates that these two trials have different settings for:

- SCF Dosage Time
- Chiller Temperature
- Core/Skin Ratio
- Maximum Barrel Temperature

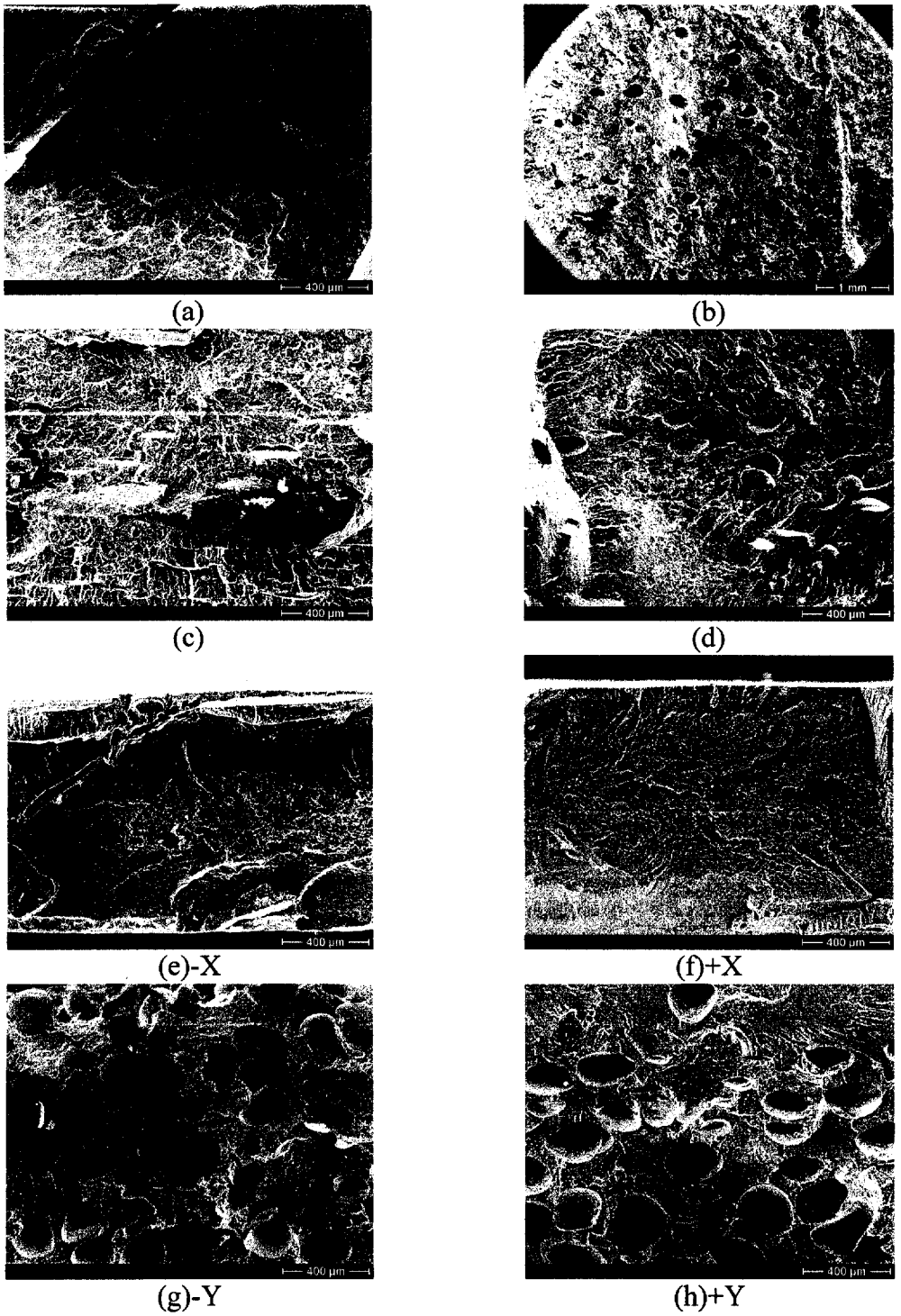

Figure 5.4 SEM images along the length of the fill for standard order 4. The locations of the images can be seen in Figure 4.3.

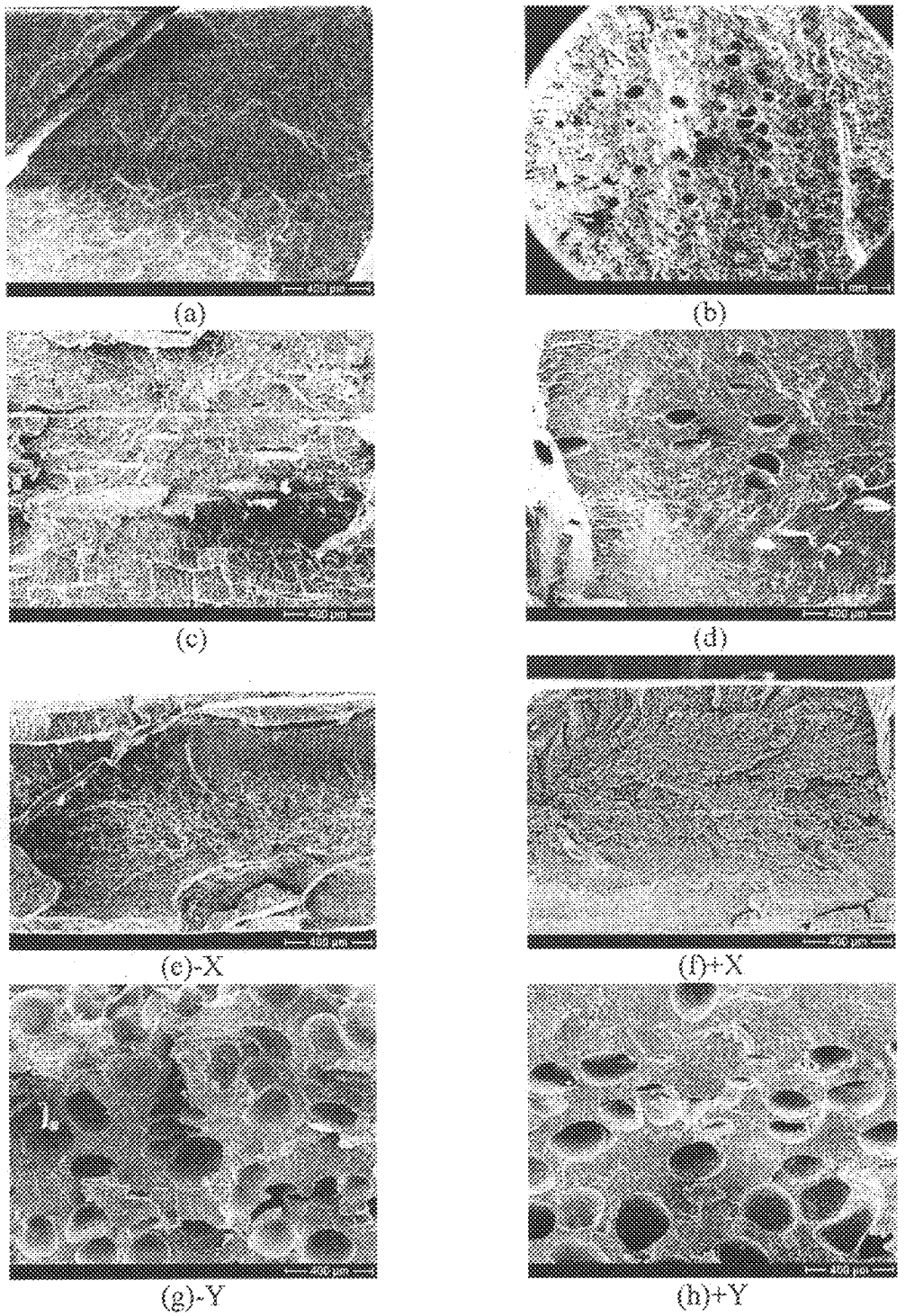

Figure 5.4 SEM images along the length of the fill for standard order 4. The locations of the images can be seen in Figure 4.3.

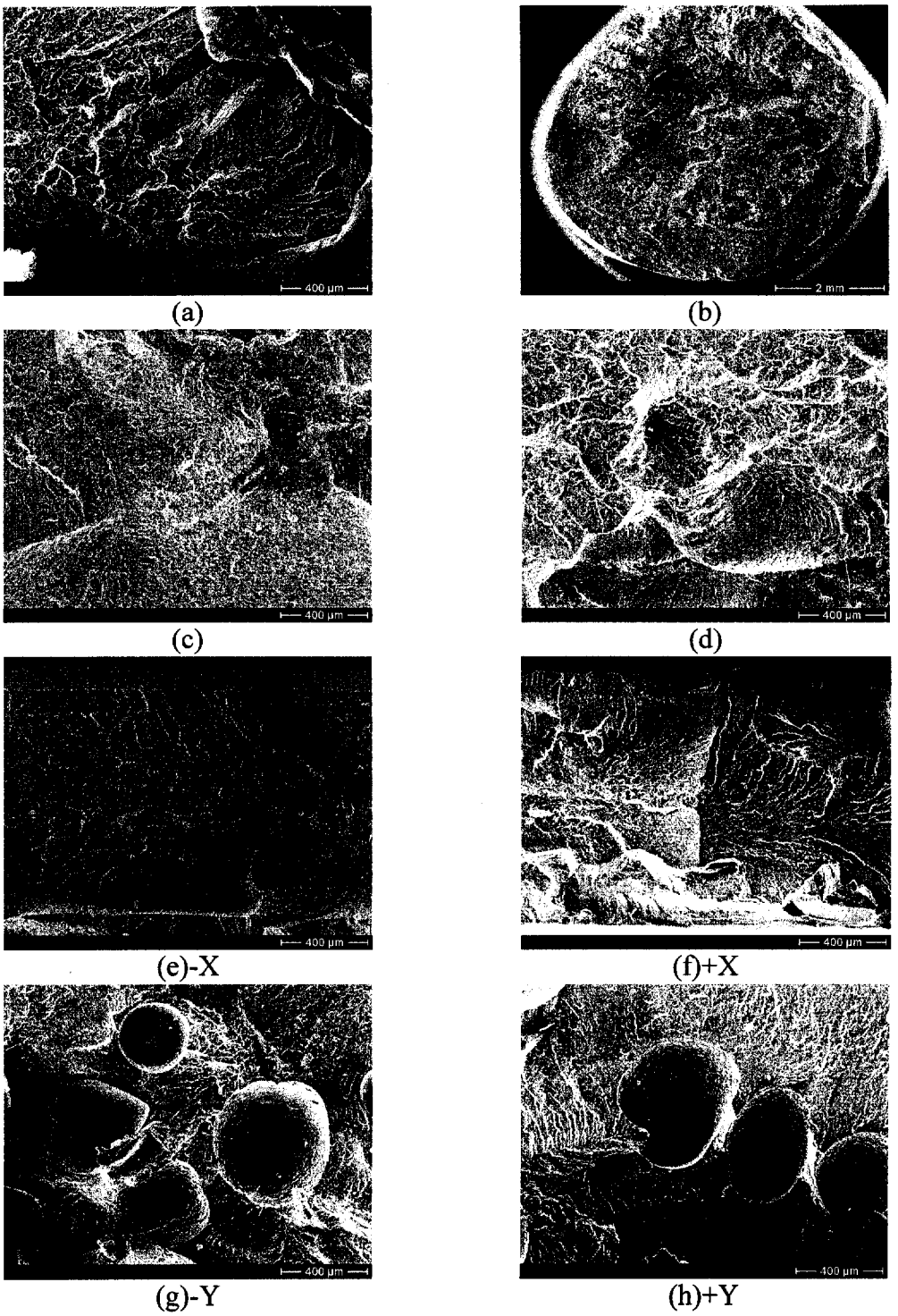

Figure 5.5 SEM images along the length of the fill for standard order 15. The locations of the images can be seen in Figure 4.3.

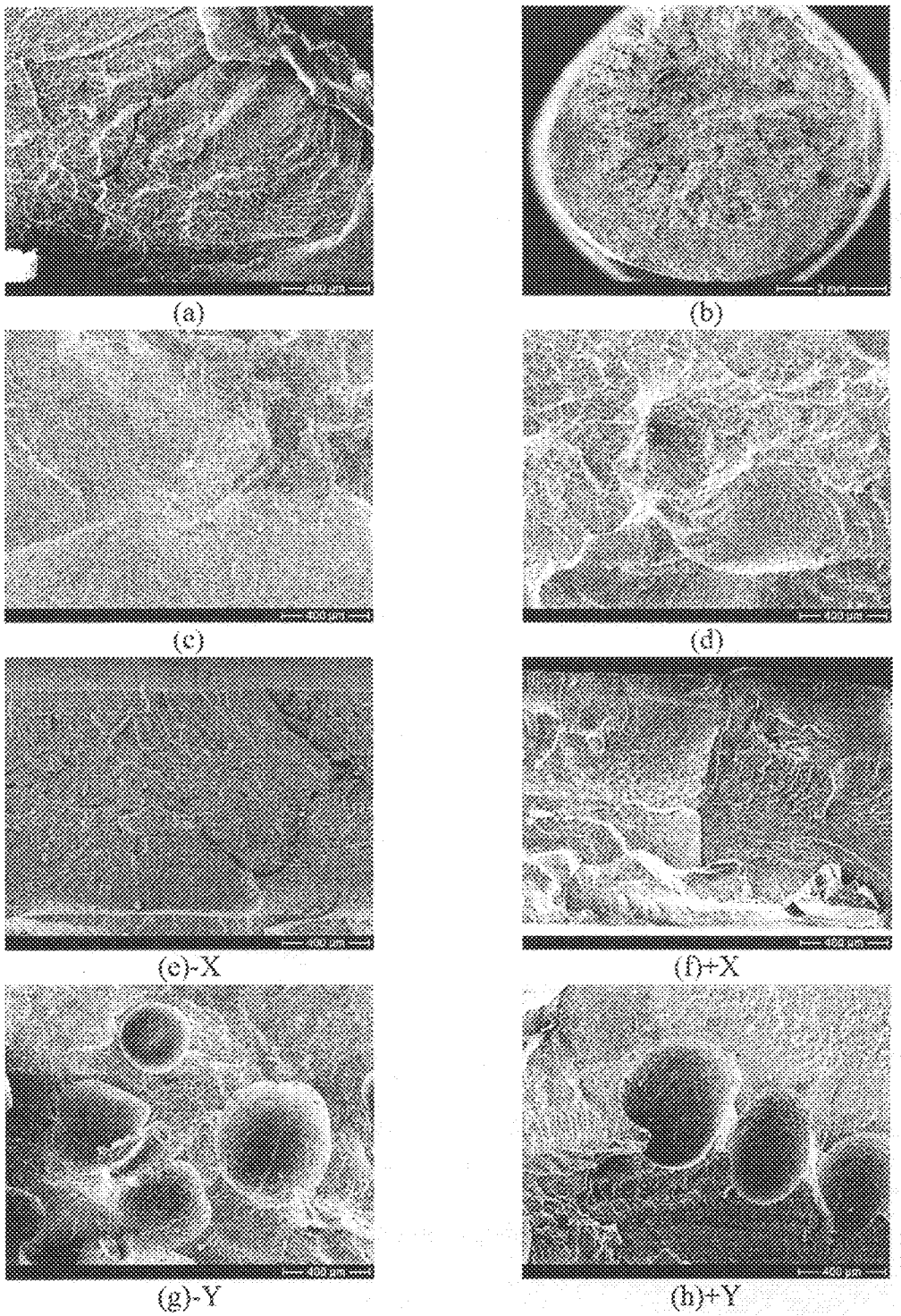

Figure 5.5 SEM images along the length of the fill for standard order 15. The locations of the images can be seen in Figure 4.3.

These differences correlate mainly to a difference in the wt% SCF content, a lower melt temperature, and a faster cooling rate. The increase in cooling rate and the decrease in melt temperature increases the melt strength of the polymer, and hinders the cell growth. Also, the increase in the wt% SCF content reduces the cell size due to increased nucleation [15, 25].

5.4 Results and Discussion

Directly correlating to the microcellular injection molding study, the SCF dosage time had the most influence on reducing the S&W. Additionally, the core/skin ratio played a role in determining the minimum S&W due to the core penetration and its importance, along with the SCF dosage time, in determining the wt% SCF content.

5.4.1 Wt% SCF Content

The wt% SCF content for the four combinations of parameter settings has been evaluated. Examination of the data indicated that the switchover position occurred at 3 cm^3 throughout the experiment. Therefore, using equation 5.1, the core shot weight was calculated to be 23.4 g and 17.1 g for the high and low core/skin ratios, respectively. Using equation 4.1, the wt% SCF content levels can be found in Table 5.3.

Table 5.3 The wt% SCF content resulting from different parameter settings.

SCF Dosage Time (sec)	Core/Skin Ratio	Wt% SCF Content
1.5	0.53	0.196
1.5	0.4	0.268
4	0.53	0.523
4	0.4	0.715

It can be seen that the wt% SCF content varies most greatly due to the SCF dosage time. However, given a fixed SCF dosage time, a smaller core/skin ratio (meaning less core material) would lead to a higher wt% SCF content. In the microcellular injection molding experiments, excellent results were obtained using a maximum wt% SCF content of 0.59%. The decrease in the S&W due to the increase in the SCF dosage time and decrease in the core/skin ratio is significant until the wt% SCF content approaches 0.5% and begins to plateau around 0.7%. This is clearer when viewing the average S&W versus the SCF dosage time and the wt% SCF content in Figures 5.6 and 5.7, respectively. The slight trend upward in S&W at 0.715 wt% SCF content in Figure 5.7 may be attributed to different core penetrations, and will be discussed below.

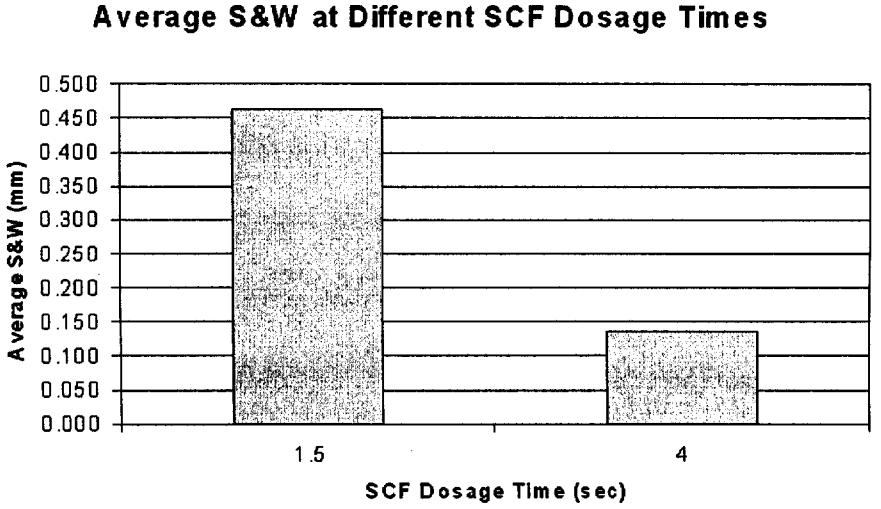

Figure 5.6 The average S&W of the walls at the high and low SCF dosage times.

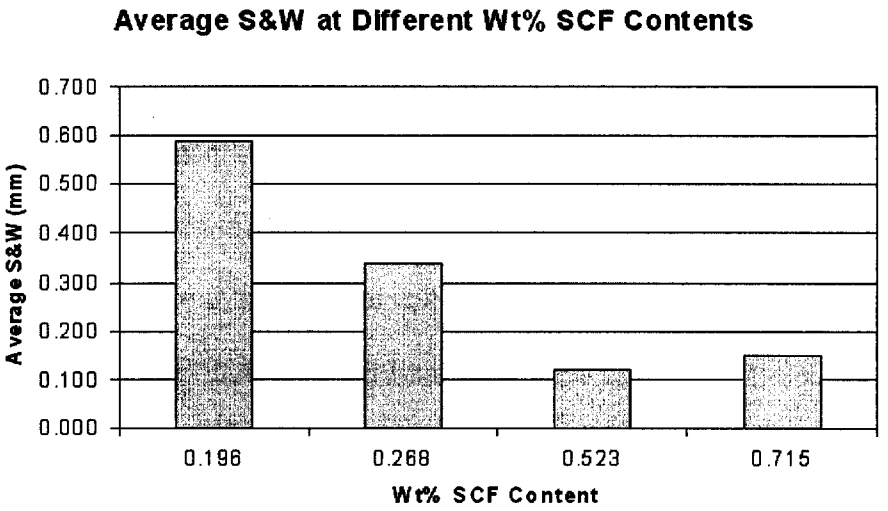

Figure 5.7 The average S&W of the walls at the various wt% SCF contents. The slight trend upward at 0.715% may be attributed to a lack of core penetration.

5.4.2 Optimal Parameters

5.4.2.1 S&W in the X directions

There are several combinations of parameters that will result in minimal S&W in the X directions. Examining the normal probability plots and using them to determine the optimal parameters may result in error due to the direction of the S&W response. Examination of the regression models show that setting the parameters to achieve the minimum S&W will actually result in a part that is warped outward on some walls. Because of the complex relationship, the direction and magnitude of the effects must be taken into account, and the regression models in Appendix 2 should be used.

5.4.2.2 S&W in the Y directions

The optimal parameter settings for the Y directions depend on the SCF dosage time and the core/skin ratio. We have seen from the microcellular injection molding results that increasing the wt% SCF content will lead to better S&W results. However, in the case of microcellular co-injection molding, as seen in Figure 5.7, the average S&W actually increases (very slightly, however) at the high wt% SCF content. Because of the dependence of the wt% SCF content on the core shot volume and the SCF dosage time, we actually have much less core penetration at the high wt% SCF content. This is probably the reason for the slight increase in S&W at the high wt% SCF content. If one were to maintain the same wt% SCF content with different levels of core penetration, one could assume that better S&W results would be obtained with more core penetration. In this study, a more in-depth look at the effects of the wt% SCF content and the core penetration will be presented later in this chapter.

5.4.2.3 Average S&W

In order to determine the optimal process parameters for reducing the average S&W, the method detailed in 2.4.3 was used, and then compared to the actual values. The estimated average S&W for each trial, as well as the actual average S&W, can be seen in Table 5.4.

Table 5.4 Predicted and actual S&W for each trial of the experiment.

Standard Order	Regression Model (mm)	Actual (mm)
1	0.233	0.217
2	0.172	0.172
3	0.344	0.171
4	0.074	0.080
5	0.326	0.398
6	0.129	0.113
7	0.532	0.608
8	0.150	0.184
9	0.503	0.447
10	0.088	0.049
11	0.627	0.722
12	0.073	0.071
13	0.557	0.485
14	0.124	0.046
15	0.750	0.803
16	0.261	0.341
17	0.239	0.394
18	0.205	0.272
19	0.309	0.282
20	0.174	0.205
21	0.293	0.297
22	0.123	0.187
23	0.432	0.383
24	0.173	0.184
25	0.470	0.403
26	0.082	0.081
27	0.527	0.507
28	0.088	0.090
29	0.563	0.630
30	0.052	0.080
31	0.715	0.674
32	0.210	0.192

This data, along with the estimated S&W for the other 32 trials, can be seen in Figure 5.8. While the results in Table 5.4 do not agree exactly, one must take into account the

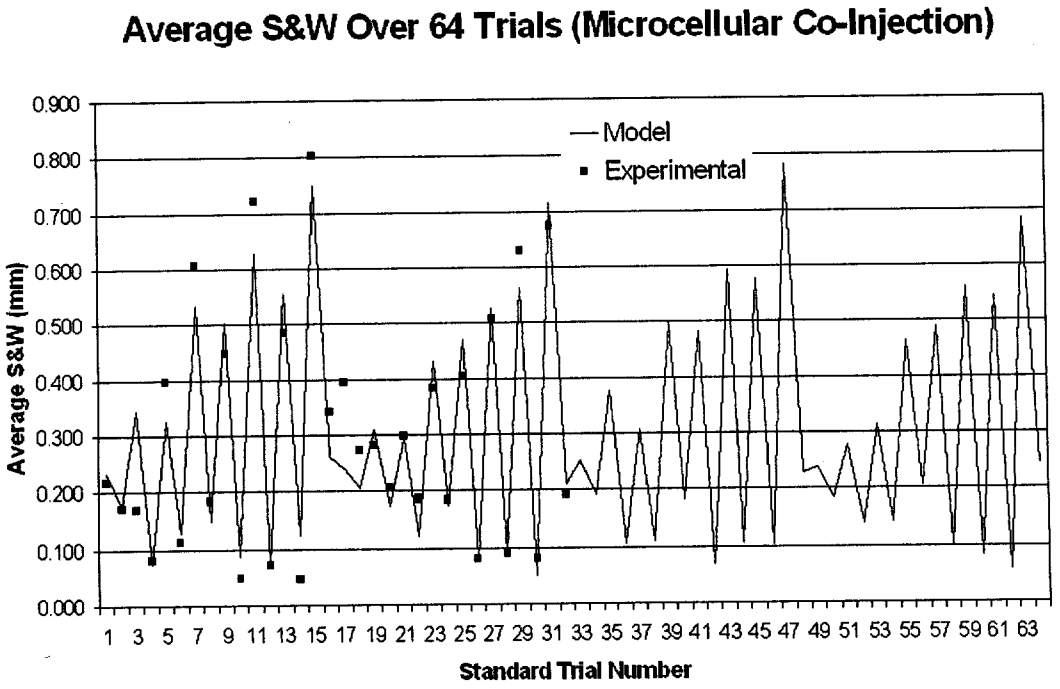

Figure 5.8 The average S&W determined from the regression models for all 64 trials. The peaks and valleys correlate to the high and low values of the SCF dosage time, which determines the wt% SCF content.

measurement variability, as well as machine and material fluctuations, even at constant parameter settings. These variations in part quality at constant parameter settings, due to machine and material fluctuations, were discussed in Section 3.3.2.3. Furthermore, the residual analysis passed the tests/checks needed to validate the regression models.

Examination of the data reveals that several combinations of parameters result in S&W of less than 100 microns on average in the four directions. These combinations of parameters show virtually identical results when comparing the regression model and the

actual results from the experiment. Visual examination of these parts can provide no further insight into the difference in the S&W, as it is not possible to detect variation in the warpage of the walls on the order of microns. The optimal processing conditions for the microcellular co-injection molding experiment can be seen in Table 5.5.

Table 5.5 Optimal parameters for achieving the minimum average S&W.

Standard Order	SCF Dosage Time (sec)	Vert. Injection Speed (mm/sec)	Chiller Temp. (°C)	Core/Skin Ratio	Switchover Time (°C)	Max. Vert. Barrel Temp. (°C)
30	4	40	40	0.53	0.5	205
12	4	120	20	0.53	0	230
4	4	120	20	0.4	0	205
26	4	40	20	0.53	0.5	205
28	4	120	20	0.53	0.5	205
10	4	40	20	0.53	0	205

With the exception of standard orders 30 and 4, which have a different chiller temperature and core/skin ratio, respectively, all of the optimal parameter settings include the maximum SCF dosage time and core/skin ratio, and the minimum chiller temperature. As mentioned previously, the wt% SCF content appears to have little increasing benefits above 0.5%, so the benefit of more core penetration seems to aid in reducing the S&W by using a higher core/skin ratio. Additionally, the cool chiller temperature leads to a cooler mold. This cooler mold also enhances the core penetration by creating a thicker skin layer.

5.4.4 Estimating the other 32 trials

Using the regression models, the other 32 possible combinations of parameters can be evaluated. While there is no actual data for these parameter combinations, residual analysis provided the means by which to accept the estimated result as accurate. Table 5.6 displays the estimated S&W value for three parameter combinations. Since these are based on the regression models, no actual data is present to compare them to. However, the results for obtaining minimal S&W agree with the results from Table 5.5, namely a high SCF dosage time, high core/skin ratio, and high vertical barrel temperature.

Table 5.6 Estimated S&W for the other 32 trials.

St. Order	SCF Dosage Time (sec)	Vertical Inj. Speed (mm/sec)	Chiller Temp. (°C)	Core/Skin Ratio	Switchover Time (sec)	Max. Vert. Barrel Temp. (°C)	Regression Model (mm)
n/a	4	40	40	0.53	0.5	230	0.057
n/a	4	40	20	0.53	0.0	230	0.069
n/a	4	120	20	0.53	0.5	230	0.083

5.4.5 Core Penetration

Based on equations 4.1 and 5.1, the wt% SCF content can be calculated for different SCF dosage times and core/skin ratios, and is shown in Table 5.3. It is obvious that the wt% SCF content will be highest at the maximum SCF dosage time and the minimum core/skin ratio. However, this high wt% SCF content also means that the core penetration will be less, due to the low core/skin ratio.

In this study, it was shown that increasing the wt% SCF content above 0.5% has little effect on further reducing the S&W. Because of the high wt% SCF content with the low

core/skin ratio, the S&W results based on differing core penetrations were similar, due to the high wt% SCF content compensating for the lack of core penetration. In fact, comparing the S&W of standard orders 4 and 26 shows near identical results (cf. Table 5.4). Examination of the core penetration shows stark contrasts however, as shown in Figure 5.9.

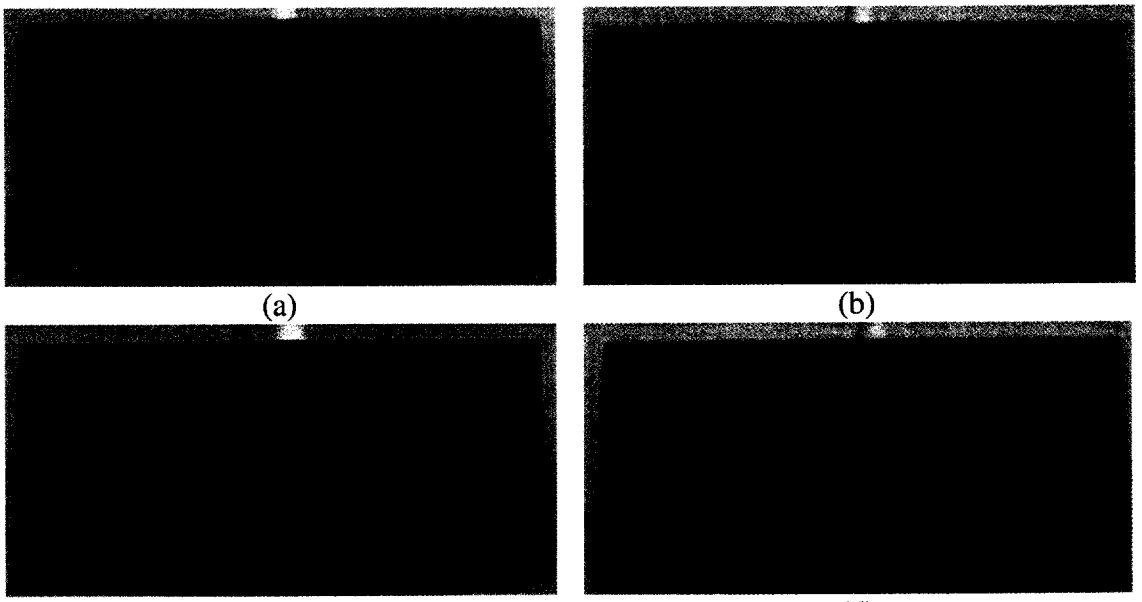

Figure 5.9 (a) The core penetration along the –X wall for standard order 4, (b) the core penetration along the –X wall for standard order 26, (c) the core penetration along the –Y wall for standard order 4, and (d) the core penetration along the –Y wall for standard order 26.

These results indicate that with either high or low core penetration, excellent S&W results can be obtained with microcellular co-injection molding. Using a high core/skin ratio would be ideal for molders wanting to use a commodity resin or regrind as their core

core/skin ratio, the S&W results based on differing core penetrations were similar, due to the high wt% SCF content compensating for the lack of core penetration. In fact, comparing the S&W of standard orders 4 and 26 shows near identical results (cf. Table 5.4). Examination of the core penetration shows stark contrasts however, as shown in Figure 5.9.

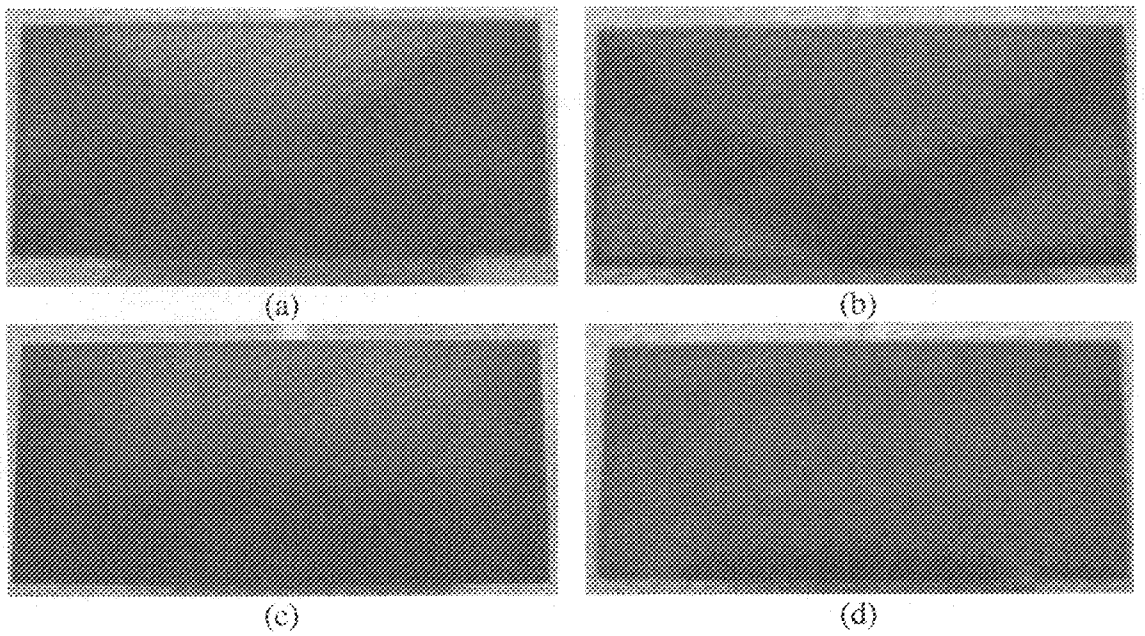

Figure 5.9 (a) The core penetration along the –X wall for standard order 4, (b) the core penetration along the –X wall for standard order 26, (c) the core penetration along the –Y wall for standard order 4, and (d) the core penetration along the –Y wall for standard order 26.

These results indicate that with either high or low core penetration, excellent S&W results can be obtained with microcellular co-injection molding. Using a high core/skin ratio would be ideal for molders wanting to use a commodity resin or regrind as their core

material. Additionally, if a molder was molding parts with a complex geometry and breakthrough was a common defect, it might be possible to use less core material and still obtain the desired reduction in S&W, all while minimizing the possibility of breakthrough. This research indicates that at low core penetration and high wt% SCF content, it is indeed possible to obtain results similar to those obtained with the high core penetration. With microcellular co-injection molding, the estimated average S&W of each wall was 0.052 mm, and the actual average S&W was 0.046 mm.

5.4.6 Dimensional Stability

As discussed in Section 3.3.4, the standard deviation of the parts for each trial was evaluated to determine the part-to-part variation. These dimensional stability results will be compared to results from the other two experiments and discussed in the conclusions chapter of this thesis.

5.5 Chapter Summary

In order to effectively reduce the S&W of the PP box part, increasing the wt% SCF content will have the most significant impact. The increase in wt% SCF content increases the cell density and decreases the cell size. The results indicate that the core penetration further reduces the S&W when the wt% SCF content is held constant. However, it was observed that the core penetration is not critical for reducing the S&W, and may allow for increased S&W reduction in geometrically complex parts while reducing the possibility of breakthrough.

Chapter 6

Conclusions

In this research, three injection molding studies were run separately in order to investigate the effects of process parameters on the shrinkage and warpage (S&W) of a PP box part. The S&W results from the conventional injection molding, microcellular injection molding, and microcellular co-injection molding were compared in order to quantitatively define the reduction in S&W achievable with each process. The microstructure of the microcellular injection molded parts and the microcellular co-injection molded parts was examined and compared. Utilizing design of experiments (DOE) for each of the experiments, significant main and two-factor interaction effects were identified and investigated to gain a better understanding of the process dynamics.

The dimensional stability of the parts resulting from each process was examined, as was the average weight reduction for the three processes. These results have been compiled to further the knowledge of microcellular injection molding and microcellular co-injection molding, focusing on optimal process parameters for reducing the S&W for each process. The results and comparison of these three experiments are presented below.

6.1 Quantitative Comparison of S&W

In Chapters 3 through 5, figures displaying the estimated average S&W over the course of 64 trials were presented. These results are compiled into Figure 6.1, making it easy to compare the average S&W at the different combinations of process parameters. Quantitative comparisons of these numbers indicate it is possible to reduce the S&W of the PP box part using microcellular injection molding and microcellular co-injection molding by approximately 90% when compared to conventional injection molding at optimal parameters. This is due to the absence of the high pressure pack/hold stage in microcellular injection molding and microcellular co-injection molding, as well as the extended and homogeneous packing pressure due to the nucleation and growth of the cells throughout the cavity. Increasing the wt% SCF content for the microcellular injection molding and microcellular co-injection molding will result in the best S&W reduction results. Increasing the wt% SCF content can be accomplished without adding any costs to the molded part due to the fact that the nitrogen is constantly flowing, whether or not it is being injected into the barrel. However, one must take into account that as the wt% SCF content is increased, so is the possibility of post blow and the

polymer-gas solution coming out of single-phase. Therefore, excessively increasing the wt% SCF content may result in an increase in cycle time due to the longer cooling cycle needed, or inconsistent part quality due to the lack of the single-phase polymer-gas solution.

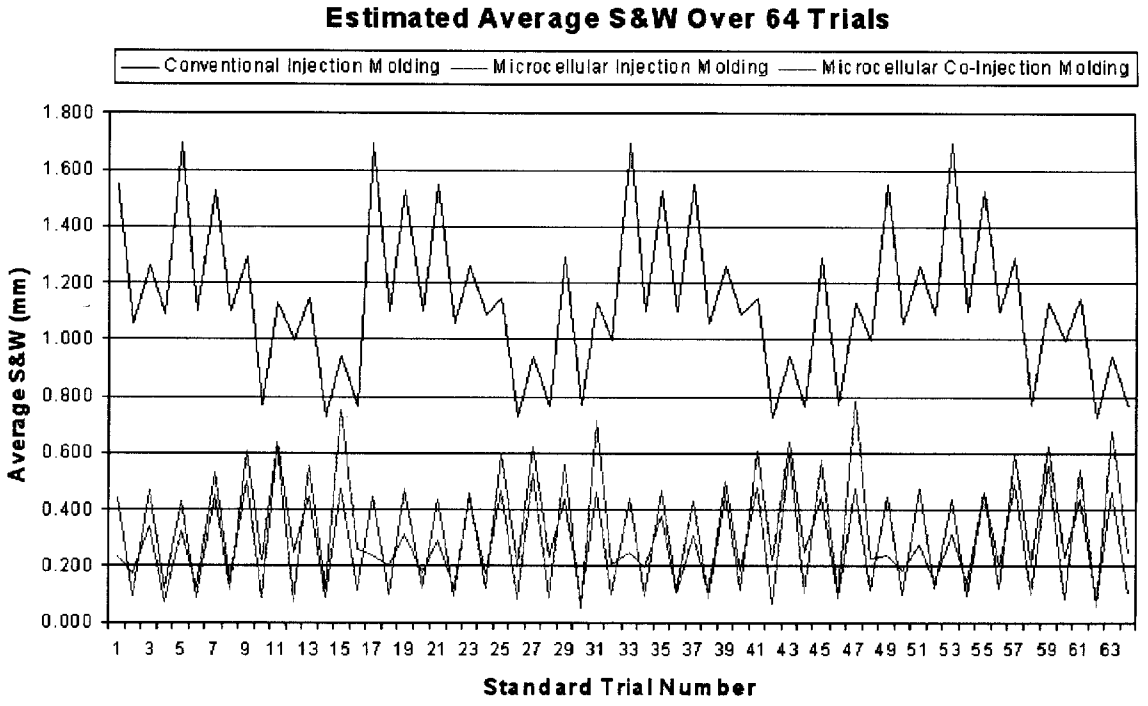

Figure 6.1 The estimated average S&W determined from the regression models for all 64 trials for the three injection molding processes.

Due to race-tracking in the part and the resulting molecular alignment, a slow injection speed will result in less S&W in the X walls. This characteristic is evident in the X walls not only because of the race-tracking effect, but also due to the lack of cell structure. However, a high injection speed will result in less S&W in the Y walls because of better cell nucleation and growth due to a more rapid pressure drop rate.

6.2 Effect of Microstructure on the S&W

The microstructure of microcellular injection and co-injection molded parts was examined. Previous literature indicated that a small cell size and high cell density is crucial concerning the mechanical properties such as tensile and impact strengths. With respect to S&W, the microstructure is correlated to the results. Increasing the wt% SCF content decreased cell size and increased cell density, reducing the S&W. However, when discussing the mechanical properties, the cell size must be equal to or less than 100 microns in order to avoid a large drop off in mechanical properties. Cells larger than this were observed for both injection molding processes, but excellent results were still obtained. This indicates that while cell structure is important for reducing the S&W of microcellular injection molded parts and microcellular co-injection molded parts, the criteria for maximum cell size and minimum cell density is more forgiving.

The PP microstructure was not ideal for microcellular injection molding and microcellular co-injection molding. This was not unexpected; however, due to the low melt strength of the PP and previous studies noting the poor cell structure when using PP. Within the microcellular injection and co-injection experiments, small pockets of cells on the order of 1 to 10 microns were observed. Such localized regions of small and dense cells and are believed to be the result of talc's effect as a nucleating agent and local talc concentrations in the polymer resulting from hand mixing the talc with the polymer pellets prior to injection molding. In order to achieve a higher cell density and decreased cell size, PP may be compounded with talc concentrations of 30 to 40%, which has been shown to result in a better cell structure.

6.3 Quantitative Comparison of Dimensional Stability and Weight Reduction

The dimensional stability is discussed in Chapters 3 through 5, and is quantitatively compared here. These results indicate that the microcellular injection molding process is the least susceptible to outside disturbances. Microcellular co-injection molding has additional process parameters when compared to conventional injection molding, but it maintains similar results due to the microcellular core dominating the formation of the part. The thick Y walls were the least susceptible to part variation due to the increased effect of the hold pressure in conventional injection molding and the wt% SCF content in microcellular injection molding and microcellular co-injection molding.

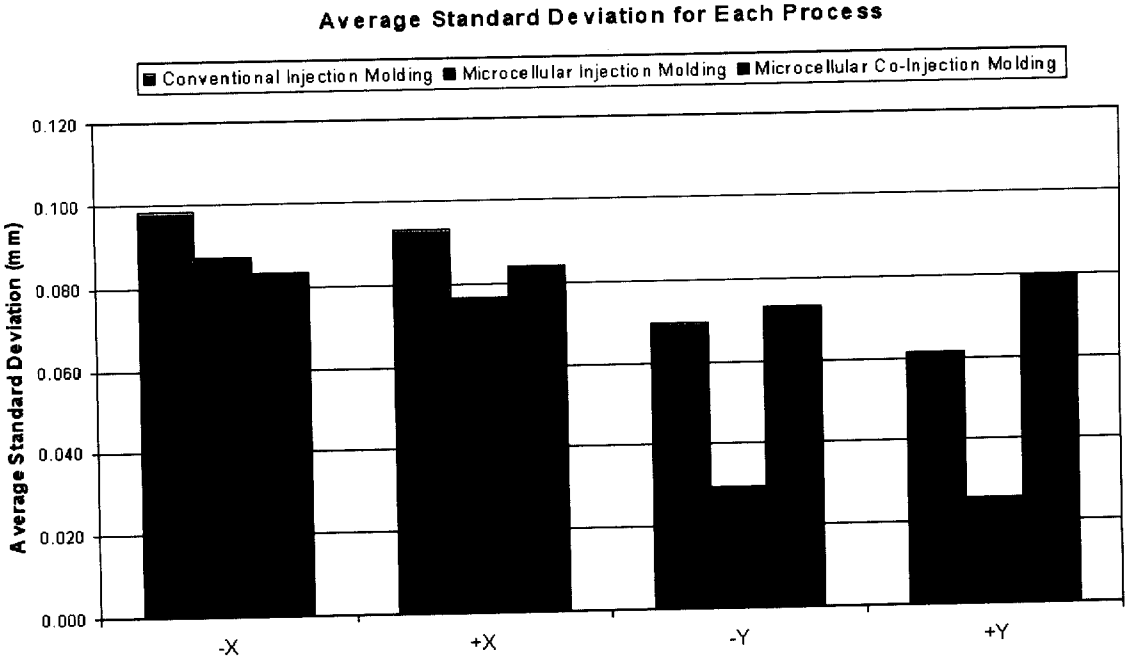

Figure 6.2 The average standard deviation for the three processes in each direction.

6.3 Quantitative Comparison of Dimensional Stability and Weight Reduction

The dimensional stability is discussed in Chapters 3 through 5, and is quantitatively compared here. These results indicate that the microcellular injection molding process is the least susceptible to outside disturbances. Microcellular co-injection molding has additional process parameters when compared to conventional injection molding, but it maintains similar results due to the microcellular core dominating the formation of the part. The thick Y walls were the least susceptible to part variation due to the increased effect of the hold pressure in conventional injection molding and the wt% SCF content in microcellular injection molding and microcellular co-injection molding.

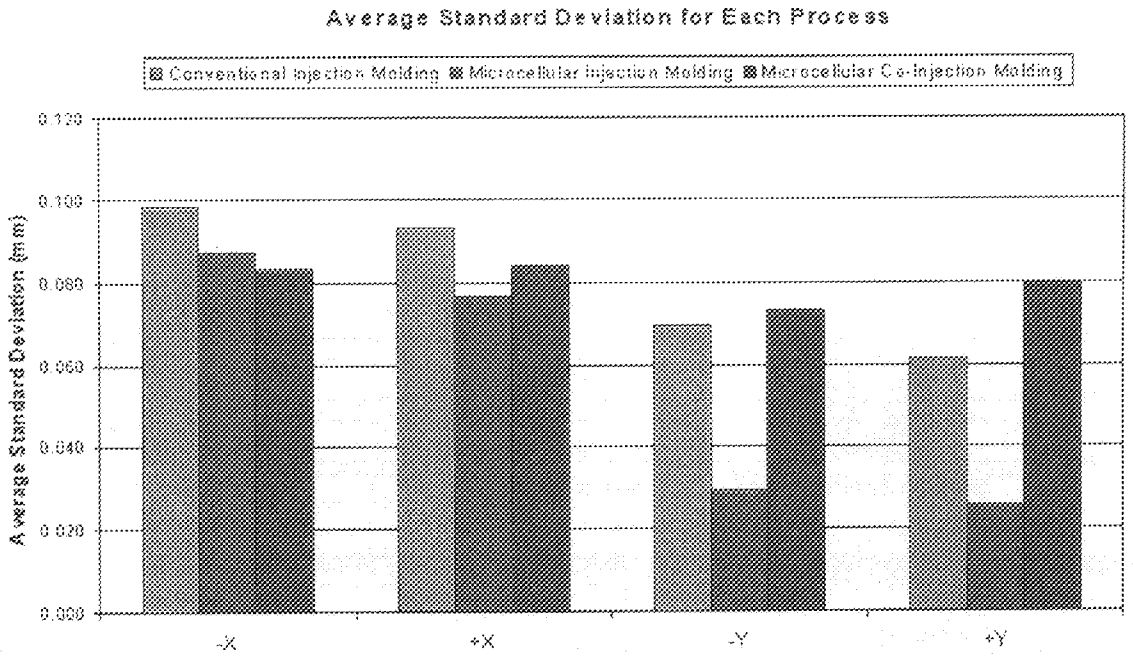

Figure 6.2 The average standard deviation for the three processes in each direction.

While determining the optimal parameters for achieving the minimum S&W and quantitatively comparing these results was the goal of this research, the weight reduction obtained using microcellular injection molding and microcellular co-injection molding processes was also documented. The average weight reduction over the course of all 32 trials was 2.83% and 1.03% for microcellular injection molding and microcellular co-injection molding, respectively. Therefore, using these two processes, one can drastically reduce the amount of S&W while also reducing material consumption, and hence, the part weight.

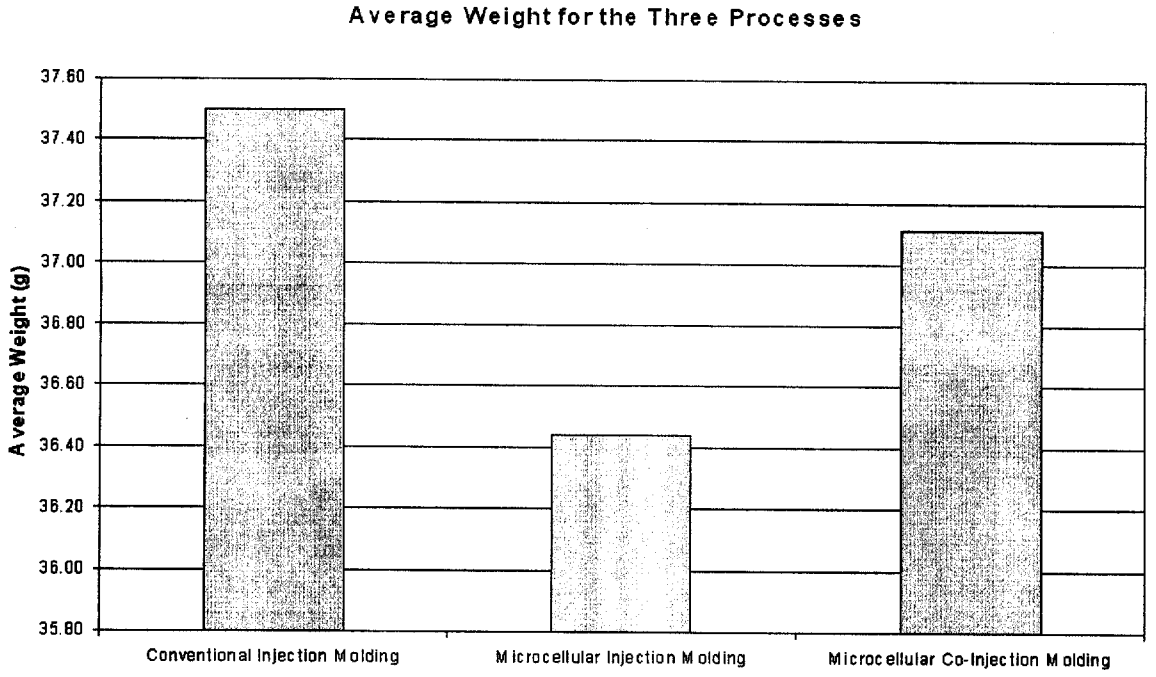

Figure 6.3 The average part weight observed over the course of all 32 trials for each process.

Appendix 1

Below are examples of the processing sheet used for the three injection molding experiments. They include any observed phenomena, as well as the processing parameters held constant throughout the entire experiments.

2	5/2/2004	29
Run #	Date	Standard Trial #

Independent Variable Settings:

X1	X2	X3	X4		X5		X6
Hold Time	Cool Time	Inj. Speed	Hold Pres.		Melt Temp.		Mold Temp.
(sec)	(sec)	(ccm/sec)	(bar)		(deg C)	(deg C)	(deg C)
3	20	50	600	Zone 5	230	230	40
				Zone 4	225	225	
				Zone 3	220	220	
				Zone 2	215	215	
				Zone 1	210	210	
					Set Value	Act. Value	

Variables held constant:

1) Shot Volume (ccm)	53
2) Switchover Position (ccm)	3
3) Parts per run	10
4) Back Pressure (bar)	60
5) Recovery Speed (rpm)	318
6)	

Procedure to reach SS

Mold SS Range = 63.5°C ± 1°C
Minimum of 5 parts to be run

Comments:

1) Good run

2)

3)

A.1 Example of a processing sheet collected for each run of the conventional injection molding experiment.

6	7/21/2004	3
Run #	Date	Standard Trial #

Independent Variable Settings:

A	B		C		D	E	F
SCF Dosage Time	Shot Vol.		Max. Barrel Temp.		Inj. Speed	Chiller Temp.	Cool Time
(sec)	(ccm)		(deg C)	(deg C)	(ccm/sec)	(deg C)	(sec)
4	53	Zone 5	205	205	20	20	44
		Zone 4	200	200			
		Zone 3	195	201			
		Zone 2	190	195			
		Zone 1	185	185			
			Set Value	Act. Value			

Variables held constant:

1) Recovery Speed (rpm)	318
2) Switchover Position (ccm)	2
3) Parts per run	10
4) Delivery Pressure Drop (psi)	100
5) SCF Flowrate (kg/hr)	0.11
6) Back Pressure (bar)	100
7) % Nucleating Agent (Talc)	1
8) Start Dosage Volume (ccm)	5

Procedure to reach SS

Observe SS Mold Temperature
Observe Switchover Pressure
Minimum of 10 parts to be run
Shut down for 12 minutes

Comments:

1) Part 1 = Cycle 120

2) Purged before this run and SCF was in solution. There was no cracking or popping, indicating it is in solution. Everything looked great!

3)

A.2 Example of a processing sheet collected for each run of the microcellular injection molding experiment.

12	4/20/2005	6
Random #	Date	Standard Trial #

Independent Variable Settings:

A	B	C	D	E		F	
SCF Dosage Time	Vertical Inj Speed	Chiller Temp	Core/Skin Ratio	Switchover Time		Vertical Barrel Temp	
(sec)	(ccm/sec)	(deg C)	(ccm)/(ccm)	(sec)		(deg C)	(deg C)
4	20	40	22c/33s	0	Zone 5	205	205
					Zone 4	200	200
					Zone 3	195	195
					Zone 2	190	190
					Zone 1	185	185

Variables held constant:

1) Cooling Time (s)	35
2) Switchover Position (ccm)	3
3) Parts per run	10
4) Back Pressure (bar)	100
5) Recovery Speed (rpm)	318
6) Barrel 1 Injection Speed (ccm/s)	60
7) Barrel 1 Temp (deg C)	230

Procedure to reach SS

Mold SS Range = 58.5°C ± 1°C
Minimum of 10 parts to be run

Comments:

1) In solution after purge.

2)

3)

A.3 Example of a processing sheet collected for each run of the microcellular co-injection molding experiment.

Appendix 2

Residual Checking

The residual error and standardized residual errors, described by equations 2.2 and 2.3, have to pass a series of test/checks, described in 2.6.3. Examples of the visual methods for validating the residuals can be found in at the end of Appendix 2 (A.13 through A.15). While these must be used, the regression models and standardized residuals will only be discussed here in detail. Using the methods detailed within equation 2.1 and the coefficients in Tables A.4 through A.6, regression models were developed for each of the four directions for each experiment, and can be seen in Tables A.7 through A.9. The method by which effects and coefficients are calculated is well documented, and information regarding how to do this can be found in [51] and the references cited within.

The residuals and standardized residuals are located in Tables A.10 through A.12. Noting that standardized residuals above 3 or 4 standard deviations can be considered outliers, these were examined. None of the standardized residuals for any of the four measurement directions was above 3. This signifies the regression models were sufficient for predicting the S&W for any set of parameters within the process window. Additionally, if the model does not agree with the actual value and high residuals occur, it indicates errors made during the experiment due to human interaction or process failure. One can be confident that the experimental results were accurate by carrying out the experiments in a systematic manner, and by using residual analysis, both statistical and visual.

Table A.4 Coefficients used for deriving regression models for the conventional injection molding experiment.

Factor/Interaction	Coeffecient (defined as the Effect divided by 2)			
	–X	+X	–Y	+Y
Average	0.8093	–0.8127	1.3784	1.4205
A	–0.5763	–0.8455	–0.1924	–0.1962
B	–0.2154	–0.2341	–0.0930	–0.0328
C	0.1521	0.2505	0.0693	0.0284
D	–0.2291	–0.3165	–0.2096	–0.2887
E	0.1162	0.1139	0.0042	0.0446
F	–0.0853	-0.0308	–0.0484	–0.0649
A*B	0.0799	0.1018	–0.0214	0.0137
A*C	–0.0396	0.1293	–0.0519	–0.0267
A*D	–0.0679	–0.0672	–0.1400	–0.1123
A*E	0.0458	–0.0250	0.0054	–0.0098
A*F	0.0022	0.1239	–0.0121	0.0007
B*C	–0.0593	–0.0968	0.0031	–0.0153
B*D	0.0115	0.0158	0.0876	0.0112
B*E	–0.0990	–0.1181	0.0194	0.0057
B*F	–0.1877	–0.2236	–0.0163	–0.0263
C*D	0.0065	0.0622	–0.0219	–0.0313
C*E	0.0726	0.0785	0.0233	0.0519
C*F	0.1012	0.1408	0.0417	0.0174
D*E	–0.0368	–0.1703	0.0363	–0.0001
D*F	–0.0032	0.0240	–0.0860	–0.0409
E*F	–0.0490	–0.0682	–0.0401	–0.0148
A*B*C	–0.0571	–0.1020	–0.0443	–0.0780
A*B*D	0.0723	0.1043	0.0639	0.0519
A*B*E	0.0827	0.0167	0.0531	0.0742
A*B*F	–0.0774	–0.0775	0.0001	–0.0431
A*C*D	–0.0714	–0.0248	–0.0851	–0.0463
A*C*E	0.0918	0.0850	–0.0370	0.0085
A*C*F	0.0418	0.0272	0.0452	0.0428
A*D*E	0.0378	0.0657	0.0147	0.0156
A*D*F	0.0084	–0.0119	–0.0061	–0.0191
A*E*F	0.0363	0.1064	–0.0281	–0.0082

Table A.5 Coefficients used for deriving regression models for the microcellular injection molding experiment.

Factor/Interaction	Coeffecient (defined as the Effect divided by 2)			
	–X	+X	–Y	+Y
Average	0.4131	0.4489	0.2648	0.1256
A	–0.2583	–0.2790	–0.1227	–0.0652
B	0.0226	0.0749	0.0000	–0.0212
C	–0.0419	–0.0582	–0.0372	–0.0102
D	0.1164	0.0961	–0.0647	0.0025
E	0.0156	0.0104	–0.0139	0.0043
F	–0.0651	–0.0403	–0.0124	–0.0168
A*B	0.0098	–0.0002	–0.0046	0.0095
A*C	0.0674	–0.0076	0.0002	0.0276
A*D	–0.0659	–0.0346	–0.0207	–0.0027
A*E	–0.0134	–0.0069	0.0048	0.0057
A*F	0.0266	0.0403	0.0113	–0.0062
B*C	0.0061	–0.0042	–0.0024	0.0069
B*D	0.0016	-0.0199	0.0028	0.0083
B*E	0.0076	0.0024	0.0013	–0.0008
B*F	–0.0083	–0.0138	–0.0051	–0.0033
C*D	–0.1089	–0.0661	0.0303	0.0123
C*E	–0.0143	–0.0031	–0.0015	–0.0050
C*F	–0.0229	–0.0059	–0.0043	–0.0049
D*E	–0.0581	0.0063	0.0061	–0.0197
D*F	–0.0232	–0.0166	0.0016	–0.0115
E*F	–0.0511	–0.0324	0.0053	0.0012
A*B*C	0.0458	0.0219	–0.0029	0.0045
A*B*D	0.0013	0.0016	–0.0066	–0.0077
A*B*E	–0.0219	–0.0116	0.0034	–0.0085
A*B*F	0.0122	0.0219	–0.001	0.0033
A*C*D	0.0217	–0.0356	–0.0116	–0.0002
A*C*E	0.0154	–0.0214	–0.0058	0.0135
A*C*F	0.0321	–0.0008	–0.0127	0.0102
A*D*E	0.0299	0.0204	0.0038	–0.0070
A*D*F	–0.0167	–0.0233	0.0003	0.0063
A*E*F	0.0050	–0.0044	–0.0022	–0.0068

Table A.6 Coefficients used for deriving regression models for the microcellular co-injection molding experiment.

Factor/Interaction	Coeffecient (defined as the Effect divided by 2)			
	–X	+X	–Y	+Y
Average	0.2100	0.3685	0.1534	0.1729
A	–0.2839	–0.1917	–0.2670	–0.2078
B	0.1230	0.1200	0.0200	–0.0070
C	0.1237	0.1058	0.0121	0.0234
D	0.1647	0.0583	0.0981	0.0784
E	–0.0805	–0.0189	0.0000	–0.0057
F	–0.0132	–0.0437	–0.0004	0.0144
A*B	–0.0030	0.0398	0.0010	–0.0014
A*C	–0.0167	0.0392	–0.0232	–0.0180
A*D	0.0075	0.0129	–0.0494	–0.0517
A*E	–0.0095	–0.0195	–0.0062	–0.0002
A*F	–0.0237	0.0038	–0.0129	–0.0215
B*C	0.0033	0.0815	0.0273	0.0004
B*D	0.0136	0.0247	0.0182	0.0111
B*E	0.0097	–0.0291	–0.0540	–0.0404
B*F	–0.0524	–0.0567	–0.0200	–0.0264
C*D	–0.0063	–0.0153	0.0048	–0.0036
C*E	0.0003	–0.0213	–0.0044	–0.0057
C*F	–0.0091	–0.003	0.0149	0.0233
D*E	0.0262	0.0005	–0.0171	0.0027
D*F	–0.0155	–0.0017	0.0150	0.0098
E*F	0.0293	0.0318	0.0142	0.0189
A*B*C	0.0003	0.0147	0.0013	–0.0128
A*B*D	–0.0353	–0.0193	–0.0139	–0.0150
A*B*E	–0.0082	–0.0158	0.0291	0.0399
A*B*F	0.0147	0.0097	0.0129	0.0292
A*C*D	–0.0036	–0.0142	0.0145	0.0098
A*C*E	0.0258	0.0173	0.0016	0.0088
A*C*F	–0.0226	0.0087	–0.0056	–0.0179
A*D*E	0.0275	0.0174	0.0050	0.0134
A*D*F	0.0053	–0.0157	–0.0154	–0.0066
A*E*F	–0.0013	0.0103	–0.0209	–0.0116

Table A.7 Regression models derived for the conventional injection molding experiment.

Conventional Injection Molding Experiment	
Response	Regression Model
–X	$\hat{Y} = 0.8093 - 0.5763A - 0.2291D - 0.2154B - 0.1877BF - 0.0853F$
+X	$\hat{Y} = -0.1827 - 0.8455A - 0.3165D - 0.2341B - 0.2236BF - 0.0308F$
–Y	$\hat{Y} = 1.3784 - 0.2096D - 0.1924A - 0.1400AD$
+Y	$\hat{Y} = 1.4204 - 0.2887D - 0.1962A - 0.1123AD$

Table A.8 Regression models derived for the microcellular injection molding experiment.

Microcellular Injection Molding Experiment	
Response	Regression Model
–X	$\hat{y} = 0.4131 - 0.2583A + 0.1164D - 0.1089CD - .0419C$
+X	$\hat{y} = 0.4489 - 0.2790A + 0.0961D + 0.0749B - 0.0661CD - 0.0582C$
–Y	$\hat{y} = 0.2648 - 0.1227A - 0.0647D - 0.0372C + 0.0302CD - 0.0207AD - 0.0139E$
+Y	$\hat{y} = 0.1256 - 0.0652A + 0.0276AC - 0.0212B - 0.0197DE - 0.0102C + 0.0043E + 0.0025D$

Table A.9 Regression models derived for the microcellular co-injection molding experiment.

Microcellular Co-Injection Molding Experiment	
Response	Regression Model
–X	$\hat{y} = 0.2100 - 0.2839A + 0.1647D + 0.1237C + 0.1230B - 0.0805E - 0.0524BF$
+X	$\hat{y} = 0.3685 - 0.1917A + 0.1200B + 0.158C + 0.1230B - 0.0815BC - 0.0583D$
–Y	$\hat{y} = 0.1534 - 0.2670A + 0.0981D - 0.0540BE - 0.0494AD$
+Y	$\hat{y} = 0.1729 - 0.2078A + 0.0784D - 0.0517AD$

Table A.10 Residuals and standardized residuals for the conventional injection molding experiment.

	–X		+X		–Y		+Y	
Standard Order	ε_{ij}	d_{ij}	ε_{ij}	d_{ij}	ε_{ij}	d_{ij}	ε_{ij}	d_{ij}
1	–0.469	–1.33	–0.423	–0.82	0.059	0.24	–0.038	–0.20
2	–0.291	–0.83	–0.604	–1.18	0.229	0.93	0.059	0.31
3	–0.068	–0.19	–0.388	–0.76	–0.041	–0.17	–0.062	–0.32
4	0.233	0.66	0.148	0.29	–0.391	–1.58	0.004	0.02
5	–0.163	–0.47	–0.477	–0.93	0.104	0.42	–0.278	–1.45
6	–0.206	–0.59	–0.151	–0.29	0.356	1.44	0.107	0.56
7	–0.151	–0.43	–0.481	–0.94	–0.029	–0.12	0.098	0.51
8	–0.109	–0.31	0.101	0.20	–0.030	–0.12	–0.246	–1.28
9	–0.325	–0.93	–0.094	–0.18	–0.167	–0.68	–0.056	–0.29
10	–0.365	–1.04	–0.835	–1.63	0.165	0.67	0.121	0.63
11	–0.263	–0.75	–0.162	–0.32	–0.089	–0.36	–0.108	–0.56
12	–0.018	–0.05	0.069	0.14	–0.166	–0.67	–0.087	–0.45
13	0.269	0.76	0.306	0.60	0.162	0.65	0.067	0.35
14	–0.171	–0.49	0.421	0.82	–0.041	–0.17	–0.029	–0.15
15	0.608	1.73	0.606	1.18	0.013	0.05	–0.057	–0.30
16	–0.370	–1.05	0.138	0.27	–0.199	–0.81	–0.205	–1.07
17	–0.031	–0.09	–0.092	–0.18	0.087	0.35	0.082	0.43
18	–0.128	–0.36	–0.384	–0.75	0.107	0.43	–0.193	–1.01
19	–0.158	–0.45	0.497	0.97	–0.336	–1.36	–0.142	–0.74
20	–0.253	–0.72	–0.262	–0.51	–0.444	–1.79	–0.186	–0.97
21	0.468	1.33	0.776	1.51	0.133	0.54	0.258	1.34
22	0.912	2.60	1.481	2.89	0.370	1.50	0.357	1.86
23	0.030	0.08	0.049	0.10	0.026	0.10	0.083	0.43
24	0.384	1.09	0.207	0.40	–0.120	–0.81	0.100	0.52
25	0.370	1.05	0.552	1.08	0.013	0.05	0.229	1.19
26	–0.452	–1.29	–0.899	–1.75	–0.278	–1.13	–0.289	–1.51
27	–0.588	–1.67	–0.861	–1.68	–0.494	–2.00	–0.345	–1.80
28	0.372	1.06	–0.273	–0.53	0.639	2.58	0.560	2.91
29	0.522	1.48	0.265	0.52	0.184	0.74	0.109	0.57
30	0.522	0.17	0.156	0.30	0.007	0.03	0.022	0.11
31	–0.048	–0.14	–0.077	–0.15	0.379	1.53	0.162	0.84
32	0.398	1.13	0.684	1.33	–0.124	–0.50	–0.091	–0.48

Table A.11 Residuals and standardized residuals for the microcellular injection molding experiment.

	–X		+X		–Y		+Y	
Standard Order	ε_{ij}	d_{ij}	ε_{ij}	d_{ij}	ε_{ij}	d_{ij}	ε_{ij}	d_{ij}
1	–0.236	–1.41	–0.035	–0.34	0.063	2.14	0.019	0.49
2	0.034	0.20	0.071	0.69	0.003	0.10	–0.014	–0.35
3	–0.139	–0.83	–0.076	–0.74	–0.025	–0.84	–0.024	–0.62
4	–0.059	–0.35	–0.077	–0.75	–0.019	–0.64	0.035	0.90
5	–0.206	–1.23	–0.123	–1.20	–0.027	–0.91	0.037	0.97
6	–0.068	–0.41	0.003	0.03	0.052	1.76	–0.053	–1.38
7	–0.151	–0.90	–0.031	–0.30	0.017	0.58	0.008	0.20
8	0.237	1.42	0.233	2.28	–0.016	–0.54	–0.008	–0.21
9	0.194	1.16	0.011	0.10	–0.054	–1.84	–0.041	–1.05
10	–0.080	–0.48	–0.014	–0.14	–0.024	–0.80	0.015	0.39
11	0.215	1.29	0.074	0.72	0.054	1.82	–0.005	–0.14
12	–0.168	–1.01	–0.061	–0.60	–0.010	–0.33	–0.025	–0.64
13	0.198	1.18	0.133	1.30	0.011	0.36	0.076	1.96
14	–0.080	–0.48	–0.110	–1.07	–0.014	–0.47	–0.046	–1.18
15	–0.108	–0.65	–0.092	–0.89	0.001	0.02	–0.025	–0.64
16	0.169	1.01	–0.074	–0.72	–0.012	–0.40	0.051	1.31
17	–0.021	–0.13	–0.130	–1.27	–0.014	–0.48	0.073	1.88
18	0.144	0.86	0.015	0.15	–0.042	–1.43	0.059	1.53
19	0.315	1.88	0.214	2.09	0.023	0.78	–0.028	–0.72
20	–0.037	–0.22	0.017	0.17	0.011	0.37	–0.021	–0.55
21	0.149	0.89	0.062	0.61	–0.003	–0.10	–0.038	–0.97
22	0.037	0.22	–0.024	–0.23	–0.010	–0.34	–0.017	–0.45
23	–0.239	–1.43	–0.160	–1.56	–0.034	–1.15	–0.068	–1.77
24	0.242	1.45	0.037	0.37	0.021	0.71	0.041	1.06
25	0.122	0.73	0.019	0.18	–0.011	–0.36	–0.003	–0.08
26	–0.289	–1.73	0.031	0.30	0.059	2.00	–0.053	–1.38
27	0.088	0.53	–0.137	–1.34	–0.035	–1.17	0.009	0.24
28	–0.083	–0.5	0.080	0.78	0.020	0.68	0.004	0.10
29	–0.304	–1.82	0.061	0.60	–0.002	–0.06	–0.047	–1.22
30	0.045	0.27	0.029	0.29	0.012	0.41	0.033	0.85
31	0.121	0.72	0.208	2.04	0.036	1.23	0.057	1.47
32	–0.040	–0.24	–0.158	–1.54	–0.032	–1.08	0.000	0.01

Table A.12 Residuals and standardized residuals for the microcellular co-injection molding experiment.

	–X		+X		–Y		+Y	
Standard Order	ε_{ij}	d_{ij}	ε_{ij}	d_{ij}	ε_{ij}	d_{ij}	ε_{ij}	d_{ij}
1	0.003	0.04	0.056	0.46	–0.009	–0.12	–0.114	–1.21
2	0.051	0.62	–0.117	–0.97	0.074	1.00	–0.009	–0.09
3	–0.129	–1.58	–0.199	–1.65	–0.216	–2.91	–0.147	–1.56
4	0.097	1.19	0.153	1.27	–0.017	–0.22	0.055	0.58
5	0.144	1.76	0.053	0.44	0.001	0.02	0.088	0.94
6	0.090	1.10	0.034	0.28	–0.040	–0.53	0.050	0.53
7	–0.032	–0.39	0.072	0.60	0.110	1.48	0.151	1.61
8	–0.015	–0.18	0.104	0.87	–0.042	–0.56	–0.008	–0.08
9	–0.113	–1.38	–0.004	–0.03	–0.030	–0.40	–0.078	–0.83
10	0.091	1.11	0.002	0.02	0.069	0.93	0.000	0.00
11	0.032	0.39	0.147	1.22	0.064	0.86	0.136	1.45
12	–0.029	–0.35	–0.057	–0.47	–0.068	–0.92	–0.032	–0.34
13	–0.014	–0.16	–0.001	–0.01	–0.100	–1.35	–0.174	–1.85
14	–0.175	–2.14	–0.104	–0.87	0.034	0.46	0.014	0.15
15	0.032	0.39	–0.129	–1.07	0.129	1.74	0.180	1.92
16	–0.033	–0.41	0.293	2.43	0.039	0.52	–0.023	–0.24
17	0.132	1.61	0.228	1.89	0.107	1.44	0.154	1.64
18	–0.138	–1.69	–0.169	–1.41	0.063	0.85	–0.021	–0.22
19	–0.054	–0.65	0.119	0.99	–0.063	–0.85	–0.114	–1.21
20	–0.013	–0.15	–0.192	–1.60	0.000	0.01	–0.023	–0.24
21	–0.066	–0.81	0.051	0.42	0.033	0.45	–0.003	–0.03
22	–0.107	–1.31	0.063	0.52	–0.085	–1.14	–0.003	–0.03
23	0.061	0.75	–0.276	–2.29	0.036	0.49	–0.018	–0.19
24	–0.025	–0.31	0.021	0.18	0.044	0.60	–0.043	–0.45
25	–0.089	–1.09	–0.022	–0.18	–0.102	–1.37	–0.054	–0.57
26	0.090	1.10	0.027	0.23	–0.052	–0.70	–0.009	–0.09
27	0.084	1.03	–0.011	–0.09	–0.035	–0.47	–0.117	–1.24
28	–0.015	–0.19	0.040	0.33	0.019	0.25	–0.006	–0.06
29	–0.022	–0.27	–0.042	–0.35	0.107	1.44	0.223	2.38
30	0.123	1.51	–0.054	–0.45	–0.072	–0.97	0.044	0.47
31	0.030	0.36	–0.042	–0.35	–0.034	–0.46	–0.118	–1.25
32	0.009	0.11	–0.043	–0.36	0.032	0.43	0.011	0.12

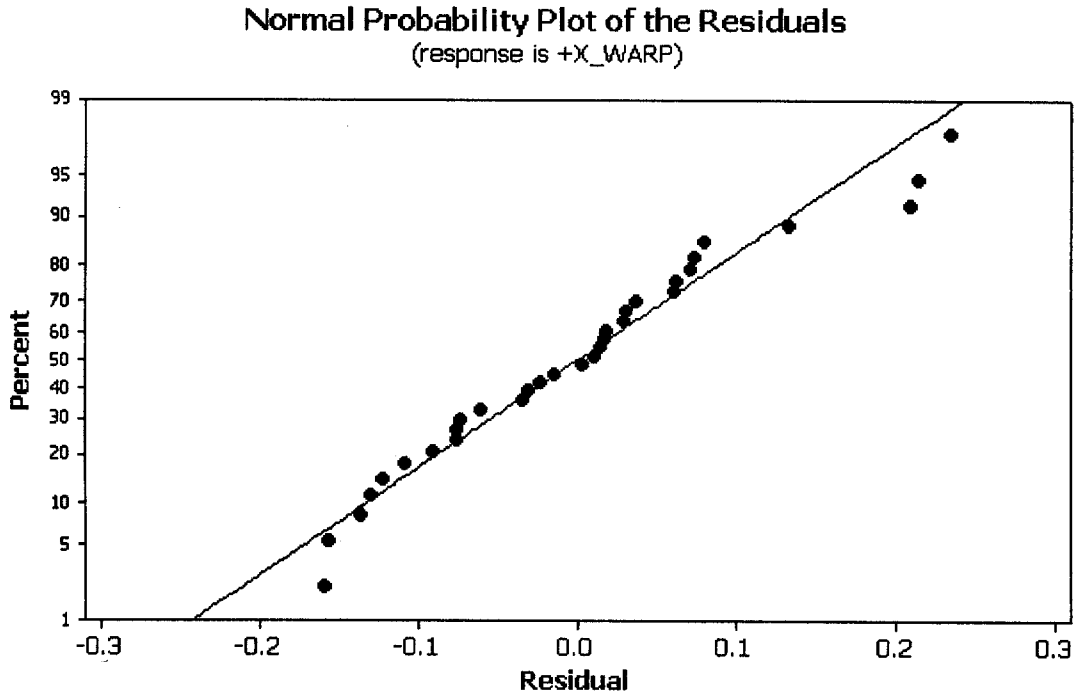

A.13 Normal probability plot of the residuals for microcellular injection molding.

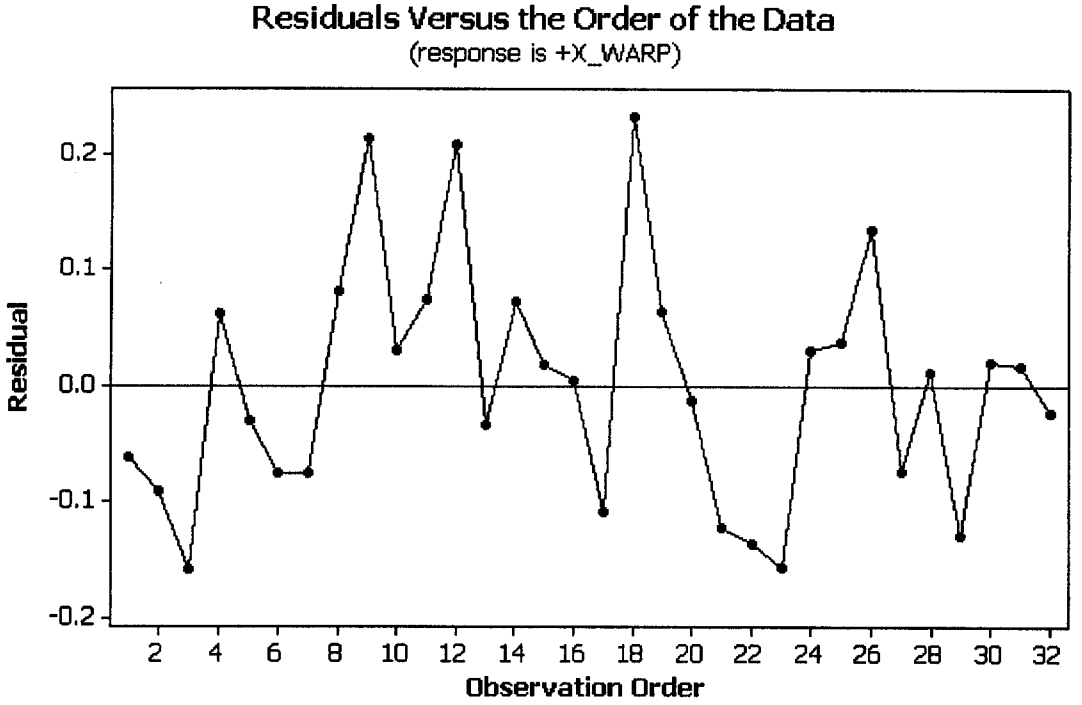

A.14 Residuals versus the random trial number for microcellular injection molding.

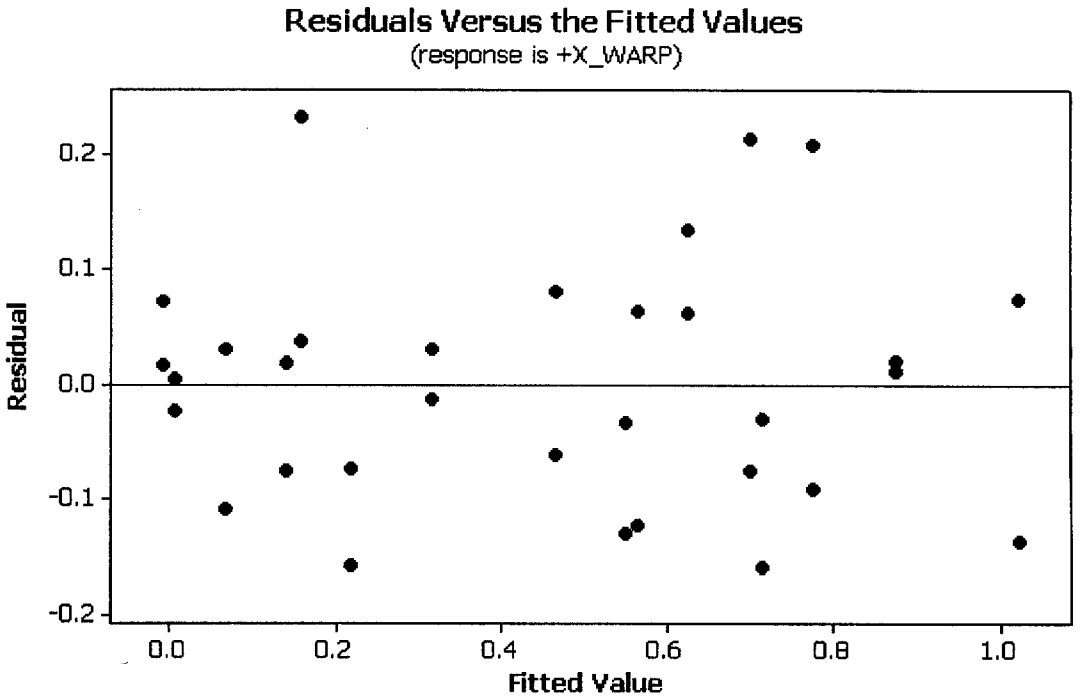

A.15 Residuals versus the regression model value for microcellular injection molding.

Appendix 3

These two-factor interaction diagrams are discussed briefly in Chapters 4 and 5. Due to the fact that each of the interaction effects is only present for one of the four directions, they were not analyzed in detail. However, these effects were included in the regression models used for estimating the S&W.

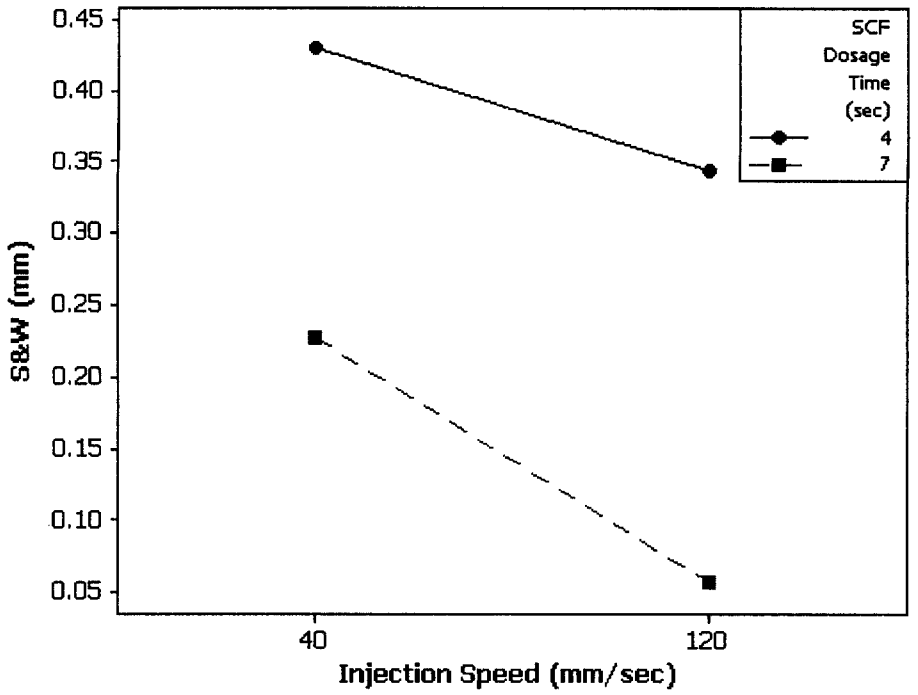

A.16 Interaction effect between SCF dosage time and injection speed in the –Y direction for microcellular injection molding.

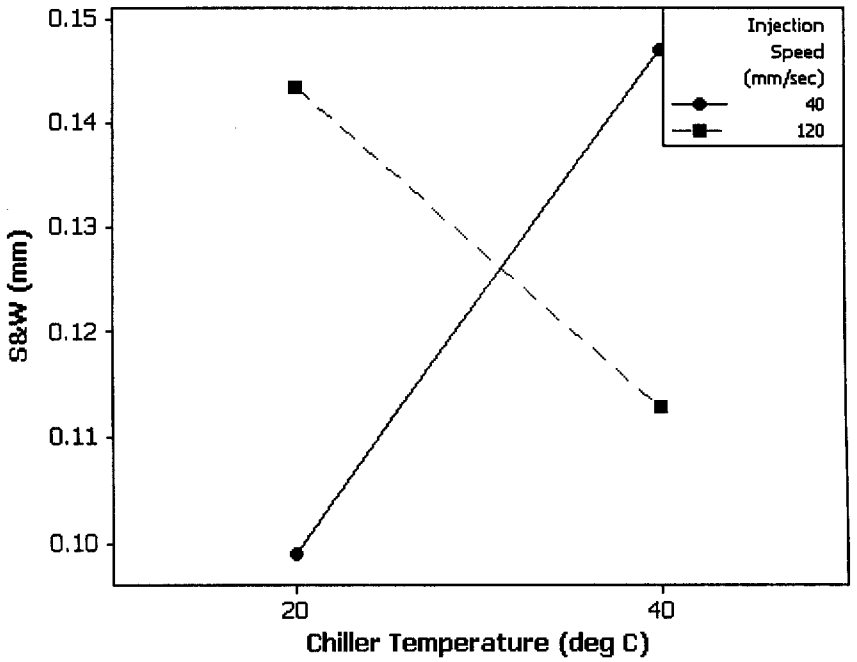

A.17 Interaction effect between injection speed and chiller temperature in the +Y direction for microcellular injection molding.

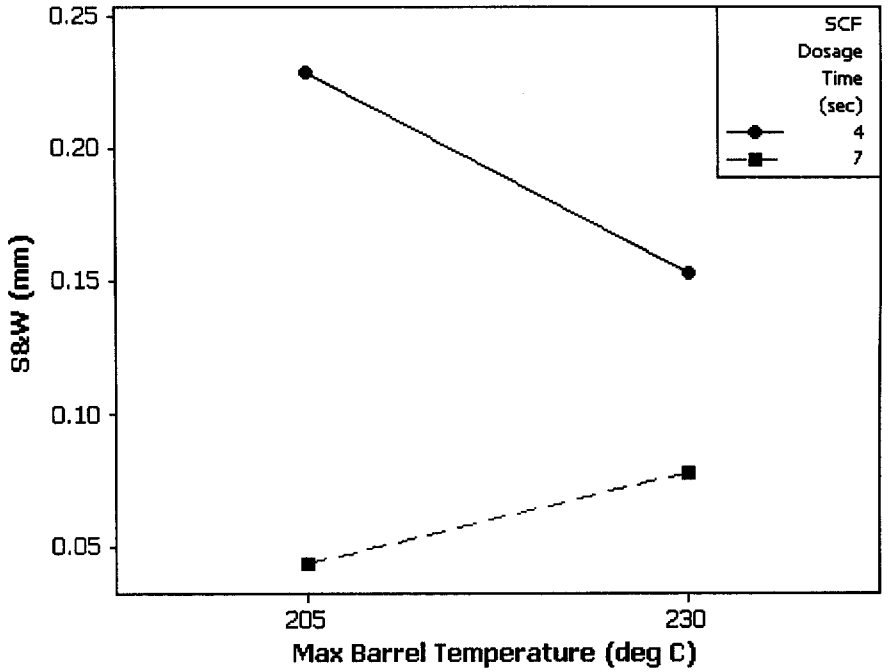

A.18 Interaction effect between SCF dosage time and maximum barrel temperature in the +Y direction for microcellular injection molding.

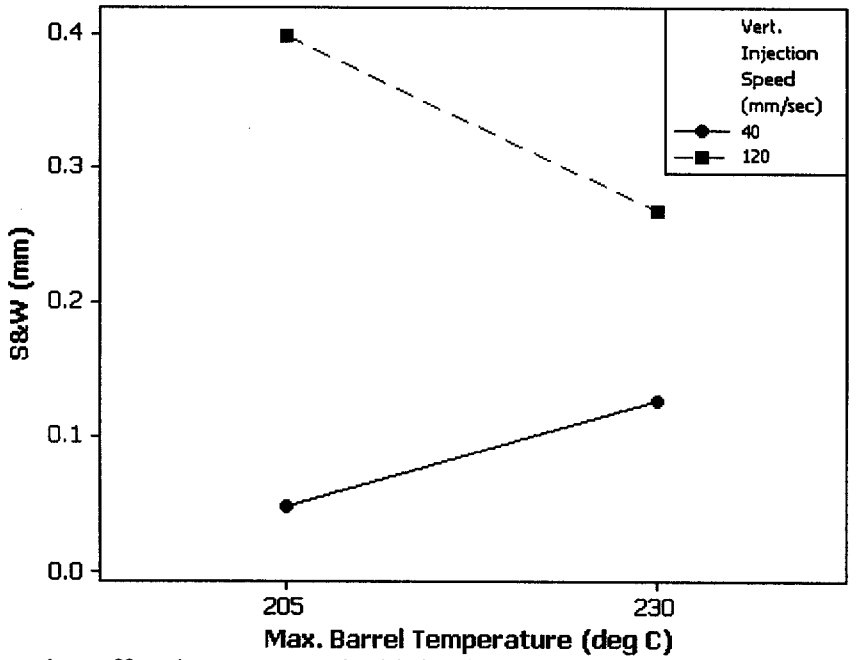

A.19 Interaction effect between vertical injection speed and the maximum vertical barrel temperature in the –X direction for microcellular co-injection molding.

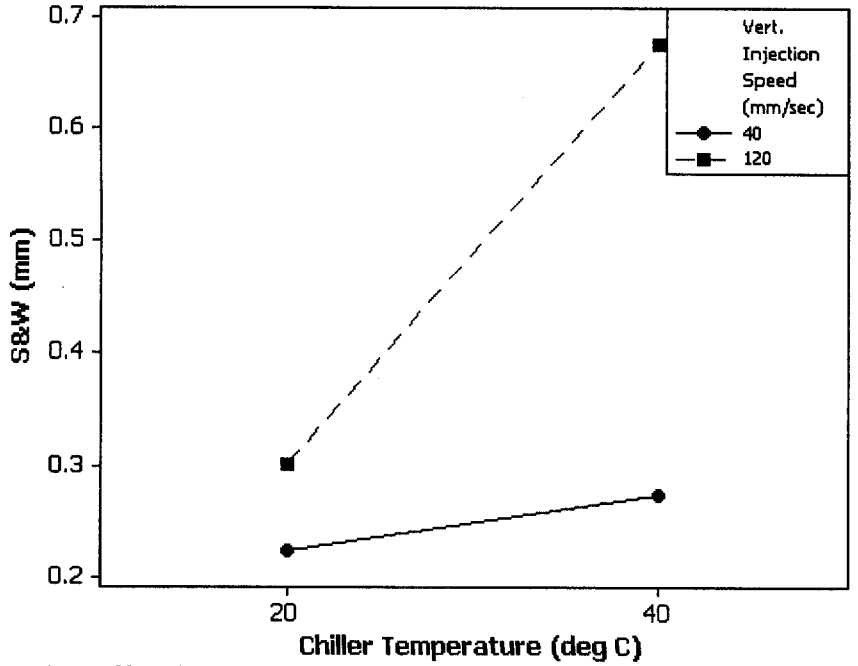

A.20 Interaction effect between the vertical injection speed and the chiller temperature in the +X direction for microcellular co-injection molding.

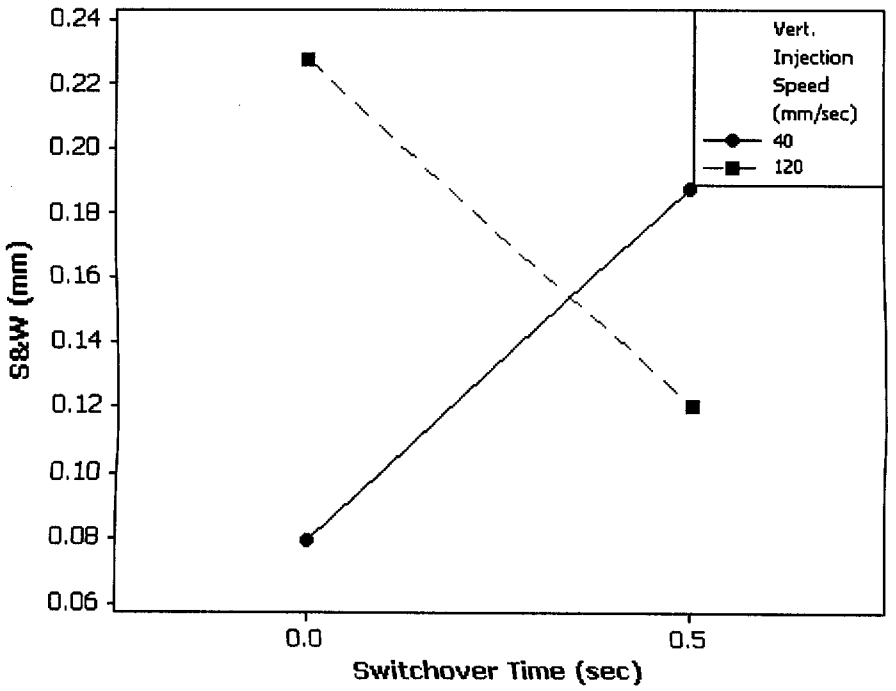

A.21 Interaction effect between the vertical injection speed and the switchover time in the –Y direction for microcellular co-injection molding.

References

1. The Society of Plastics Industry website - http://www.socplas.org/about/index.htm
2. Plastics Datasource website – www.plasticsdatasource.org
3. Suh, N. P., Chapter 3 in *Innovation in Polymer Processing – Molding*, Stevenson, J. F, (Ed.), Hanser Publishers, Munich, **93** (1996).
4. Cha, S. W., *Ph.D. Thesis*, *Massachusetts Institute of Technology*, Cambridge, MA (1994).
5. Kumar, V., *Ph.D. Thesis*, *Massachusetts Institute of Technology*, Cambridge, MA (1988).
6. John, S. B., *S.B. Thesis, Massachusetts Institute of Technology*, Cambridge, MA (1994).
7. Park, C. B., Doroudiani S. and Kortschot, M. T. *Polymer Engineering and Science*, **38**, 1205 (1998).
8. Seeler, K. A. and Kumar, V. *Journal of Reinforced Plastics and Composites*, **12**, 359 (1993).
9. Elkovitch, M. D., Lee, J. and Tomasko, D. L., *Polymer Engineering and Science*, **41**, 2108 (2001).
10. Gulari, E. and Manke, C. W. *219th ACS National Meeting, I&EC –106, San Francisco, CA, March 26-30* (2000).
11. Royer, J. R., Gay, Y. J., Desimone, J. M., and Khan, S. A., *J. Polym. Sci., Part B: Polym. Phys.*, ***38**, 3168 (2000).*

12. Kwag, C., Manke, C. W. and Gulari, E. *Journal of Polymer Science, Part B: Polymer Physics*, **37**, 2771 (1999).

13. Zhang, Z. and Handa, Y. P., *Journal of Polymer Science, Part B: Polymer Physics*, **36**, 977 (1998).

14. Handa, Y. P., Kruus, P. and O'Neill, M., *Journal of Polymer Science, Part B: Polymer Physics*, **34**, 2635 (1996).

15. Turng, L. S., *Journal of Injection Molding Technology*, **5**, 160 (2001).

16. Baldwin, D. F., *Ph.D. Thesis, Massachusetts Institute of Technology*, Cambridge, MA (1994).

17. Park, C. B., *Ph.D. Thesis, Massachusetts Institute of Technology*, Cambridge, MA (1993).

18. Okamoto, K., *Microcellular Processing*, Cincinnati, Hanser Gardner Publications, Inc., (2003).

19. Xu, J. and Pierick, D., *Journal of Injection Molding Technology*, **5**, 152 (2001).

20. Turng, L. S. and Kharbas, H. A., *Polymer Engineering and Science*, **43**, 157 (2003).

21. Habibi-Naini, S. and Schlummer, C., *ANTEC 2005 CD ROM.*

22. Colton, J. S. and Suh, N. P., *Polymer Engineering and Science*, **27**, 485 (1987).

23. Colton, J. S. and Suh, N. P., *Polymer Engineering and Science*, **27**, 493 (1987).

24. Kramschuster, A., Cavitt, R., Ermer, D., Chen, Z. B., Turng, L. S., *Polymer Engineering and Science*, **45**, 1408 (2005).

25. Jacobsen, K. and Pierick, D., *ANTEC 2000 CD ROM.*

26. Trexel Website Homepage- www.trexel.com

27. Turng, L. S. and Kharbas, H., *Polymer Engineering and Science*, **43**, 157 (2003).

28. Kharbas, H., Nelson, P., Yuan, M., Gong, S., Turng, L. S. and Spindler, R., *Journal of Polymer Composites*, **24**, 655 (2003).

29. Park, C. B., Baldwin, D. F. and Suh, N. P., *Cellular and Microcellular Materials, ASME,* 53, 109 (1994).

30. Yuan, M., Turng, L. S., Caulfield, D. F., Hunt, C. and Spindler, R., *Polymer Engineering and Science*, **44**, 673 (2004).

31. Kharbas, H., *M.S. Thesis, University of Wisconsin – Madison*, Madison, WI (2003).

32. Smith, C., "MuCell Gloss breakthrough set to double Trexel's sales," *Plastics & Rubber Weekly*, (October 2004).

33. Bledzki, A., Kirschling, H., Steinbichler, G., Egger, P., *ANTEC 2004 CD ROM.*

34. Bledzki, A., Kirschling, H., Steinbichler, G., Egger, P., *PPS-21 2005 CD ROM.*

35. Turng, L. S. and Kharbas, H., *International Polymer Processing*, **19**, 77 (2004).

36. Dr Ing, Erich Escales, Sasbachwalden; *German Plastics, Translation of Kunststoffe*, **60**.

37. Selden.R., *Journal of Injection Molding Technolgy*, **1**, 189 (1997).

38. Avery, J. A., *Injection Molding Alternatives – A Guide for Designers and Product Engineers*, Hanser, Munich, (1998).

39. Turng, L. S., Wang, V. W and Wang, K. K., " Numerical Simulation of the Co-injection Molding Process," *Transaction of the ASME*, **115**, 48 (1993).

40. McRoskey, J., *GPEC 2004 CD ROM.*

41. Blundy, J., Reitan, D., Steele, J., *ANTEC 1998 CD ROM.*

42. Santhanam N., *Ph.D. Thesis*, *Cornell University*, Ithaca, New York (1992).

43. Santhanam N., Chiang H. H., Himasekhar K., Tuschak P., Wang K. K., *Advanced Polymer Technology*, **11**, 77 (1992).

44. C-MOLD Design Guide, 3rd Edition, Ithaca, New York (1999).

45. Park, C. B. and Cheung, L. K., *Polymer Engineering and Science*, **37**, 1 (1997).

46. Rachtanapun, P., Matuana, L. M., and Selke, S. E. M., *ANTEC 2003 CD ROM*.

47. Chandra, A., Gong, S., Turng, L. S., Gramann, P., *ANTEC 2004 CD ROM*.

48. Chandra, A., Gong, S., Turng, L. S., Gramann, P., Cordes, H., *Polymer Engineering and Science*, **45**, 52 (2005).

49. *Polypropylene: An A to Z reference*, Kluwer Publishers, (1999).

50. Chen, L., Straff, R., and Wang, X., *SPE Annual Technical Papers CD-ROM*, (2001).

51. Lee, C., Sheth, H. and Kim, R., "Gas Absorption with Filled Polymer Systems," *www.trexel.com, Technical Papers and Presentations*.

52. Antony, J., *Design of Experiments for Engineers and Scientists*, Butterworth-Heinemann, Burlinton, MA (2003).

53. Montgomery, D. C., *Design and Analysis of Experiments*, John Wiley & Sons, Inc., (1984).

54. Ermer, D. S. and E-Hok, R. Y., *Contributed Publications of the Measurement Quality Division*, American Society for Quality, **2** (1997).

55. Wheeler, D. J. and Lyday, R. W., *Evaluating the Measurement Process*, SPC Press, Inc., Knoxville, (1989).

56. Xu, J., Kishbaugh, L. and Casale, M., *SPE Annual Technical Papers CD-ROM*, (2002).

57. Gong, S., Yuan, M., Chandra, A., Kharbas, H., Osorio, A., Turng, L. S., *International Polymer Processing*, **20**, 202 (2005).

58. Chen, L., Blizard, K., Wang, X., *SPE Annual Technical Papers CD-ROM*, (2001).

59. Derdouri, A., Garcia-Rejon, A., Nguyen, K. T., Simard, Y., Koppi, K. A., and Salamon, B. A., *ANTEC 1999 CD ROM*.

60. Watanabe, D., Hamada, H., and Tomari, K., *ANTEC 2001 CD ROM*.

61. Watanabe, D., Hamada, H., and Tomari, K., *ANTEC 2002 CD ROM*.

62. Patcharaphun, S. and Mennig, G., *PPS-21 2005 CD-ROM*.

Approved

Lih-Sheng Turng

Date 10/18/05

Lih-Sheng Turng

Associate Professor